University of South Bohemia
Faculty of Science

Assaying mitochondrial cell number, morphology and respiration status in the emerging three lineages of the preimplantation stage mouse embryo

Master's thesis

Bc. Valeriy Kutsyna

Supervisor: prof. Alexander W. Bruce, Ph.D.

České Budějovice 2023

Master's Thesis

Kutsyna, V., 2023: Assaying mitochondrial cell number, morphology and respiration status in the emerging three lineages of the preimplantation stage mouse embryo. Mgr. Thesis, in English. – 72p., Faculty of Science, University of South Bohemia, České Budějovice, Czech republic.

Anotace:

The aim of this master thesis was to assay mitochondrial cell number, morphology and respiration status in the emerging three lineages of the preimplantation stage mouse embryo.

Prohlášení

Prohlašuji, že jsem autorem této diplomové práce a že jsem ji vypracoval pouze s použitím pramenů a literatury uvedených v seznamu citované literatury.

V Českých Budějovicích, 13.04. 2023 …….

Valeriy Kutsyna

Acknowledgements

First of all, I would like to thank my supervisor prof. Alexander W. Bruce, Ph.D. for his invaluable advice and guidance throughout my exciting two-year stay at his lab. Next, I would like to say a huge thank you to Martina, Becky, Pablo, Lenka and Valeriya for their help, mentoring, constant support and friendly atmosphere in our lab. My gratitude also goes out to Andy and Jana for being the best lab-mates and troubleshooters. I'm much obliged to my family and friends for sticking with me and supporting me during the last couple of years. Finally, I'm forever indebted to every human being who decided to defend my home, Ukraine, since 2014 and 2022.

Честь і слава загиблим героям. Навіки.

Abstract

Mitochondria play crucial cellular roles, ranging through oxidative phosphorylation and generation of ATP, control of intra-cellular Ca^{2+} signalling cascades, regulation of redox cellular potential, maintenance and balance of reactive oxygen species levels, and are strongly associated with apoptosis, among many other physiological processes. In mammalian preimplantation development, it is claimed the quality of maternally inherited mitochondria is directly related to embryo integrity and the ability of blastocyst stage embryos to implant; as well as influencing development through to adulthood and an association with certain pathologies. However, systematic and comprehensive research into mitochondrial morphology and function in relation to the emerging three blastocyst stage lineages (*i.e.* trophectoderm/TE, primitive endoderm/PrE and epiblast/EPI) is still relatively scarce. Accordingly, using immuno-fluorescence based confocal microscopy imaging and a subsequent computationally based approach, we have assayed the membrane potential activity (utilizing Mitotracker Red (CMXRos)) of mitochondria at the late mouse blastocyst stage; and specifically within the emerging inner cell mass (ICM) and TE lineages. Additionally, we have explored the role of p38-MAPK activity in mitochondria maturation dynamics, utilizing chemical inhibition and quantitative real-time polymerase chain reaction technique. The obtained results indicate an increased ratio of highly-polarized mitochondria in differentiating TE cells (associated with a tubular network morphology), accompanied by comparatively less-polarized mitochondria in the blastocyst inner cell mass lineages. Conversely, a reduced degree of membrane polarization in TE cells, coupled with a significantly increased ratio of polarization in ICM mitochondria of p38-MAPK inhibited embryos was observed. Moreover, a comparatively robust increase in mitochondrial morphological parameters (*e.g.* branch length, number of branches), coupled with a transcriptional downregulation of electron transport chain-related mRNA transcripts was demonstrated in p38-MAPKi embryos. Reliable derivation of baseline data describing preimplantation mouse embryo mitochondrial status will act as a foundation for future functional studies related to identified cell-signalling pathways and candidate mitochondrial structural genes implicated in the derivation of specific blastocyst cell lineages.

Key words:

preimplantation mouse embryonic development, blastocyst, trophectoderm, primitive endoderm, epiblast, mitochondria, p38-MAPK inhibition (p38-MAPKi).

Table of contents

Glossary of abbreviations

AIF – apoptosis-inducing factor

ATP – adenosine triphosphate

AMOT – angiomotin protein

CDX2 – caudal-related homeobox 2 transcription factor protein

CTCF – corrected total cell fluorescence

DRP1 – dynamin-related protein-1

EPI – epiblast

ERK – extracellular signal regulated kinase protein

ESC – embryonic stem cell

ETC – electron transport chain

FGF4 – fibroblast growth factor 4 protein

FGFR - fibroblast growth factor receptor protein

GATA2/4/6 – GATA binding protein 2/4/6

ICM – inner cell mass

IF – immuno-fluorescence

IVF – *in vitro* fertilization

MAPK – mitogen activated kinase protein

MMP – mitochondrial membrane potential

mtDNA – mitochondrial deoxyribonucleic acid

MTR – MitoTracker Red (CMXRos)

NANOG – homeobox transcription factor NANOG protein

OCT4 – octamer-binding transcription factor 4 protein, also known as POU5F1 – POU class 5 homeobox 1

OXPHOS – oxidative phosphorylation

ROS – reactive oxygen species

RT-qPCR – quantitative real-time polymerase chain reaction

PrE – primitive endoderm

SOX2 - SRY-box transcription factor 2 protein

TCA – tricarboxylic acid

TE – trophectoderm

TEAD4 – transcriptional enhanced associate domain 4 transcription factor protein

TOS – threshold overlap score

YAP – yes associated protein

ZGA – zygotic genome activation

1. Introduction

1.1 Preimplantation mouse embryonic development: from oocyte to implantation

1.1.1. Preimplantation mouse embryo development

Preimplantation mouse development is characterised by distinct periods of cleavage (cell division and differentiation), culminating with the formation of a embryonic structure, containing an outer epithelial layer cell layer, supporting an encapsulated inner cell mass (ICM) and a fluid-containing cavity, called the blastocyst and its subsequent implantation into the uterus wall. The three unique blastocyst cell lineages emerge throughout preimplantation development are defined as the epiblast (EPI), the primitive endoderm (PrE), both resident in the ICM, and the trophectoderm (TE). The EPI gives rise to the cells of the embryo proper, while the PrE, on the other hand, forms extraembryonic yolk sac membranes, that play a crucial role in nutrient uptake and waste disposal during early development. The TE forming the outer layer of the blastocyst, eventually give rise to the embryonic component of the placenta. Understanding the development and specification of these three lineages is important for improving the success of assisted reproductive technologies and for gaining fundamental insight into early embryonic development. The quality of mitochondria is crucial for successful embryo development and maturation, as they are the primary energy producers in cells. Furthermore, the distinct morphological and physiological characteristics observed in the mitochondria of different cell lineages highlight the importance of energy metabolism regulation and maintenance in this process.

1.1.2. Fertilization

Preimplantation mouse embryo development originates after fertilization and continues up until blastocyst stage embryo implantation. Fertilization can be described as the fusion of a single haploid sperm cell and a metaphase II-arrested oocyte resulting in a 1-cell totipotent diploid zygote, later giving rise to all extraembryonic tissues, and the embryo/foetus itself. To successfully fertilize an oocyte, sperm cells must navigate through the uterine passage up into uterotubal junction, and to ampulla of oviduct. While migration is underway, spermatozoa undergo a series of molecular changes, collectively called capacitation — chemical reactions essential for oocyte fertilization, sperm transport, resulting in faster flagella motility and better spatiotemporal navigation (Stival *et al.*, 2016). Nevertheless,

most of the sperm passage is still ensured by muscle contractions of uterus. Capacitation is succeeded by sperm penetration of the outer cumulus mass (*corona radiata*), surrounding the oocyte along with *zona pellucida* layer (ZP). Sperm penetration is possible due to the activity of the acrosome and trypsin-like enzyme. Adhesion to the oocyte plasma membrane, causes a critical activated release of Ca^{2+} into the ooplasm, leading to exocytosis of oocyte cortical granules whose contents result in changes in molecular structure of ZP, resulting in inability of slower spermatozoa to penetrate it; thus preventing polyspermic fertilization events (Figure 1; Cheeseman *et al*., 2016; Tokuhiro *et* Dean, 2018).

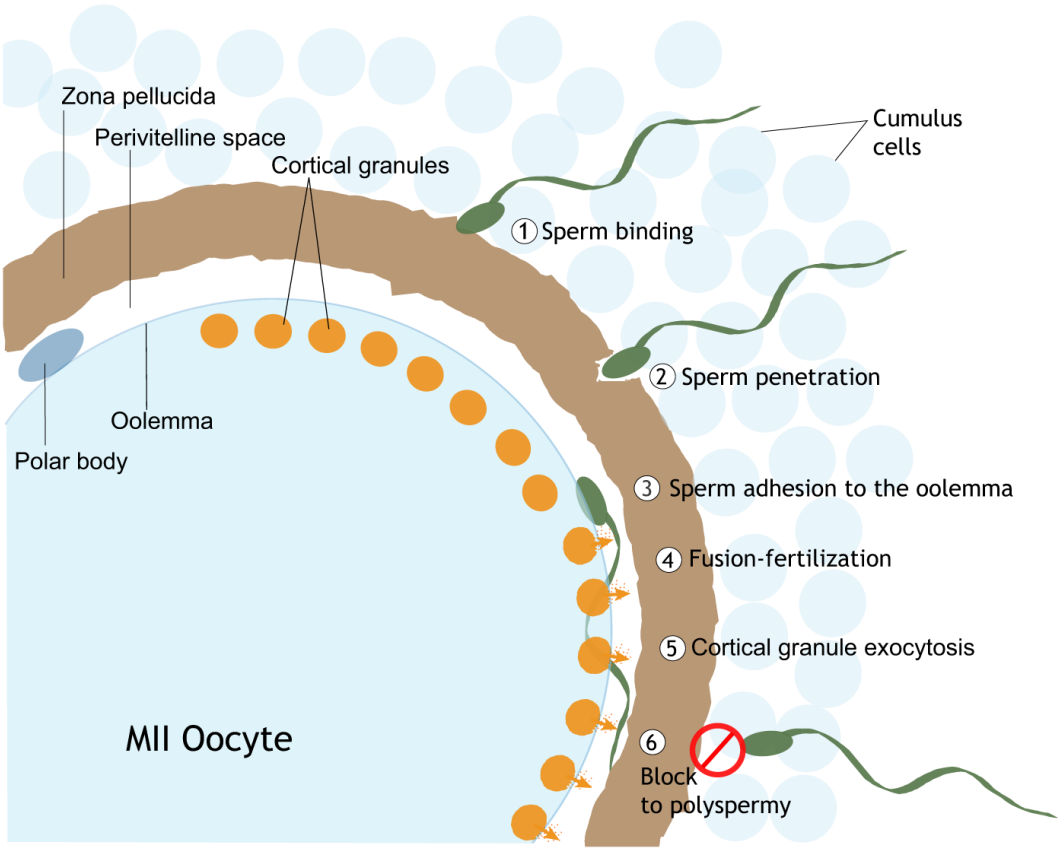

Figure 1. Schematic representation of essential processes and factors participating in mammalian fertilization. Sperm penetration of the metaphase II (MII) oocyte cumulus cells and *zona pellucida* kickstarts fertilization. After a single sperm cell manages to reach the oolema, the egg plasma membrane, cortical granules exocytosed from within the periphery of the oocyte, within the cortical region just beneath the plasma membrane, lead to the formation of a fertilization envelope that prevents polyspermy, thus, allowing the single sperm cell to successfully fertilize the egg (taken from Bhakta *et al.*, 2019).

1.1.3. Overview of cleavage division events

Subsequent stages of totipotent zygote development are characterized by a series of atypical cell divisions, with no general volume increase, also known as cleavage division. Embryonic cells, resulting from such divisions are referred to as blastomeres. Prior to the cleavage

division stages, embryo development is ultimately dependent on maternally provided proteins and mRNA reserves that are stored in the oocyte. These factors are necessary for early developmental events including embryonic genome activation and cell-fate specification. During the first cleavage division (from zygote to 2-cell) a noticeable change in the embryo's transcriptome marks the beginning of zygotic genome activation (ZGA). ZGA is implemented in 2 waves: the minor burst, conducted as soon as 7 hours after zygote pronuclei are formed, being possibly associated with protamine exchange in the male pronucleus. Around the end of 2-cell stage, major ZGA result in maternal mRNA decay, together with rearrangements in chromatin structure such as DNA methylation, changes in nucleosome positioning and replacement of canonical histone proteins (reviewed in Svoboda, 2018). ZGA in responsible for establishing totipotency in blastomeres, thus it is a crucial process in mammalian embryo development — embryos that fail in ZGA mostly do not progress beyond the 2-cell stage (Schulz *et* Harrison, 2019).

One of the most actively researched topics in early mammalian developmental biology is focused on understanding the underlying mechanisms responsible for biased positional and later functional distribution, and self-organization of blastomeres across the whole embryo. The first cleavage division usually happens 24 hours after fertilization, while the following ones take place every 12 to 20 hours (Artus *et* Cohen-Tannoudji, 2008). Coincident with the prolonged timing of 2-cell stage blastomere cell cycles, such blastomeres are also the only type of mouse embryonic cell individually capable of developing into a complete embryo/ organism, indicating decreasing totipotency of blastomeres throughout development (Morris *et* Zernicka-Goetz, 2012). While 4-cell stage and early 8-cell stage blastomeres are still able to contribute to extra-embryonic and embryonic fate, the late dividing 8-cell stage blastomeres have undergone morphological compaction and polarization events, responsible for setting up a future lineage specifications, while embryos at later stages also self-regulating the number of polar/apolar and outer/inner cells, that later contribute to the trophectoderm or inner cell mass lineages (Fleming, 1987). Both compaction and polarization occur concurrently: the former event involving physical reshaping of blastomeres, in which cells flatten and increase their contact area, forming a tightly packed spherical cell mass, while the latter involves establishment of apico-basal polarity by localisation of specific polarity factors (Varelas *et al.*, 2010; Ziomek *et* Johnson, 1980). Key factors mediating compaction and, later, blastocyst formation include E-cadherin and β-

catenin. E-cadherin is a member of the transmembrane protein complex that mediates calcium-dependent cell-cell adhesion, whereas β-catenin is a cytoplasmic proteins that interact with the intracellular domain of cadherins and link them to the actin cytoskeleton (De Vries *et al.*, 2004). Consequently, the newly-reshaped embryo can be split into areas of cell contact (baso-lateral for outer cells and ubiquitous for inner cells) and contact-free zones (apical area of outer cells). The unique apical domains of outer cells are marked with increased presence of F-actin, localised atypical protein kinase C/ partitioning defective complex (aPKC–PAR complex), ezrin, microvilli and factors, contributing an apical-baso-lateral axis of intra-cellular polarity (Korotkevich *et al.*, 2017). The differential spatial segregation and inheritance of apical-basolateral polarity of 8-cell daughter blastomeres represent the first wave of potential internalization of apolar cells to the nascent ICM, also referred to asymmetric divisions. During the 16- to 32-cell transition, polarized outer 16-cell stage blastomeres can contribute an additional population of inner cells in a second wave of cell internalization. Therefore, at the early blastocyst 32-cell stage, the pluripotent ICM comprises its initial full complement of EPI and PrE progenitors and the outer polarized and differentiating TE cells initiate their irreversible cell-fate commitment (Morris *et al.*, 2010; Posfai *et al.*, 2017). The factors influencing the frequency by which asymmetric division types occur (either at the 8- to 16- or 16- to 32-cell transitions), and whether they represent inherent randomness, are not completely understood. However, the intra-cellular position of nuclei along the embryonic radial axis (outer-cell apico-baso-lateral axis) and the orientation and size of the apical domain play an important role in orientating ensuing divisions (Ajduk *et al.*, 2014). Indeed, an important trait of the apical domain of outer cells is its ability to recruit one of the mitotic spindle poles, which helps in orienting and establishing a particular degree of uneven inheritance of the apical domain between the resulting daughter cells. Newly-divided cells can acquire, depending on a mitotic spindle angle, either apolar (transversal plane of division), polar (sagittal plane) or mixed condition (oblique or “uneven” plane). It is speculated that the fate of those “unequal” cells specifically depends on differential distribution of E-cadherin in each daughter progeny (reviewed in Johnson, 2009).

1.1.4. First cell-fate decision — trophectoderm and inner cell mass

The first cell-fate decision between TE and ICM can be considered as initiating from the 8-cell stage onwards. This phase is characterized by the amplification of cell contacts by all blastomeres during the process of embryo compaction, leading to the formation of an

intracellular axis of apical-basolateral polarity. The Hippo signalling pathway plays a critical role in the regulation of differentiation during first cell-fate decision (Figure 2). The Hippo pathway is regulated by a complex network of upstream signalling molecules and proteins, including the MST1/2 kinases, the LATS1/2 kinases, and the scaffold proteins SAV1 and MOB1. During the 8- to 16-cell stage division, the Hippo pathway is active and inhibits the activity of the transcriptional co-activators YAP and TAZ, binding partners of the transcription factor TEAD4, by preventing their translocation into the nucleus and the activation of their target genes. The TEAD4 transcription factor is a key downstream effector of the Hippo pathway and is activated (by interaction, in the nucleus, with YAP/TAZ) when the Hippo pathway is inhibited. Indeed, in outer TE cells, the Hippo pathway is actively inhibited, leading to the activation of TEAD4 transcriptional complex and the expression of its downstream target genes. These genes include *Gata2*, *Gata3* and *Cdx2* - markers of the future TE, that they are involved in the transcriptional regulation of cell proliferation, differentiation, and cell-fate determination in the developing embryo (reviewed in Alberio, 2020). Conversely, the inner unpolarized cells maintain an active Hippo pathway, that leads to YAP/TAZ phosphorylation, via AMOT-LATS-NF2 complex, and ensures they are sequestered to the cytoplasm and do not enter the nucleus; thus preventing *Cdx2* (and other TE-related gene) transcription but also ensuring an actively transcribing pluripotent *Sox2* gene (reviewed in Chazaud *et* Yamanaka, 2016). By the end of 16-32-cell transition, the embryo has primarily managed to establish a spatial and polarity specific identity of each cell and, in turn, is able to initiate the second cell-fate decision division. Importantly, the embryo's self-organizing properties allow it to regulate a constant ratio of inner and outer cells utilizing an intrinsic mechanism of cell-shape remodelling and resegregation up to 32-cell stage and even further in development (Johnson, 2009).

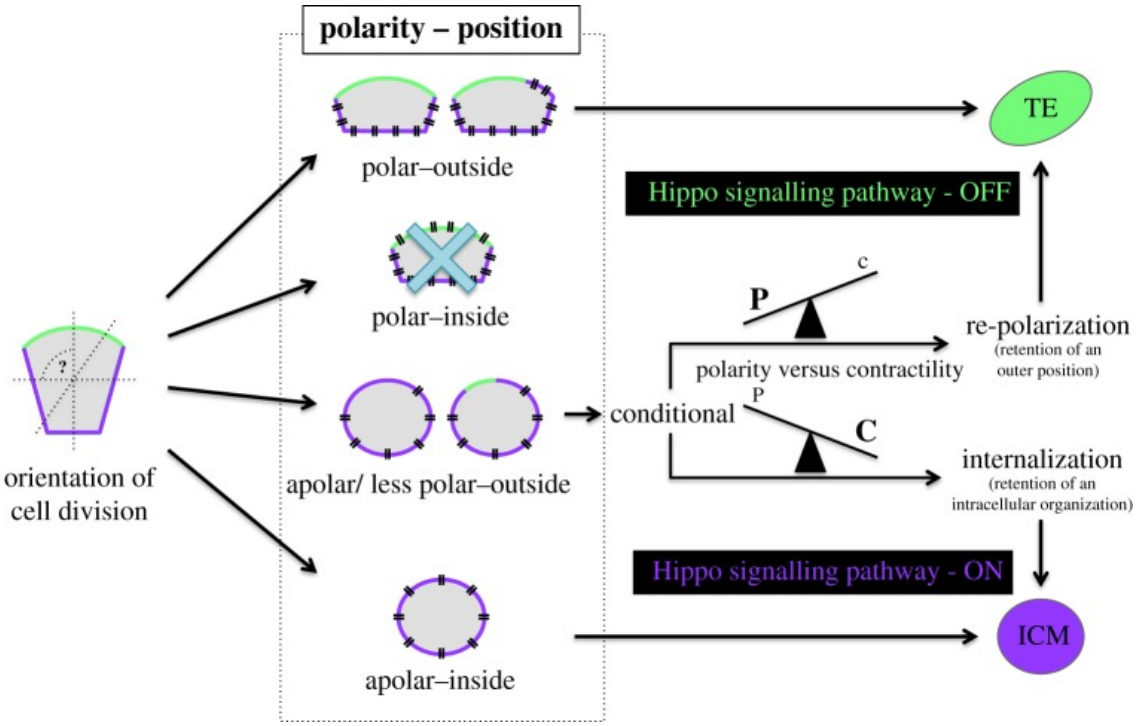

Figure 2. A schematic depiction of polarity-dependent cell-positioning model of the first cell-fate decision in preimplantation mouse embryo development. At the 16-cell stage, newly formed blastomeres inherit different degrees of apical (contactless domain) or basolateral (cell contacts) polarity factors, based upon the orientation of division of their mother 8-cell stage cell. The degree of factor acquisition is dependent on the plane of cell division, thus generating daughter cells with varying amount of apical domain, or none at all. Blastomeres, inheriting apical - basolateral polarity factors and an outer position are destined to develop into extraembryonic trophectoderm, via preventing Hippo signalling activation. Inside polar cells with no apical domain factors activate the Hippo pathway and contribute to the embryonic inner cell mass. The existence of internalized polar daughter cells is not derived. Outside located blastomeres with no apical polarity factors or small amount are either internalized via actomyosin contractility, or less frequently repolarize in the outside area (taken from Mihajlović *et* Bruce, 2017).

1.1.5. Second cell-fate decision — epiblast and primitive endoderm

At the 32-cell stage, as the blastocyst cavity forms, blastomeres are already classified as either outer cells or inner cell mass (ICM), the second cell-fate decision pushes embryonic development further, leading to the formation of a fluid filled cavity containing blastocyst comprising three morphologically distinct cell lineages: an already epithelialized flat rod-like outer trophectoderm lineage (TE, marked by CDX2 expression), further subdivided into polar TE (adjacent to ICM) and mural TE (at the abembryonic pole), and an ICM, consisting of deeply located pluripotent epiblast (EPI, marked by NANOG expression), superficial primitive endoderm (PrE, marked by GATA6 expression), and a small number of yet unspecified cells (marked by NANOG and GATA6 coexpression). Following implantation, all three lineages will differentiate/contribute progeny into morphologically and functionally

independent structures: TE cells will form placental tissue, PrE will contribute to yolk sac formation, as well as parietal and visceral endoderm, and pluripotent EPI cells will serve as a foundation of a future embryo (Figure 3).

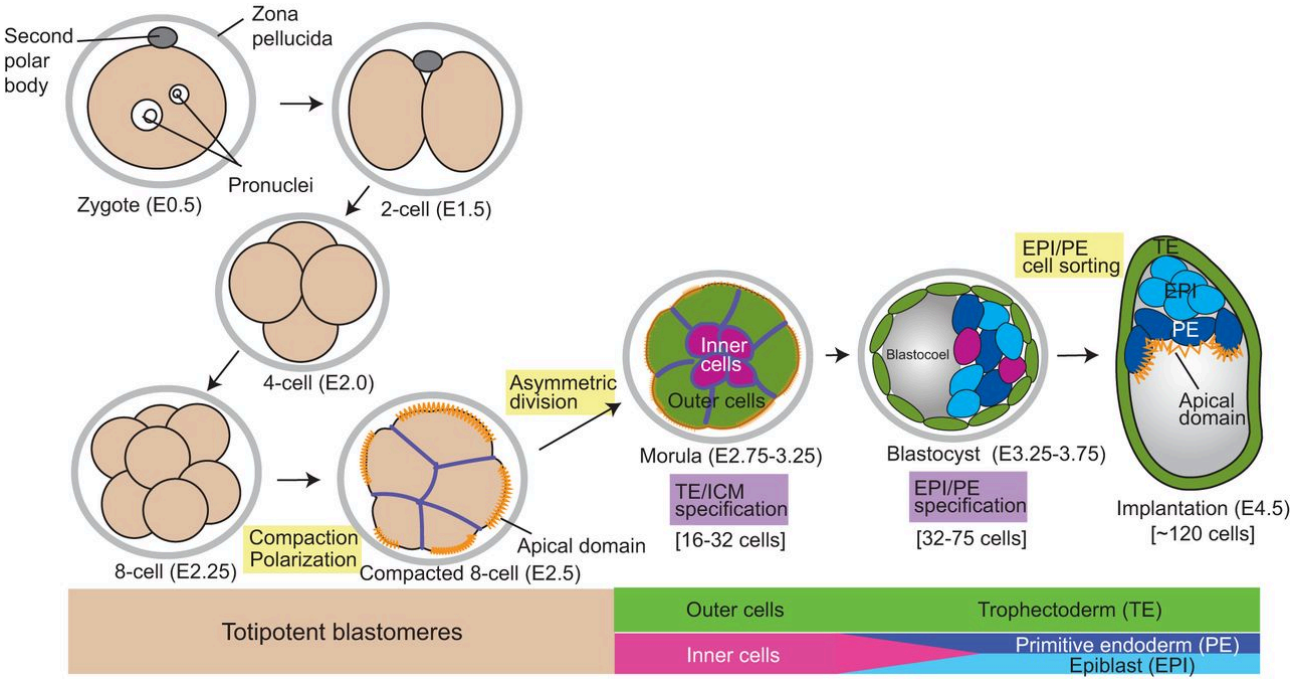

Figure 3. A generalized representation of preimplantation mouse development up to the implantation period. A brief summary of preimplantation mouse embryo development from fertlilized zygote to fully developed E4.5 stage (late blastocyst) embryo. The figure depicts timings of pluripotent-to-differentiating blastomere development, the number of cells at each stage, progressing lineage specification and corresponding derivation events (taken from Chazaud *et* Yamanaka, 2016).

Starting from the late 16-cell stage, a certain blastomeres form an osmotic gradient powered by Na^+/H^+ pumps in the apical side and Na^+/K^+ ATPase complex located basolaterally, thus creating an internal fluid-filled cavity and significantly increasing volume of the embryo (Dumortier *et al.*, 2019). The presence of the cavity is thought to be an important factor preceding the second cell-fate division and a number of models detailing PrE cell differentiation have been proposed. The "positional induction" model states that ICM cells that are in contact with the cavity are destined to differentiate into another extraembryonic tissue, namely the primitive endoderm (PrE) as they contribute to the facilitation of osmotic water transfer across the TE monolayer via Na^+/K^+ ATPases and aquaporins. Conversely, cells residing deeper in the ICM are meant to remain as a pluripotent epiblast (EPI), and later develop into embryo proper (Rubio *et* Simón, 2021). Although, the absence of a confirmed signalling molecule derived from the cavity undermines the validity of the "positional

induction" model (Ryan *et al.*, 2019). An alternative "salt and pepper" theory proposes a three-step model of PrE lineage specification to explain the acquisition of the second cell-fate decision. The first step of the model involves stochastic processes that lead to the co-expression, within cells of the ICM, of NANOG and GATA6 at the 32-cell (E3.5) stage. The second step occurs at the 64-cell (E4.0) stage, where inhibitory regulatory pathways mature and mutual exclusion of NANOG and GATA6 expression occurs in individual cells. This results in the formation of a spatially randomized heterogeneous population of ICM cells expressing either NANOG or GATA6, termed the emergence of a "salt and pepper" pattern distribution of EPI and PrE progenitor cells. The third step involves cell sorting within the ICM, driven by active and/or passive cell movements, which leads to the final spatial segregation of the EPI and PrE cell lineages at around the 128-cell stage (reviewed in Zernicka-Goetz *et al.*, 2009). However, mathematical modeling suggests that stochastic processes are unlikely to be the driving force behind the "salt and pepper" distribution of GATA6 and NANOG proteins throughout the ICM (Bessonnard *et al.*, 2014).

The "time inside-time outside" hypothesis is another model that proposes the developmental history of an individual early blastocyst ICM cells influences its eventual fate as either EPI or PrE progenitor (Bruce *et* Zernicka-Goetz, 2010). One of the causative reasons of the onset of heterogeneity in the ICM population from the 32-cell stage onwards, might be connected to observations suggesting, that inner cells derived from the first asymmetric division (8-16-cell stage) are biased to becoming EPI progenitors, while cells generated from second asymmetric division (16-32-cell stage) are significantly more often PrE progenitors (Morris *et al.*, 2010). Nonetheless, the following rules of specification are strongly dependent on the number of internalized cells after the first asymmetric division. It is implied, the intricacies behind such regulation mechanisms are mediated by fibroblast growth factor (FGF) signalling: blastomeres derived after 1st asymmetric division show higher level of FGF4 protein/mRNA expression, that could influences the initiation of PrE formation in neighbouring ICM cells via a paracrine mechanism (Krupa *et al.*, 2014). On the contrary, inner cells produced by the second round of division possess higher mRNA levels of *Fgfr2*, a receptor that recognizes the FGF4 molecule, thus kickstarting, or at least augmenting, the PrE differentiation pathway — depicted in Figure 4. Therefore, in cases when the number of inner cells, emerging after the 8- to16-cell stage is small, the levels of expressed/secreted FGF4 are not enough to activate the FGFR2 receptors of neighbouring blastomeres until the

second round of asymmetric division, thus majority of cells are oriented towards the EPI lineage. Conversely, in situations when the produced number of cells after the 1st round is high enough (>3 inner cells), the stimulation threshold is reached, allowing a number of cells to acquire PrE fate (Figure 4).

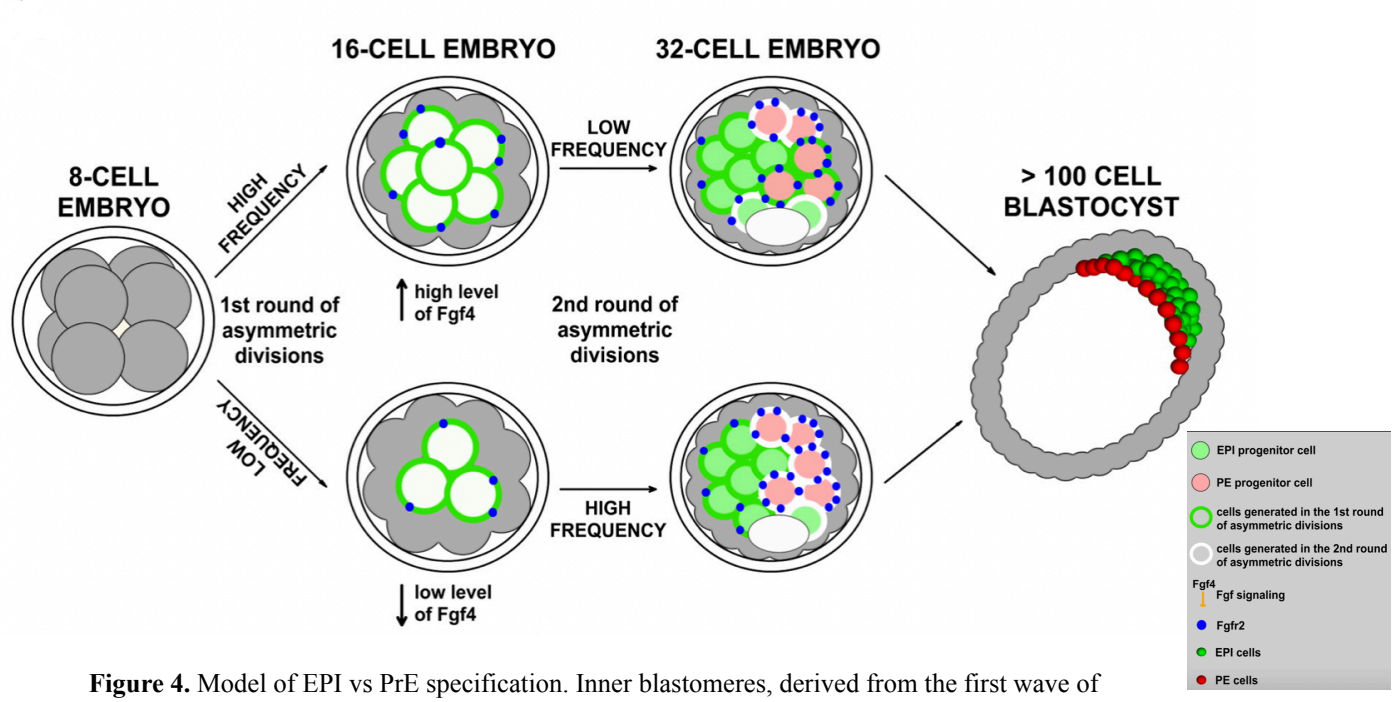

Figure 4. Model of EPI vs PrE specification. Inner blastomeres, derived from the first wave of asymmetric cell division express elevated levels of *Fgf4* mRNA and reduced levels of *Fgfr2* mRNA, compared to those, created during the 2nd wave. When enough inner cells originating from the 1st asymmetric division are created, extracellular FGF4 levels rise, thus, exceeding a threshold required to initiate some PrE derivation. In contrast, when the number of inner cells created during 8-16-cell stage is not sufficient, not enough FGF4 is secreted, leading to unbalanced derivation of mainly EPI progenitors. As a consequence, the 2nd wave produces elevated number of the PrE population, also confirmed by increased levels of *Fgfr2* expression, requiring less FGF4 demanded for PrE specification (taken from Krupa *et al*., 2014)

The paracrine mechanism of FGF signalling is propagated downstream via the mitogen-activated-kinase/extracellular signal-regulated kinase (MAPK/ERK) pathway. After FGF4 ligand binds to its transmembrane FGFR1/2 receptors, several tyrosine residues become autophosphorylated, increasing receptor activity. The ongoing phosphorylation is then followed by recruitment of adaptor proteins, belonging to the mitogen-activated protein kinase (MAPK) family, thus connecting the FGF4 and MAPK pathways. Subsequent signal transduction is further characterised by multiple protein phosphorylation reactions originating from the cytoplasmic domain of FGFR1/2 tyrosine residues culminating with the activation of RAS; involved in multiple essential physiological processes. Activated RAS is

able to recruit the RAF family of kinase proteins, which then phosphorylates mitogen activated protein kinase kinases 1 and 2 (MEK1/2), part of the MAPK cascade. Final elements of the ERK pathway include activated ERK1/2 kinases, translocation to the nucleus and a dictation of cellular response via transcriptional activation of various biologically important genes and eventual proteins (Krupa *et al.*, 2014; McCubrey *et al.*, 2007; Yamanaka *et al.*, 2010; Figure 5).

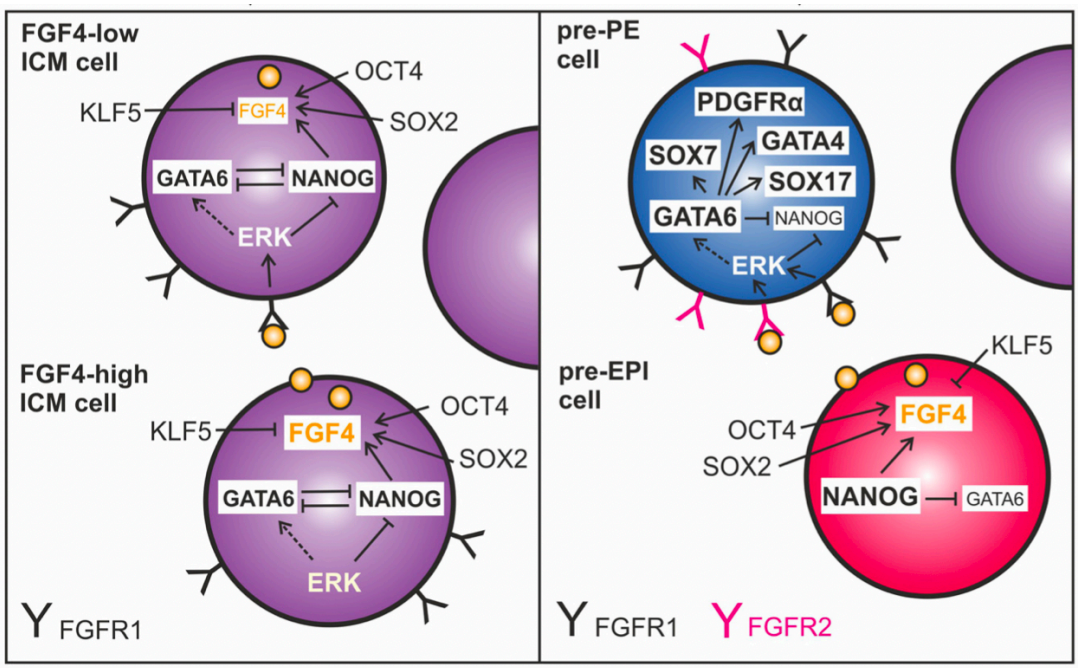

Figure 5. The role of FGF4/ERK signaling in preimplantation mouse embryogenesis. FGF4/ERK cascade regulates EPI/PrE specification across the ICM. Before full development of the blastocyst is established, every cell within ICM expresses FGFR1 receptor and both EPI and PrE specific factors (such as NANOG for EPI and GATA6 for PrE) simultaneously. Continuous with blastocyst cavity establishment, FGF4 is translated from future EPI cells, promoting GATA6 expression in neighbouring blastomeres via a paracrine mechanism. In these cells FGF4, acting through FGFR1 and FGFR2, maintains GATA6 expression and downregulates NANOG (i.e., activates the PrE specification program). Next, it induces expression of several late PrE markers, such as SOX17, PDGFRα, GATA4, SOX7 (Taken from Soszyńska *et al.,* 2019).

In the context of the second cell-fate decision, MEK1/2 and ERK1/2 are extremely important in PrE derivation, as pharmacological inhibition of MEK throughout the entire blastocyst maturation period completely blocks PrE differentiation (resulting in pan-ICM expression of EPI markers). At the same time, it is speculated that ERK2 also regulates propagation of polar trophectoderm cells, as *Erk2*$^{-/-}$ embryos die early during embryogenesis due to a defect in trophoblast development (Saba-El-Leil *et al.*, 2003).

Besides taking part in PrE specification and maintenance, the FGF/ERK pathway seems to have an unexpected role in the EPI specification: as *Fgf4*$^{-/-}$, as well as *Fgfr1*$^{-/-}$ and *Fgfr2*$^{-/-}$ double knockout embryos are distinct in maintaining elevated expression of NANOG compared to wild-type embryos by the late blastocyst stage, implying antagonistic pressure of FGF4-signaling towards the pluripotent potential of blastomeres (Kang *et al.*, 2017). It is important to understand the existence of many more mechanisms governing the second cell-fate decision. For example, some recent publications report on autonomous role of the Notch pathway in both the first cell-fate decision, similar to the Hippo-signalling mechanism, as well as a regulatory element in establishing *Fgfr2* expression, crucial to EPI/PrE differentiation (Anani *et al.*, 2014; Menchero *et al.*, 2019). Similarly, members of the transforming growth factor beta (TGF-β) growth factors family, consisting of Activins, NODAL and bone morphogenetic proteins (BMPs), occupy an essential niche in PrE and EPI development and regionalization as soon as these lineages emerge, judging from perturbing phenotypes in embryos lacking various genes related to TGF-β family (Reviewed in Papanayotou *et* Collignon, 2014). Other major signalling pathways actively involved in early embryonic development, include the Wnt/β-Catenin pathway, G-protein coupled receptors (GPCRs), estrogen receptors, and RHO/Rock associated signalling (Menchero *et al.*, 2017).

1.2. p38 mitogen-activated protein kinases (p38-MAPKs)

1.2.1 General description and a mechanism of action

The p38 mitogen-activated protein kinase (p38-MAPK) pathway is a stress-induced signalling pathway, also associated with a variety of different cellular functions including cell cycle, cellular respiration, survival, development, tumorigenesis and immune response. The p38-MAPKs belong to a family of serine-threonine and tyrosine kinases, comprised of four isoforms: p38α (MAPK14), p38β (MAPK11), p38γ (MAPK12/ERK6) and p38δ (MAPK13/SAPK4) - all four are expressed in mouse preimplantation embryo development; but only the -α isoform knockouts are embryonic lethal in mice around E10.5 (the first discovered isoform; Mudgett *et al.*, 2000). The p38-MAPKs are activated through various functional upstream MAPKK (Mek3/Mkk3/Map2k3 *etc.*) phosphorylation cascades, as a response to extracellular environmental stimuli triggers, such as U.V. radiation or amino acid stress, heat shock, increased expression of cytokines and growth factors; thus contrasting with the other members of its mitogen-activated protein kinase superfamily (such as

ERK1/2), which activate through a particular ligand-receptor pattern, usually via RTKs (Remy *et al.*, 2010). As soon as p38-MAPKs are activated, a wide range downstream phosphorylation is continued, including hundreds of proteins, enzymes, transcription factors/ cofactors, epigenetic regulators, involved in protein synthesis and turnover (Cuenda *et al.,* 2007).

1.2.2. p38-MAPK role in preimplantation embryo development

In the context of preimplantation mouse embryo development, application of chemical p38-MAPK inhibition on 2-cell stage embryos mostly results in either blocked compaction event during E2.5, or cavitation failure after E3.5; each resulting in embryo death (Paliga *et al.*, 2005). Such observed phenotypes are accompanied by mRNA transcription downregulation of facilitative glucose transporter proteins, in turn reducing the adaptative capability of the preimplantation embryo to uptake and utilize glucose in variable environmental conditions (Sozen *et al.*, 2015). Moreover, treatment of E3.5 embryos with p38-MAPK inhibitor is marked by impaired cavity expansion, increased levels of cellular reactive oxygen species (ROS; Bora *et al.*, 2019) and a reduction of ICM number, accompanied by minor reductions of outer TE cells (Bora *et al.*, 2021; Maekawa *et al.*, 2005). Observed ICM impairments are further characterised by a significant impairment in PrE cell specification and differentiation (marked by GATA4 expression), at the expense of an increased population of unspecified cells (GATA6 and NANOG double positives), but a statistically unchanged number of correctly specified EPI (NANOG-positive) cells (Thamodaran *et* Bruce, 2016); invoking a failed mechanism of PrE specification and differentiation.

Besides its role in ICM development, a TE specific role in the context of FGF2 signalling and blastocyst expansion has also been reported; whereby blastocysts (E3.5-E4.5) treated with p38-MAPKi display defects in cavity expansion (Bora *et al.*, 2019; Bora *et al.*, 2021; Thamodaran *et* Bruce., 2016), while embryos microinjected with anti-FGF2 antibodies, failed to develop a cavity at all (Yang *et* Wilson, 2015). Interestingly, defects in ICM cell fate specification/differentiation have also been reported in blastocysts with impaired cavity size/ volume. A study by Ryan *et al.*, demonstrated that modifying the size of the blastocyst cavity during early maturation stages (E3.5-E4.0) by either chemical means (using ouabain to inhibit the ATP1 channel responsible for cavity fluid accumulation) or mechanical means led to decreased expression of PrE marker proteins at E4.0 (Ryan *et al.*, 2019). Intriguingly, the defects in PrE differentiation associated with p38-MAPKi closely resemble those observed

in mechanically deflated blastocysts, including reduced GATA4 expression and normal EPI specification as indicated by analysis of either NANOG or SOX2 expression. Inhibition of p38-MAPK activity has been reported to increase mouse blastocyst TE tight junction permeability and reduce aquaporin and Na^+/K^+ pumps expression (Bell *et* Watson, 2013); contributing to reduced cavity size/volume. Although the majority of derived data comes from mouse embryos, inhibited at the 32-cell (E3.5) stage, the proposed window of p38-MAPK inhibition insensitivity is reported around E3.5 + 10h stage, coinciding with blastocyst definitive maturation timing (Bora *et al.*, 2021; Posfai *et al.,* 2017; Thamodaran *et* Bruce, 2016).

An ambitious mass spectrometric phosphoproteomic and proteomic analysis, coupled with mRNA-Seq data, by Bora *et al.*, demonstrated that p38-MAPK inhibited blastocysts showed significantly reduced translational activity during the early blastocyst maturation period compared to control embryos; and the presented combined proteome and phosphoproteome results included almost 300 differentially expressed proteins, likely affected directly or indirectly by p38-MAPK inhibition (Bora *et al.*, 2021). Ontological analysis revealed dysregulation of proteins associated with translation (primarily reduced expression), as well as general depletion in phosphorylation levels of some RNA stability regulatory proteins, in turn, suggesting p38-MAPK orchestrates regulated protein synthesis during the early blastocyst and inhibitor sensitive developmental window. Moreover, additional transcriptome analyses of p38-MAPK inhibited (p38-MAPKi) embryos, performed at three different developmental stages (E3.5 + 4, +7, +10h), identified summarily varying patterns of transcription activity, peaking at E3.5 + 7h time point, nevertheless reverting back to the levels observed in control blastocysts by the E3.5 +10h period. The most differentially variable transcripts being protein translation related genes, followed by mitochondrial respiration and regulators of RNA splicing (Figure 6). The latter two functional clusters being contributed to via p38-MAPK mediated phosphorylation of the MYBBP1A protein (Bora *et al.*, 2021 (a)).

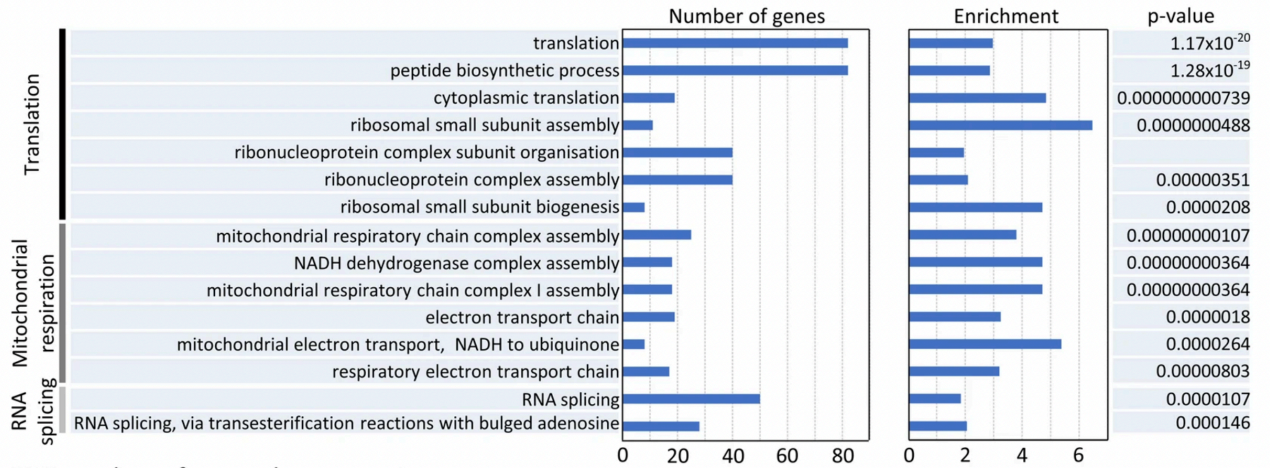

Figure 6. Statistically enriched gene ontology analysis of the top 15 terms identified in the p38-MAPK regulated transcriptome at the E3.5 +7h time-point. Transcriptomic analysis of the effect of p38-MAPKi during early blastocyst maturation reveals a distinct regulatory node governed by p38-MAPK. Marked overall mRNA increases in the inhibited condition suggests importance of p38-MAPK mediated phosphorylation of proteins as a facilitating mechanism of PrE differentiation from an uncommitted state, as well as mitochondrial respiration and RNA splicing (taken from Bora *et al.*, 2021).

1.3. Mitochondria

1.3.1. Mitochondrial structure and function

Mitochondria are double-membrane organelles responsible for producing ATP through oxidative phosphorylation (OXPHOS), taking part in the tricarboxylic (TCA) and urea cycles, also regulating Ca^{2+} homeostasis and participating in cellular stress response, apoptotic pathway and steroid biogenesis (Tuppen *et al.*, 2010). Mitochondria are comprised of two membranes: semipermeable outer and impermeable for most metabolites membranes inner (that can be arranged as folding structures called cristae), separated by inter membrane space and DNA-protein rich inner membrane matrix (Figure 7).

The outer membrane surrounds the entire mitochondrion and separates mitochondrial content from the cytosol, allowing passage of small molecules (to 10kDa) into the inter membrane space via voltage-dependent anion channel membrane proteins (also known as porins). Transfer of bigger proteins across the membrane requires special mitochondrial signal sequence (at their N terminus) and is facilitated via translocase protein units: translocase of the outer membrane (TOM) complex (from cytosol to intermembrane space) and translocase of the inner membrane (TIM) complex (from the intermembrane space into the inner membrane). The inner mitochondrial membrane is impermeable to ions and polar molecules, while protein transport is facilitated only through translocases. The inner membrane acts as a collective hub for respiratory chain complexes, where protein subunits

can be assembled and utilized for the generation of the electrochemical gradient required for OXPHOS and subsequent ATP generation. (Wagner *et al.,* 2009).

Due to the semipermeable nature of the outer membrane, the intermembrane space contains a similar protein and sugar content as in cytosol, while also possessing some unique mitochondrial enzymes responsible for catalytic (*e.g.* adrenaline oxidation), anabolic (*e.g.* ATP synthesis, elongation of fatty acids) as well as other metabolic/cell biological reactions (*e.g.* fusion and fission of mitochondria, transport of metabolites; Van Blerkom, 2011).

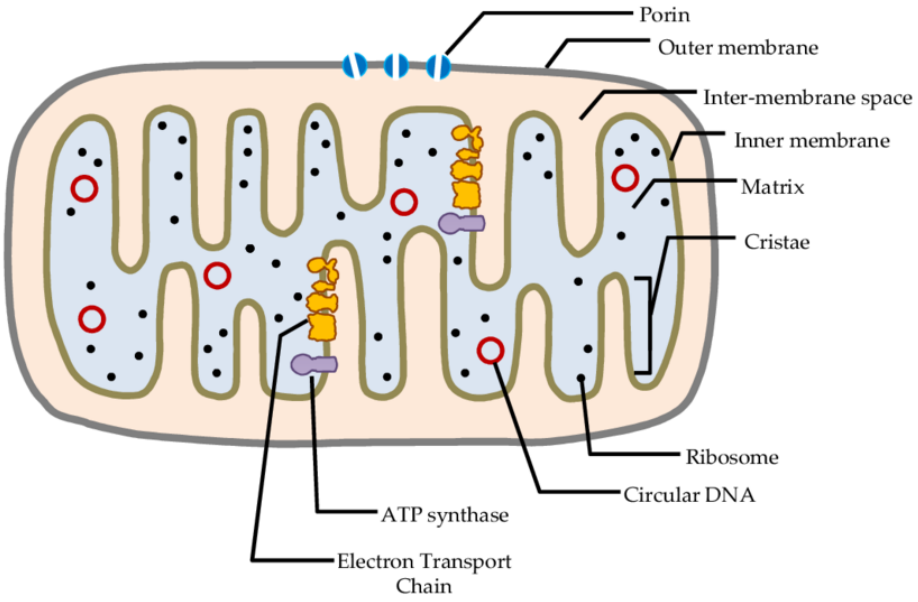

Figure 7. Mammalian mitochondrion structure. Mitochondria consists of two membranes, inner and outer, both are made of phospholipid bilayers. The presence of porin proteins enables passage of cytosolic metabolites up to 10kDa into the inter membrane space. Multiple folding of inner membrane, termed cristae, are essential to increasing effectivity of TCA cycle reactions via exposing greater surface area. Additionally, the inner membrane is also a place of residence to Electron Transport Chain (ETC) complex proteins, where OXPHOS takes place. (taken from Yusoff *et al.*, 2015)

ATP synthesis in mitochondria is dependant on generated metabolites from the TCA cycle and is possible due to the OXPHOS reactions taking place in the ETC; an interconnected system of more than 80 proteins, assembled into 5 complexes (complex I through V), responsible for H^+/proton influx from the matrix into the intermembrane space, in turn generating a strong electrochemical gradient across the cristae of the inner membrane. The rate of respiratory activity depends on the ability of ETC complexes to assemble into active super-complexes across the inner membrane (Dumollard *et al.*, 2007; Wilding *et al.*, 2001). Triglyceride and carbohydrate oxidation, reduces electron carriers in the form of NADH and

$FADH_2$, that transfer electrons to acceptor molecules in the ETC, in the inner mitochondrial membrane.

This process starts with oxidation of NADH by complex I or succinate/ $FADH_2$ by complex II. Coenzyme Q receives these electrons and passes them on to Complex III. The electrons are then transferred to cytochrome c (mobile electron carrier protein, similar in function to Coenzyme Q), before moving on to Complex IV. Finally, the electrons are passed to ½ O_2 to produce H_2O. The energy released during electron passage through complexes I, III, and IV, is used for proton pumping from the mitochondrial matrix across the inner membrane to the intermembrane space. Protons then diffuse back via complex V, ATP synthase, and the concentrated energy, manifested as an electrochemical gradient, enables complex V to phosphorylate adenosine diphosphate (ADP) forming ATP (Dumollard *et al.*, 2007; Wilding *et al.,* 2001; Yusoff *et al.*, 2015). The ETC-related reactions of mitochondria OXPHOS are summarized in Figure 8.

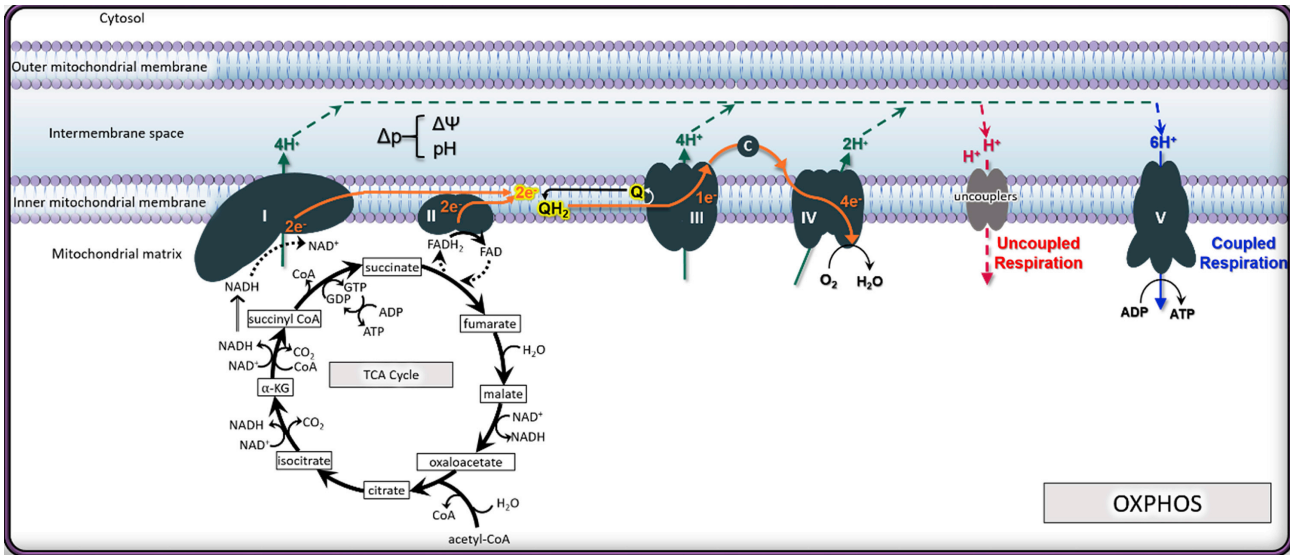

Figure 8. The mitochondrial electron transport chain (taken from Nolfi-Donegan *et al.*, 2020).

1.3.2. Mitochondria in oocytes and early embryos

Fundamentally, oocyte, zygote and embryonic maturation would be impossible without ATP production due to severe impairments originating from metabolic depletion/deficit. Mitochondrial intricate morphology and regulatory function, amidst intensive ATP production, are considered essential factors for successful fertilization and developmental

progression of the oocyte and future embryo (Van Blerkom, 2011). During oogenesis there is an amplification in mitochondrial number, starting with ovarian progenitor stem cells possessing around 100 mitochondria, increasing to 200 in oogonia and 10 000 in primordial follicle oocytes and 100 000 mitochondria in mature metaphase II (MII) oocyte. Additionally, the copy number of mtDNA considered to be maximal in MII oocytes, as during the early embryonic cleavage stages mtDNA replication is absent during cell divisions, and up until the ICM and TE lineages are already established and the embryo is prepared for implantation (Pikó et Taylor, 1987). The average number of mtDNA copies in mammalian oocyte is around 200 000, while the number of mitochondria is half of that, meaning every mitochondrion bears very few mtDNA copies, around 1-2 (Cummins, 1998). Using the mouse model, a minimal threshold, required for successful post-implantation development has been established as ~50000 copies per oocyte (Wai *et al.*, 2010). Mitochondria in MI oocytes are round, possessing a comparatively small number of cristae and a dense matrix, with the most prominent morphological characteristics being pericortical localization of mitochondria, as opposed to surrounding meiotic spindle in MII oocytes, apical/perinuclear localization in 2-cell up to 8-cell stage embryos and predominantly perinuclear in 16-cell upwards (Harvey, 2019; Van Blerkom, 2011). Mitochondrial translocation to the perinuclear region commences prior to oocyte germinal vesicle breakdown and is linked with several energy consuming processes, such as the development of microtubular arrays from perinuclear microtubule organizing centres, formation of polar bodies and chromosomal segregation (Van Blerkom *et* Runner, 1984).

Yet another distinctive feature of oocytes, as well as cleavage stage embryo blastomeres, is the occurrence of a mitochondrial microzonation at a sub-plasmalemmal domain. Although comprising only 3-5% of mitochondria pool, the sub-plasmalemmal mitochondria exhibit significantly increased mitochondria membrane potential (MMP) — the electrical potential difference (voltage) across the inner mitochondrial membrane, created by the uneven distribution of ions across the membrane. Specifically, the potential difference arises from the separation of protons (H^+) on one side of the inner mitochondrial membrane (the intermembrane space) from the protons on the other side (the inner matrix). The proposed hypothesis for such a phenomena is often associated with mitochondria-regulated intercellular signal transduction or inhibition of sperm penetration and cortical granule exocytosis via membrane potential-regulated mechanisms (Van Blerkom, 2008).

Throughout early embryonic lineage development, mitochondria undergo drastic morphological, spatiotemporal and physiological development, generalized by formation of intricate networks of mature cristae upon implantation, but also specific changes, attributed to each blastocyst cell lineage (Zhou *et al.,* 2012). It is implied, that the difference in mitochondria maturation rate is directly associated with cell-specific energy demand, which may be based on increased energy consumption and metabolic switches from glycolysis to OXPHOS in differentiating cells (Van Blerkom, 2008). Mitochondria in mammalian oocytes and early stage embryos are generally undeveloped and minuscule in size (≤1m), circularly shaped and with tight cristae; contrasting with those, during mid-cleavage (8-16 cells) stage, mitochondrial morphology transitions from spherical to elliptical with noticeably increased cristae formation (Hayashi *et al.*, 2021; Sathananthan *et al.*, 2000). In accordance, human cleavage stage embryos have shown constant levels of ATP content from fertilization to the 4-cell stage, accompanied by a significant increase at the 8-16-cell stage. Following that, a noticeable decrease in ATP content was observed in compact morula and early blastocyst stages, coupled with a minor increase at the expanded late blastocyst stage (Gardner *et* Harvey, 2015). Intercellular uniformity between blastomere mitochondrial physiology and morphology ceases to exist specifically around the early blastocyst (E3.5) stage and up until implantation: as more than 80% of the preimplantation embryo ATP pool is generated in the TE, while ICM cells are maintained in a state of relative quiescence (Houghton, 2006). Indeed, in cattle, 10% - 40% of total energy storage is consumed by Na^+/K^+-ATPases located on the basolateral surfaces of the TE that are responsible for blastocyst cavity expansion (Hayashi *et al.,* 2021). The observed mitochondrial hyperpolarization of TE cells, contrasting with low membrane potential across ICM mitochondria, is often experimentally evaluated utilizing potentiometric chemical dyes (such as MitoTracker Red – a rosamine derivative chemical, containing chloromethyl moieties that can react with free sulfhydryls located across the inner mitochondrial membrane, tetramethylrhodamine methyl ester, Jc-1 or many other deltapsim or carbocyanine-sentitive reagents, which bind to the mitochondria inner membrane and allow measurements of a quantifiable degree of intensity of the membrane polarization potential; Buckman *et al.*, 2001; Lima *et al.*, 2021; Rovini *et al.*, 2021; Van Blerkom *et al.*, 2002). In addition to ATP content, MMP is an excellent indicator of cellular viability, directly reflecting the pumping of protons across the inner membrane during the process of electron transport and OXPHOS. It has been reported that MMP

changes throughout preimplantation development (Diaz *et al.*, 1999). As an example, Jc-1 staining of mouse zygotes, 2-, 4-, 8-cell, compact morula and blastocyst stage embryos indicated that MMP remained low in early (pre-8-cell) stages, but elevated during later stages (Acton *et al.* 2004). An explanation for the following observations can be sustained by the fact, that since there is no mitochondrial replication until blastocyst hatching, the initial population of mitochondria must be rationed and therefore the metabolic activity of fewer mitochondria per cell must increase to meet the rising demands of cellular activity (Pikó *et* Taylor, 1987). Consequently, in mouse embryos of the post-morula stage, TE cells possess more elongated mitochondria, compared to the ICM (Kumar *et al.*, 2018). The same situation can be observed in human and bovine embryos, as well as mesoderm differentiated human embryonic stem cells (Mohr *et* Trounson, 1982; Prowse *et al.*, 2012). The morphological maturation of mitochondria is believed to be mainly associated with the alternating metabolic consumption profile of the developing embryo (May-Panloup *et al.,* 2021.) From the zygote to morula, ATP production levels remain constant and the metabolic activity mainly revolves around OXPHOS related substrates. Prior to the blastocyst stage, pyruvate is the main energy source up until the 2-cell stage, further accompanied by glutamine and aspartate as the important ATP generating metabolites, prior to 8-cell stage, while the general rate of glucose intake, required for glycolysis, is comparatively low until the morula stage (reviewed in Absalón-Medina *et al.,* 2014; Gardner *et* Harvey, 2015). The key importance of pyruvate, not only as a nutrient source, has been demonstrated in ZGA promotion, as the absence of exogenously sourced pyruvate blocks cell-cycle functioning and further embryo development (Nagaraj *et al.*, 2017). At the morula stage there is an obvious metabolic shift in ATP production to glycolysis, while during the blastocyst stage, even greater cellular capacity to uptake glucose is apparent, as almost 50% of molecular glucose is converted into lactate via fermentative reactions, mainly in the ICM cells, suggesting TE-exclusive switch from glycolytic to the mitochondria-based OXPHOS ATP supply (Figure 9; Houghton, 2006). Indeed, on a molecular level, upregulated OXPHOS ATP production in TE mitochondria is associated with tissue-specific inactivity in Hippo signalling, specifically TEAD4-mediated transcription of TE-specific genes. Experiments on TEAD4-knockout mice demonstrate a crucial molecular mechanism of mitochondria metabolism regulation in the form of TEAD4-regulated POLRMT recruitment, which

enhances mtDNA-encoded genes transcription and is essential to proper TE development (Kumar *et al.*, 2018).

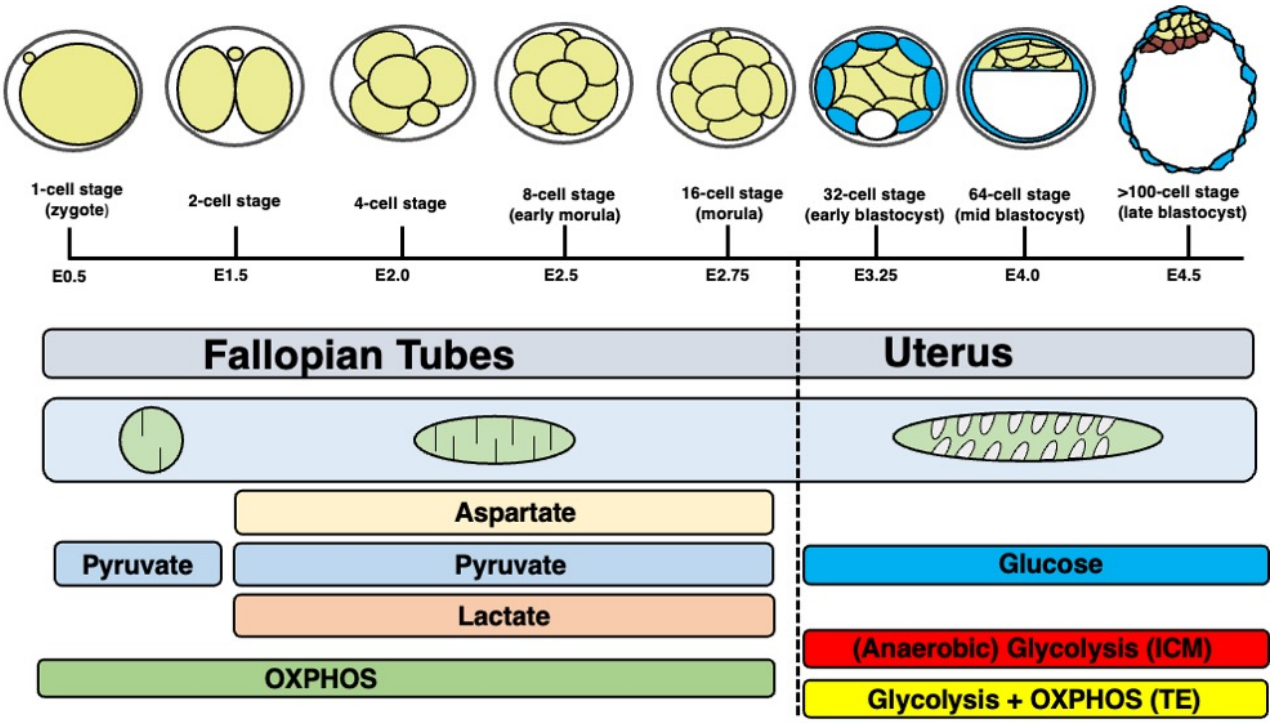

Figure 9. A schematic timeline of main energetic pathways and corresponding metabolic sources involved in embryonic development. The location of developing embryo is highlighted to demonstrate a change in maternal fluid content — consumption of sodium pyruvate and other carboxylic acids is relatively greater at the pre-compaction stages, coincident with the relatively more oxygenated environment of the oviduct. When embryo is delivered to the uterus, the oxygen tension decreases, while glucose metabolism is elevated to deal with higher energy demands. After fertilization, the zygote is dependent on tricarboxylic acids such as pyruvate, later lactate and aspartate as the primary energy sources. After compaction event, cells are metabolizing higher amounts of molecular glucose by actively utilizing glycolysis and pentose phosphate pathway (adapted from May-Panloup *et al.,* 2021).

1.3.3. Mitochondrial dysfunctions

Mitochondrial dysfunction is a hallmark of many human diseases, including cancer, neurodegenerative disorders, and metabolic diseases. Mitochondrial DNA has some unique mutagenic properties, compared to nuclear DNA. The mutation rate of mtDNA is statistically higher, which may be explained by its proximity to the respiratory chain and a leakage of ROS molecules - superoxide anions produced by incomplete transfer of electrons to oxygen, due to stress-inducing conditions (hypoxia, chemical disruption, neurological disorders *etc*.) (Deluao *et al.*, 2022). The rapid elevation of ROS levels can cause noticeable accumulation of point mutations, membrane potential depolarization and initiate mitophagy,

leading to mitochondria degradation. At least nine sites of ROS production have been discovered in mitochondria, capable of promoting intra-cellular oxidative stress, thus damaging already exposed mitochondrial DNA, that does not have protective histones (substituted by compact nucleoids) (Pikó *et* Taylor, 1987). In the human population, mitochondrial mutations are known to be highly prevalent (~1 in 200), leading to elevated incidence of diseases (~1 in 5000 births) (Schaefer *et al.*, 2008). Currently, more than 250 pathogenic mtDNA mutations have been classified, which effect respiratory chain subunits or mitochondrial protein synthesis (DiMauro *et* Schon, 2003). Mitochondrial disorders can be manifest at any age from late childhood to adulthood, owing to nuclear DNA mutations present in childhood. Multiple factors are responsible for both cellular (chromosome mis-segregation, spindle defects) and specifically mitochondrial dysfunction at the early stages of development; the most severe ones include exposure to endocrine disruptors and ROS - both environmental and as a byproduct of oxidative reactions in mitochondria, coupled with natural ageing processes (Hunt *et al.*, 2003; Perkins *et al.*, 2016). The effects of ageing on oocyte mitochondria have been assessed through several aspects, such as MMP activity, which most likely correlates with ATP production rate, although no link has been established between MMP and oocyte/embryo competence (Brand *et* Nicholls, 2010; Wu *et al.*, 2007). MII oocytes are especially susceptible towards destructive abnormalities of the ageing process, as older oocytes, under constant exposure to deleterious factors tend to possess fewer numbers of intracellular mitochondria, therefore generate less ATP (Simsek-Duran *et al.*, 2013).

1.3.4. MAPKs and mitophagy

Mitochondria are dynamic organelles that undergo constant fusion and fission events to maintain their shape and function. Disruptions to these events can lead to various mitochondrial disorders, including neurodegenerative diseases (*e.g.* Parkinson's disease), cancer (*e.g.* hepatocellular carcinoma), and metabolic disorders. Recent studies have shown that mitogen-activated protein kinase (MAPK) signalling pathways play a critical role in regulating mitochondrial fusion, fission and cellular apoptosis. Thus, dysregulation of these pathways has been linked to the development of such above described disorders (Ren *et al.*, 2020; Zhang *et al.*, 2017). The main three MAPK families - JNK, ERK1/2, and p38-MAPK participate in various cellular functions, including proliferation, apoptosis and differentiation. Among them, ERK1/2 is the most well-known MAPK with a confirmed

regulatory effect on mitochondrial dynamics. Oncogenic Ras treatment can activate ERK2, leading to the phosphorylation of DRP1, which results in an increase in mitochondrial fragmentation (Cook *et al.*, 2017). ERK2 suppresses mitochondrial fusion by phosphorylating MFN1, facilitating cytochrome c release and subsequent mitochondria apoptosis. ERK1/2 activation also participates in mitochondrial fission mediation during the early stage of induced pluripotent stem cell reprogramming by phosphorylating DRP1 (Prieto *et al.*, 2016). Besides ERK1/2 pathway, it has been shown that activation of p38-MAPK in cell cultures leads to increased mitochondrial DRP1-dependent fission, while inhibition of p38-MAPK with SB203580 promotes mitochondrial fusion and reduced fragmentation (Song *et al.*, 2021). The dynamics of this pathway have been implicated in a variety of diseases, including Parkinson's disease, Alzheimer's disease, and cancer (Gui *et al.*, 2020). More detailed description on the role of ERK1/2 and p38-MAPK, as well as other important signalling cascades in DRP1-mediated fission are highlighted in Figure 10.

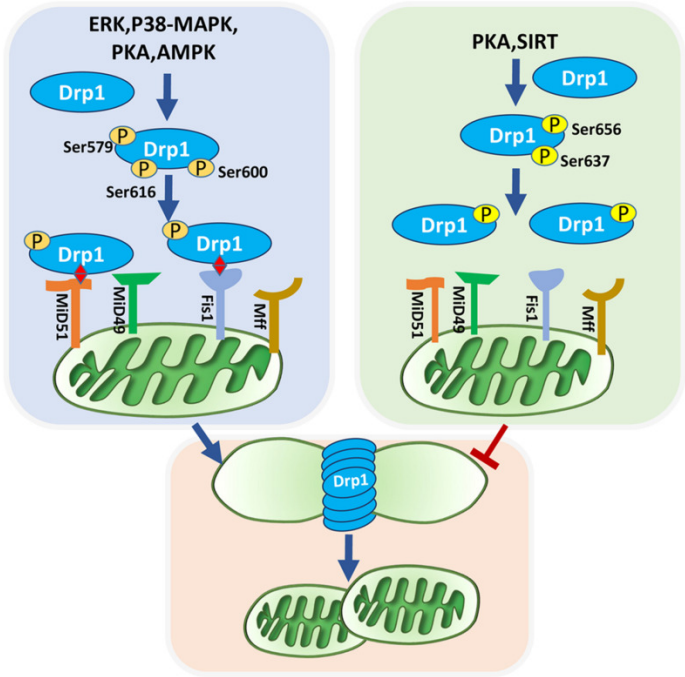

Figure 10. Schematic representation of DPR1-mediated mitochondrial fission. Mitochondrial fission involves DRP1 recruitment and anchoring on the outer mitochondrial membrane. The localization of DRP1 can be influenced by post-translational modifications, particularly phosphorylation by various enzymes, including ERK, p38-MAPK, PKA, AMPK. MAPK-, PKA- and AMPK-dependent DRP1 phosphorylation at Ser637 and Ser656 can inhibit mitochondrial fission, while phosphorylation at Ser616, Ser579, and Ser600 can promote it. To anchor DRP1 to the outer mitochondrial membrane, it binds with four receptors: FIS1, MFF, MID49, and MID51. Active DRP1 oligomers form ring-like structures that constrict to divide the mother mitochondria into daughter mitochondria (taken from Ren *et al.*, 2020).

2. Aims

The general aim of this thesis is to research mitochondrial morphology and physiology during mouse early development *in vitro*, including mitochondrial activity in the context of p38-MAPK function and its influence towards preimplantation mouse blastocyst cell lineage acquisition. The aims were divided into the following parts:

1. Provide experimental data of mitochondria morphological and physiological (membrane potential) characteristics in developing tissues of late mouse blastocyst stage preimplantation embryos.
2. Investigate the potential regulatory involvement of p38-MAPK function in mitochondria development, differentiation and lineage-specific segregation.

3. Materials and Methods

3.1. Embryo culture, selective inhibition of p38-MAPK, MitoTracker Red (CMXRos) staining, embryo fixation and immuno-fluorescence

Mouse embryos were collected from F1 hybrid (C57Bl6 × CBA/W) females, that were treated with 7.5 IU of PMSG (Folligon, MSD Animal Health, Boxmeer, Netherlands) via intra-peritoneal injections, followed by 7.5 IU of hCG (Sigma-Aldrich, USA; Cat. No. CG10) after 48 hours and then mated overnight with F1 males. 2-cell stage (E1.5) embryos were collected from oviducts of previously euthanised female mice (using cervical dislocation technique) for *in vitro* culturing. Obtained embryos were then transferred to culturing plates containing M2 medium (prewarmed at 37°C for a period of 3-4 hours) and covered in light mineral oil (Irvine Scientific, USA; Cat. No. 9305) and thereafter cultured in batches of 15 embryos in 10μL drops of KSOM media with addition of non-essential amino acids (Sigma-Aldrich USA; EmbryoMax KSOM Mouse Embryo Media; Cat. No. MR-020P-5F, combined MEM Non-Essential Amino Acids Solution Thermo Fisher Scientific, Scotland; Cat. No. 11140035, diluted to working concentrations of 0.5x — prewarmed and equilibrated in 5% CO_2 and 37^{o}C) — as described in Mihajlović *et al.* 2015.

p38-MAPK selective inhibitor, SB220025 (Calbiochem, Millipore, Germany; Cat. No. 559396) was dissolved in dimethyl sulfoxide (DMSO; Sigma-Aldrich, USA; Cat. No. D4540) and added to KSOM+AA solution at 20μM working concentration - E3.5 stage embryos were transferred to a plate, containing KSOM+AA with SB220025 and washed through approximately 6-8 drops of medium containing the inhibitor. The control group was cultured in KSOM+AA and added DMSO of an equal volume to the p38-MAPK inhibited (p38-MAPKi) group. MitoTracker Red (CMXRos) (Invitrogen, USA; Cat. No. M7512), a mitochondria membrane potential-binding red-fluorescent dye was diluted in KSOM + AA at 500nM concentration, the embryos were transferred to medium containing MitoTracker Red (MTR), washed through 3-5 drops and cultivated for 20 minutes following manufacturer-suggested protocol. After reaching E4.5 stage, embryos were washed in Tyrode's solution (Sigma-Aldrich, USA; Cat. No. T1788) to remove the *zona pellucida*, and fixed for 20 minutes in 4% paraformaldehyde (Santa Cruz Biotechnology, USA; Cat. No. sc-281692) in a 96-well plate at 37^{o}C. Following that, fixed embryos were washed in a

0.15% solution of Tween-20 (Sigma-Aldrich, USA; Cat. No. P9416) in phosphate buffered saline (PBS; Sigma-Aldrich, USA; Cat. No. BSS-1005- B; PBST) and incubated for 20 minutes at room temperature (RT). Afterwards, fixed embryos were permeabilised in 0.5% Triton-X100 (Sigma-Aldrich, USA; Cat. No. T8787) diluted in PBS for 20 minutes at RT. Next, embryos were transferred to a drop of 3% bovine serum albumin (BSA; Sigma-Aldrich, USA; Cat. No. A7906) in PBST for 30 minutes at 4^{o}C, in order to block nonspecific epitopes, followed by an overnight incubation in primary antibodies reconstituted in BSA with 1:200 concentration (all utilized primary and secondary antibodies are listed in supplementary materials, Supplementary figure 7). The next steps in embryo staining protocol includes three embryos washes through PBST at RT, 30 minute incubation in BSA at 4^{o}C and 1 hour incubation in secondary antibodies (1:500 concentration) at 4^{o}C. Finally, embryos are transferred to a drop of DNA-binding DAPI-containing Vectashield (Vector Laboratories, USA; Cat. No. H-1200) for nuclear counterstaining and, thus, were ready for confocal imaging.

3.2. Confocal microscopy imaging

Fixed embryos, used for mitochondrial membrane potential analysis of developing lineages, were stained with MTR, antibodies against lineage protein markers (NANOG for EPI, GATA4 for PrE, CDX2 for TE and a GATA6/NANOG combination for identifying double-positive unspecified ICM cells) and F-actin-binding Phalloidin 488/647 - used for cell-boundary identification, were imaged in a glass-bottomed dish using inverted laser-scanning confocal microscope (Olympus FLUOVIEW FV10i), employing laser excitation and emission wavelength settings corresponding to DAPI, MitoTracker Red and secondary fluorescently-conjugated antibody wavelength of corresponding analyzed proteins, accordingly. Each embryo was scanned in a complete series of z-sections through the whole embryo (with a step-size of 1μm). Image settings were kept unified for all scanned embryos across all imaging sessions.

Higher quality image acquisition of embryos used for colocalization analysis of active mitochondria, as well as digitalized reconstruction of mitochondria networks was employed using an Olympus FV3000 confocal laser-scanning microscope utilizing either 60x oil-immersion lens (step-size 0.5 μm) for images of embryo mitochondria reconstruction, or 100x oil-immersion lens (step-size 1 μm) for simultaneous scanning, utilized for intensity-

based colocalization analysis of highly-polarized mitochondria (represented by elevated MTR signal) and a general pool of embryonic mitochondria (showed by antibody staining against apoptosis-inducing factor, AIF, a flavoprotein residing in the mitochondrial intermembrane space).

3.3. Mitochondrial membrane potential activity in mouse preimplantation embryonic cells.

Mitochondrial membrane potential (represented by MTR fluorescence) was quantified using Fiji (ImageJ), by measuring average pixel intensities from single plane images of individual cells, the area, integrated density and mean gray value, focusing on the plane with maximum MTR intensity. Average MTR measurements were corrected for background. The Corrected Total Cell Fluorescence (CTCF) was selected as the quantification unit of the mean fluorescence intensity. *CTCF* = Integrated Density – (Area of selected cell x Mean fluorescence of background), as described in Bora *et al.* (Bora *et al.*, 2021; Schindelin *et al.*, 2012). The fluorescence intensity of each cell was calculated using Excel (Microsoft).

3.4. Colocalization analysis of active mitochondria in embryos

To locate actively respiring cells in mouse embryos, colocalization analysis between apoptosis-inducing factor (AIF) and MTR staining confocal micrographs, was performed using EzColocalization, an open source Fiji plugin (Stauffer *et al.,* 2018). Colocalization probability was measured using the Pearson's correlation coefficient. For analysis, cell boundaries of selected blastomeres were manually segmented by hand tracing with the polygon selection tool, then converted into binary masks subsequently used in the EzColocalization plugin to restrict colocalization analysis to selected cells.

The software result output is presented by Heat maps and Scatterplots. Heat maps are coloured images that depict the strength of reporter signals in a relative manner, that is generated by normalizing and rescaling the data. Heat maps can be used to identify areas where the reporter signals have the highest intensity in cells, and can also reveal if different cells within an image have substantially different intensities, which may indicate heterogeneity or unevenness in labelling.

Scatterplots show the relationship between signal intensity for two reporter channels (MTR and AIF antibody staining) for individual cells and images.

3.5. Mitochondria morphology analysis and 3D reconstruction

In order to proceed with qualitative and quantitative analysis ("morphofunctional" descriptive analysis) of mitochondrial network structure in preimplantation embryo cells, a number of post-confocal micrograph image acquisition manipulations were performed using a Fiji pipeline developed by Chaudhry *et al.* (Chaudhry *et al.* 2019). Obtained z-section projections were deconvoluted using DeconvolutionLab2 plugin for ImageJ/Fiji, in order to eliminate image-altering distortions (artificial noise and improper focus) caused by point-spread function.

Maximum projections from z-stacks were pre-processed by subtracting background (a rolling ball pixel value was determined for each biological replicate individually based on empirical judgement, in order to remove background fluorescence pixels), followed by subsequent processing steps: Sigma filter plus correction, Enhance local contrast (CLAHE, applied value of 1.8), Gamma adjustment (0.9), Despeckle, Remove outliers, Fill 3D holes, Local Thresholding using the Weighed Mean method. Thresholded images were then binarized and visualized using the analyze particles tool. Obtained binary threshold images were subjected to skeletonization (Skeletonize 2D/3D), skeleton analysis (analyze skeleton, to receive numerical amount and of branches, their length, and number of branch junctions), as well as 3D visual analysis in Mitochondria Analyzer plugin. Cell boundaries were determined using the F-actin staining (Phalloidin-488 or Phalloidin-647). 3D reconstruction of mitochondrial branch networks was performed using Volume Viewer plugin in Fiji, images were visually optimized by utilizing in-built functions. Image analysis was performed on four embryos per condition, an experiment consisted of a pair of embryos (inhibited/control), a total number of biological replicates was set to 4. A small sample size is limited by the extremely long duration of confocal microscope scanning time (7-8 hours per embryo), necessary to obtain quality and accurate representation of mitochondria networks. A brief description of the mathematical descriptors utilized to quantify mitochondrial morphology is listed in Figure 11.

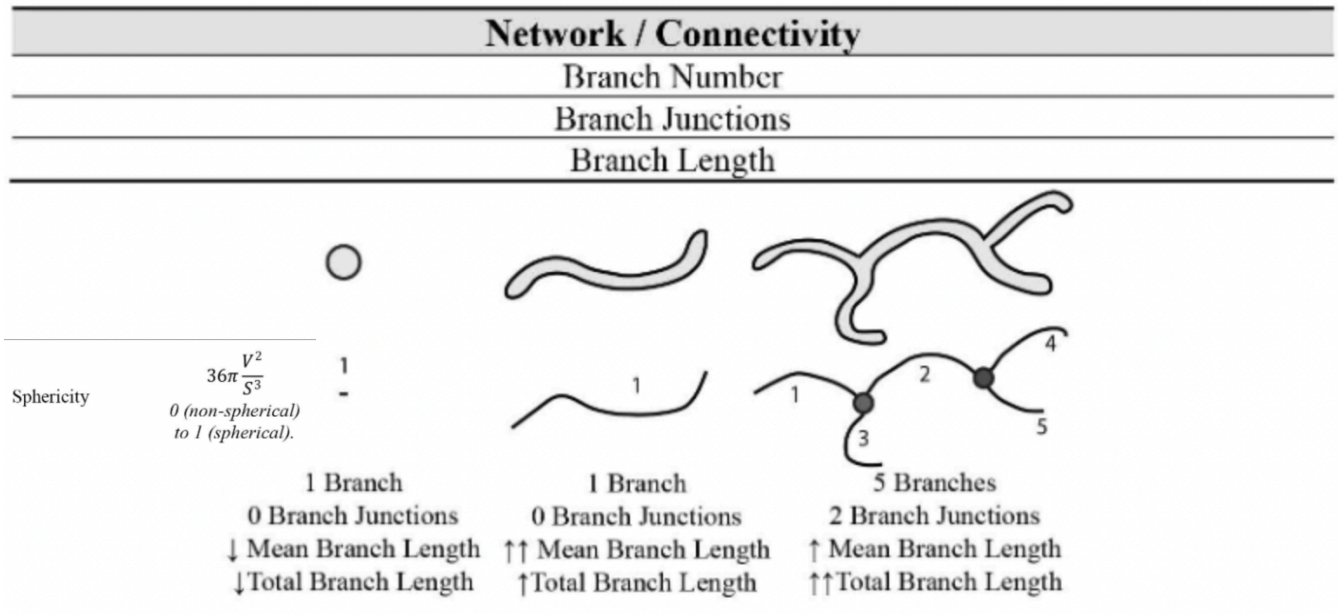

Figure 11. Summary of the parameters used to describe mitochondrial network connectivity and an illustration of skeletonization analysis, including a mathematical definition of the object sphericity. Skeletonized analysis produces objects, representing a mitochondrial network, from confocal images, of the late mouse blastocysts. Output objects include a punctate object with no branch junctions and minimal branch length; a long single tubular object with no branch junctions but higher branch length; and a complex object with multiple branches and junctions (gray dots), and the highest total branch length.

3.6. Quantitative real-time PCR (RT-qPCR)

Approximately 25 E4.5 stage embryos from either p38-MAPK inhibited or control conditions were collected and processed for RNA extraction and isolation using an ARCTURUS PicoPure RNA Isolation Kit (Thermo Fisher Scientific; Cat. No. KIT0204); following the manufacturer's protocol. The entire eluted volume of total RNA was immediately DNase treated with TURBO DNase (Thermo Fisher Scientific; Cat. No. AM2238) with respect to the manufacturer's protocol. Acquired samples were then subjected to cDNA synthesis using SuperScript III Reverse Transcriptase (Thermo Fisher Scientific; Cat. No. 18080044) according to the manufacturer's protocol with oligo d(T)16 primers (Thermo Fisher Scientific; Cat. No. N8080128) dNTP Mix (Thermo Fisher Scientific; Cat. No. R0192) and RNase inhibition (Thermo Fisher Scientific; Cat. No. N8080119). Synthesised cDNA was diluted with nuclease free water (1:2) and used as template (0.3 µl per reaction) in 10µl SYBR Green-based RT-qPCR reactions, using C1000 Touch Thermal Cycler (Bio-Rad) and the PCR cycling conditions detailed in Figure 12. Initial analysis was performed with the accompanying Bio-Rad CFX Manager software. Triplicate measurements were obtained for each gene (oligonucleotide primer pair sequences are

provided in the supplementary data, Supplementary figure 6) from two technical replicates per biological replicate, two biological replicates per transcript. Resulting gene transcript specific units were internally normalized against *H2afz* (H2A histone family member z mRNA cDNA expression). The internally normalised expression fold changes (plus S.D.) were derived using the ΔΔCt method (Livak *et* Schmittgen, 2001).

RT-qPCR program	Temperature	Time
Denaturation	95°C	15m
Denaturation	94°C	25s
Annealing	57°C	25s
Elongation	77°	30s
PLATE READ	/	/
Melting curves	57°C - 94°C	/

39x

Figure 12. Thermal cycler program used for RT-qPCR.

3.7. Data analysis

Statistical analyses of quantitative MMP fluorescence measuring, colocalization assay , mitochondrial morhology reconstruction and RT-qPCR were performed with Prism 9 (GraphPad). Error bars on graphs represent standard error of the mean (SEM) for all the experiments besides RT-qPCR analysis, where error bars represent standard deviation (S.D.). To assess the normality of data in each set of pharmacologically treated and immuno-fluorescently stained embryos, a Shapiro-Wilk test was initially conducted. If the data distribution was found to be non-normal ($p < 0.05$) in at least one of the datasets being compared, a Mann-Whitney U test was used to analyze the datasets. In cases where the data distribution was normal ($p > 0.05$), F-tests were used to measure the variance of the two datasets. Based on the outcome of the F-test, the datasets were then compared by t-test that specified equal or unequal variance in the parameters. In graphs, * represents a p value of < 0.05, ** represents a p value of < 0.01, *** represents a p value of < 0.001, **** represents a p value of < 0.0001.

4. Results

4.1. Mitochondrial membrane polarization in E4.5 preimplantation stage mouse embryos varies between different lineages

A number articles discussed above, detail the emerging divergence in mitochondrial morphology between developing blastocyst cell lineage progenitors and, as a consequence, varied physiological outputs, on a per-cell basis, that have/been confirmed utilizing multiple approaches: electron/fluorescent microscopy (Rojansky *et al.*, 2016; Kumar *et al.*, 2018), chemical or biological inhibition of selective protein complexes (Mitchell *et al.*, 2009), mtDNA content analysis (Diez-Juan *et al.*, 2015) *etc*. The initial results (below) are intended to illustrate and complement this already existing data from the perspective of assaying mitochondria activity based on mitochondria membrane polarization properties of intracellular networks in (the emerging) mouse blastocyst lineages. MitoTracker Red (MTR), a chloromethyl-X-rosamin-based, thiol-reactive moiety dye, was selected to assay and compare mitochondria manifesting elevated membrane potential due to its many advantages over other conventional dyes (such as Jc-1, tetramethylrosamine and rhodamine 123); including its ability to maintain a mitochondrial-specific localization coupled with excellent tolerance to aldehyde-based fixation and permeabilization treatment with Triton X-100, followed by particular suitability for multi-colour fluorescent experiments due to appropriate spectral distance of red fluorescence from the green fluorescence of other probes. Moreover, MTR has been reported to outperform alternatives, as shown in additional data in flow cytometry experiments (Buckman *et al.*, 2001; Marcondes *et al.*, 2018); *e.g.* MitoTracker dyes are able to detect alterations in the internal mitochondrial membrane that gradually lose their crista ridges.

To obtain and analyse E4.5 stage embryo scans with chemically stained mitochondria membrane potential characteristics, 2-cell (E1.5) stage mouse embryos were cultured until the 32-cell stage (E3.5) and then transferred to KSOM+AA plates containing DMSO until E4.5 stage (Figure 13). Following the protocol described in Materials and Methods, embryos were transferred and incubated for 20 minutes in KSOM+AA medium containing MTR, washed in Tyrode's solution to remove *zona pellucida* and fixed in 4% paraformaldehyde. Following that, embryos were washed through PBST, permeabilized in Triton-X100, washed

again in PBST and transferred to BSA. Next, embryos were stained with primary antibodies overnight, then washed through PBST and stained with secondary antibodies. Finally, they were mounted in DAPI-Vectashield mounting medium. The prepared embryos were classified into the following groups: EPI (NANOG+), PrE (GATA4+), TE (either CDX2+ or empirically selected based on their observable outside location) and uncommitted ICM (GATA6-NANOG double positives). All experiments are noted in the supplementary materials (Supplementary figures 1, 2, 3, 4). Analysing the generated images and data results, an evident divergence in mitochondria membrane potential (MMP, the electrochemical gradient that exists across the inner mitochondrial membrane generated by the proton-pumping action of the ETC, reflecting the process of electron transport and ATP production rate via OXPHOS) can be derived (Figure 13). As anticipated, the MMP intensity in TE progenitors was much more elevated (5268 ± 238.9 a.u.) compared to EPI (1626 ± 137.8 a.u.), PrE (1160 ± 103.7 a.u.) and uncommitted lineages (1587 ± 238.9 a.u.). Kruskal-Wallis ANOVA statistic tests showed significant differences between the derived values ($p < 0.0001$), while multiple comparison analyses confirmed statistical significance between TE cells and EPI, PrE and uncommitted lineages, respectively ($p < 0.0001$ in each comparison). Contrastingly, no statistical significance was observed between multiple comparison tests of ICM-exclusive cells (EPI vs. PrE $p > 0.9999$; EPI vs. Uncommitted $p > 0.9999$, PrE vs Uncommitted $p = 0.988$). These MTR related results concur with previously observed data from published articles (Kumar *et al.*, 2018; Van Blerkom, 2011), under the assumption of a correspondence between MMP activity and the morphological mitochondrial state, in turn reflects OXPHOS activity and ATP production (discussed in Diaz *et al.*, 1999; Rovini *et al.*, 2021; Zorova *et al.*, 2018). Additionally, these data provide the reference base for succeeding experiments involving a potential role for p38-MAPK-related mitochondrial regulation and development of the preimplantation stage mouse embryos. Hence, the initial data indicate a consistent increased mitochondrial energetic output of the outer (TE) lineage in comparison to those of the ICM (Figure 14).

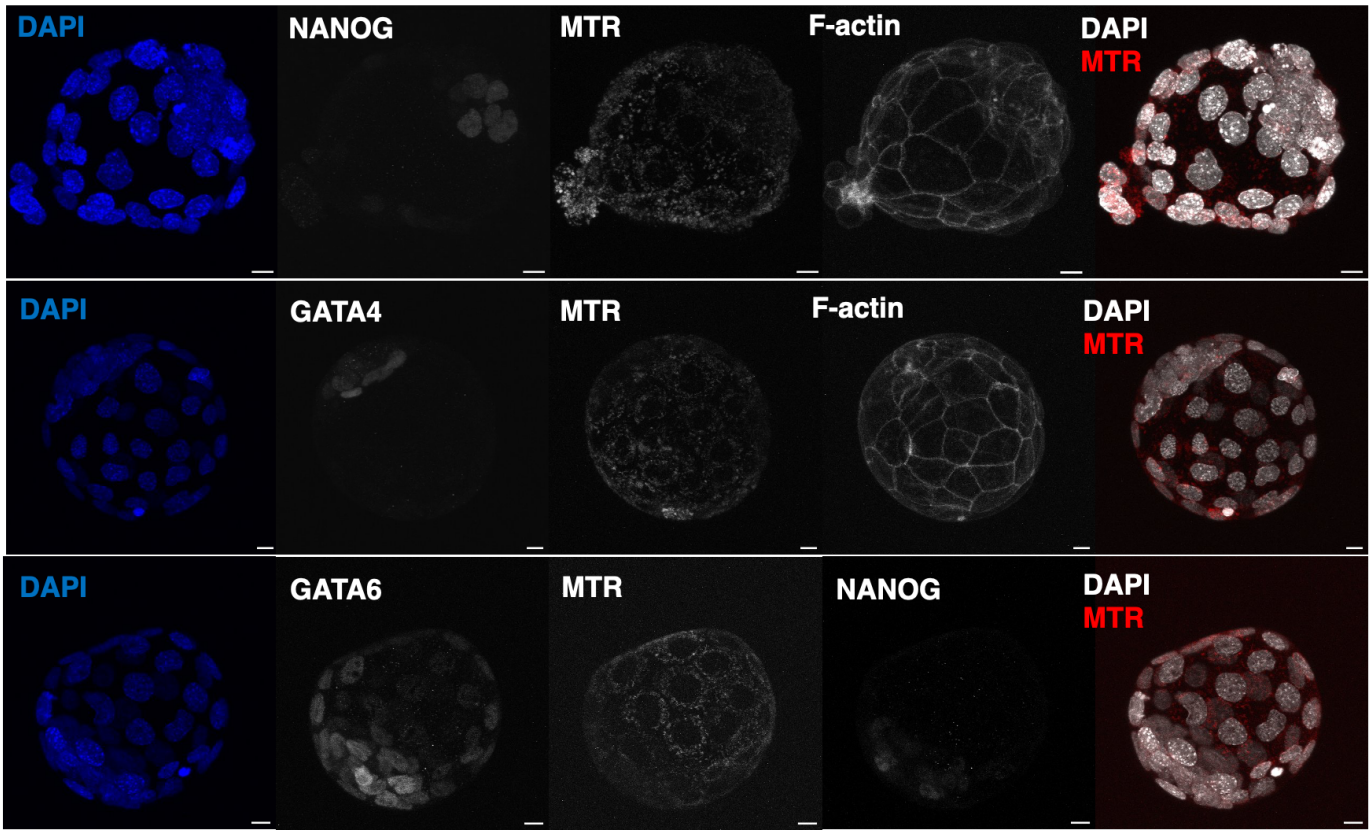

Figure 13. Confocal micrograph z-section projections of an exemplar late (E4.5) stage blastocysts incubated with MTR. Individual DAPI (blue pan-nuclear stain; total number of cells), NANOG (grayscale; EPI cells) and GATA4 (grayscale; PrE cells and GATA6 and NANOG (grayscale; uncommitted cells) and F-actin (cellular membrane boundaries, grayscale) channel micrographs, plus a merged DAPI (blue, grayscale in merged images), MitoTracker Red (grayscale, red in merged images) image are shown (scale bar = 10μm).

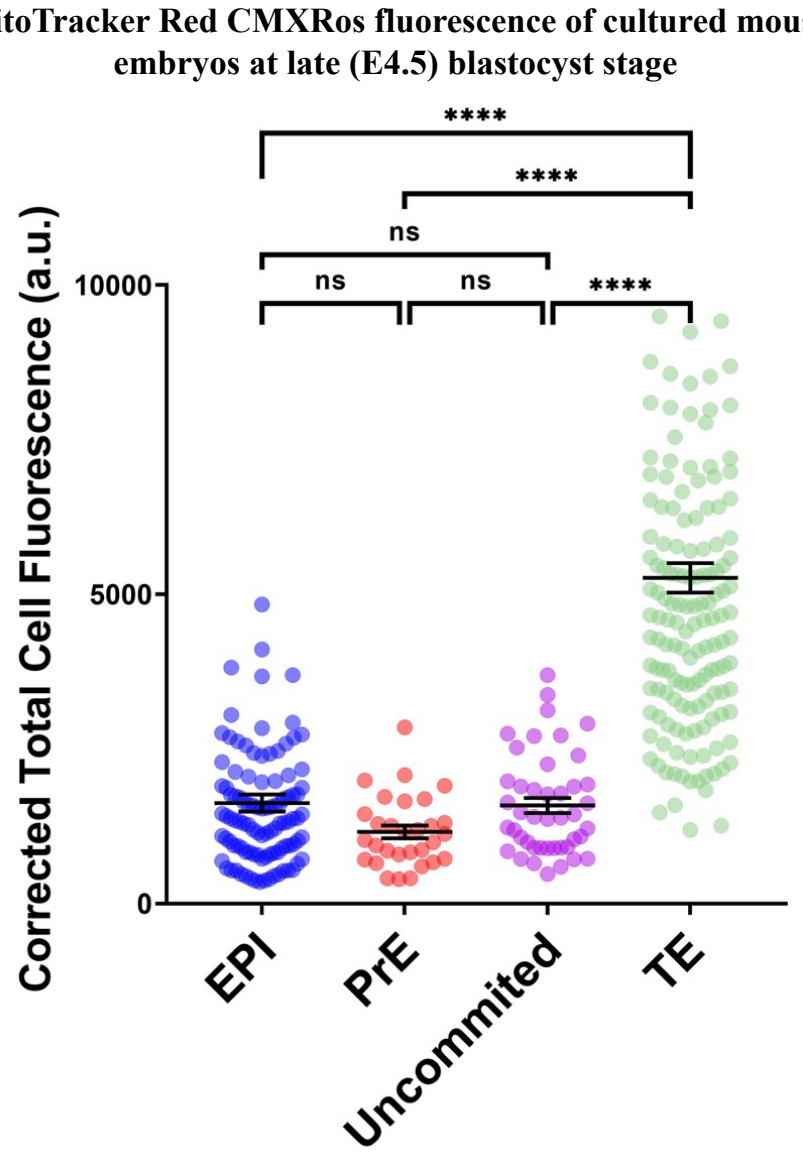

Figure 14. A scatterplot showing multi-lineage comparison Corrected Total Cell Fluorescence of MTR staining (representing mitochondria membrane potential) in E4.5-stage mouse embryos.

4.2. p38-MAPK influences mitochondria membrane potential accumulation in both TE and ICM

The subsequent experiments were performed in order to investigate the role of p38-MAPK in the context of mitochondria activity/MMP. Referencing a number of publications (Thamodaran *et al.* 2019; Bora *et al.*, 2019; Bora *et al.*, 2021) an essential function of p38-MAPK was established, as chemical inhibition between E3.5 and E3.5 +7 hour results in impaired (severity of impairment positively correlates with length of inhibitor exposure time) derivation of GATA4 expressing PrE cells, coupled with reduced blastocyst cavity size and volume by the implantation (E4.5) stage. Moreover, the key motivation for conducting the following experiments come from transcriptomic analysis of developing blastocysts

under p38-MAPKi conditions, as mitochondrial respiration-related transcripts comprised a significant proportion of differentially expressed units, the majority of units were upregulated during E3.5 +4h and E3.5 +7h, but reverted back to initial levels at E3.5 +10h stage. (the latter point being outside the determined p38-MAPK inhibition/p38-MAPKi sensitive window; Bora *et al.*, 2021).

The following experiments were conducted in a similar fashion to the initial one described above, although in these experiments the embryos were separated into p38-MAPKi and control (+DMSO) groups. A typical PrE-deficient phenotype associated with p38-MAPKi embryos was confirmed via counting GATA4-positive cells in inhibited embryos (detailed in supplementary materials) and was in agreement with already published results from our lab (Bora *et al.*, 2019; Bora *et al.*, 2021; Thamodaran *et* Bruce, 2016). According to the protocol, E3.5 stage blastocysts were transferred into culture plate media drops containing p38-MAPK inhibitor (SB220025) until they developed to E4.5 stage, while the control embryos were moved into drops containing DMSO as a vehicle control. After that, both groups were transferred to a plate containing MTR in the incubator for 20 minutes, embryos were then washed in Tyrode's solution to remove *zona pellucida* and fixed in paraformaldehyde. Afterward, embryos were prepared for IF, following the previously described protocol. The goal was set to obtain confocal scans and compare MTR staining as a correlate of MMP in all lineages of p38-MAPKi, as well as control embryos. Figure 15 highlights the protocol procedure for obtaining MTR/IF stained embryos for confocal microscopy.

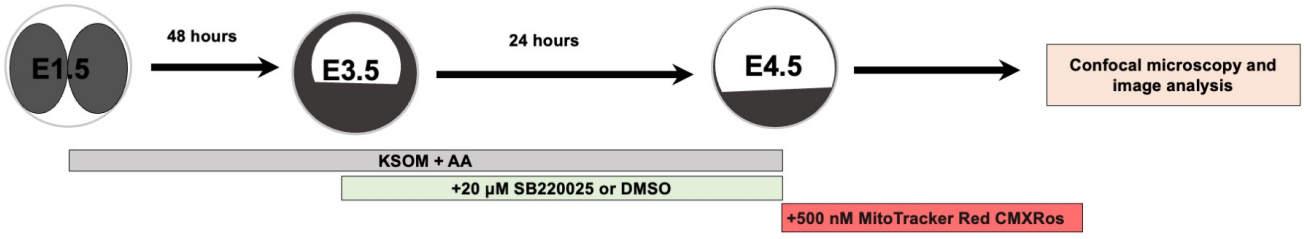

Figure 15. Scheme illustrating experimental protocol for obtaining E4.5 stage mouse blastocysts (either treated with p38-MAPK inhibitor SB220025 or control DMSO) treated with MitoTracker Red for 20 minutes. Embryos are further immune-fluorescently (IF) stained with antibodies against selected lineage marker proteins and F-actin

Analyzing the generated confocal microscopy image and derived quantitative data results within the p38-MAPKi treated embryos, a similar MMP intensity pattern to that, observed in

control blastocysts (Figure 14) was observed (Figure 16). The Kruskal-Wallis ANOVA statistic test revealed significant differences between the observed values ($p < 0.0001$). The MMP intensity in TE progenitors was shown to be much higher (4391 ± 251.2 a.u.) than in EPI (1705 ± 76.1 ± a.u.; $p < 0.0001$), and the uncommitted lineage (1806 ± 123.1 a.u. $p < 0.0001$), but surprisingly, there was no significant statistical difference between TE and PrE cells (2798 ± 307.4 a.u.; $p = 0.07$). Elevated MMP values observed in the PrE lineage caused statistical significance between the PrE and EPI, but not the PrE and uncommitted cell population (EPI vs. PrE $p = 0.0076$; EPI vs. Uncommitted $p > 0.9999$, PrE vs Uncommitted $p = 0.132$). Although, it is important to note that due to p38-MAPKi the overall number of GATA4+ PrE cells was significantly reduced (Supplementary figure 3).

MitoTracker Red CMXRos fluorescence of cultured mouse embryos under p38-MAPK inhibition at late (E4.5) blastocyst stage

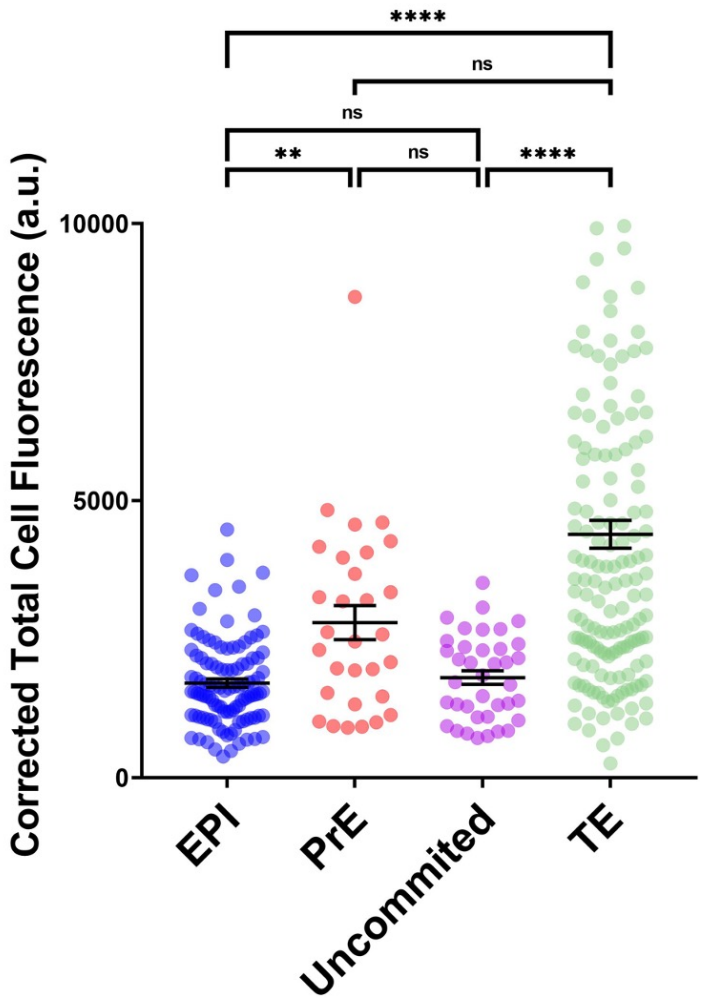

Figure 16. A scatterplot showing per cell multi-lineage comparison Corrected Total Cell Fluorescence (CTCF) of MTR staining representing mitochondria membrane potential (MMP) in p38-MAPK inhibited (E3.5 - E4.5) E4.5-stage mouse embryos. Note fewer GATA4+ PrE cells of p38-MAPKi blastocysts but with statistically higher MTR/MMP values (versus EPI).

Furthermore, statistical comparison of MMP intensity values in the TE lineage of both the p38-MAPKi and DMSO control groups was performed (Figure 17). The results indicate a higher MMP intensity in the control group of TE cells (5268 ± 238.9 a.u.) versus the p38-MAPKi group (4391 ± 251.2 a.u.; $p = 0.0003$). To gain further insight, the TE lineage was divided into two subgroups: the mural TE cells (located opposite and farthest from the ICM) and the polar TE cells (overlaying the ICM). Interestingly, no significant difference was observed between the polar (4892 ± 370.4 a.u.) and mural (5275 ± 294.5 a.u.) TE subgroups of control embryos ($p = 0.09$), but the p38-MAPKi condition showed a noticeable reduction in the values of polar TE cells (2093 ± 139.8 a.u.) compared to mural TE cells (5019 ± 314.2 a.u.; $p < 0.0001$).

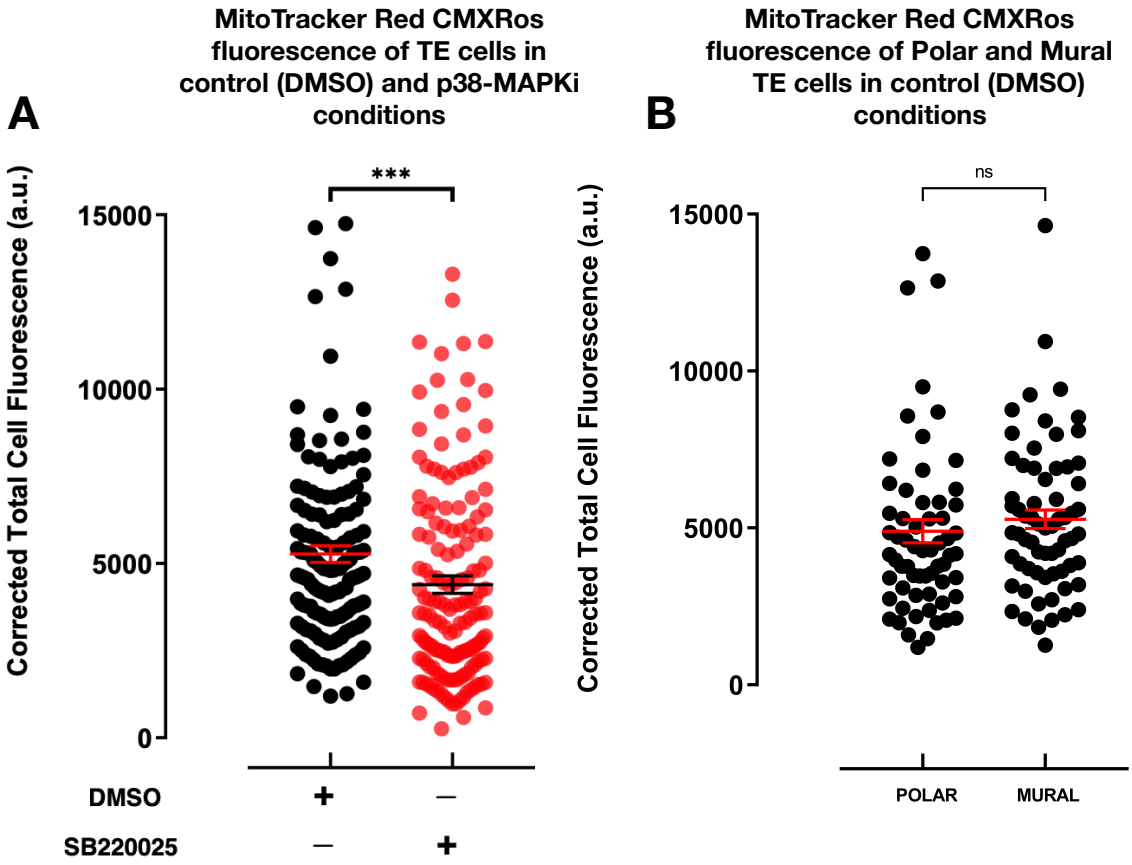

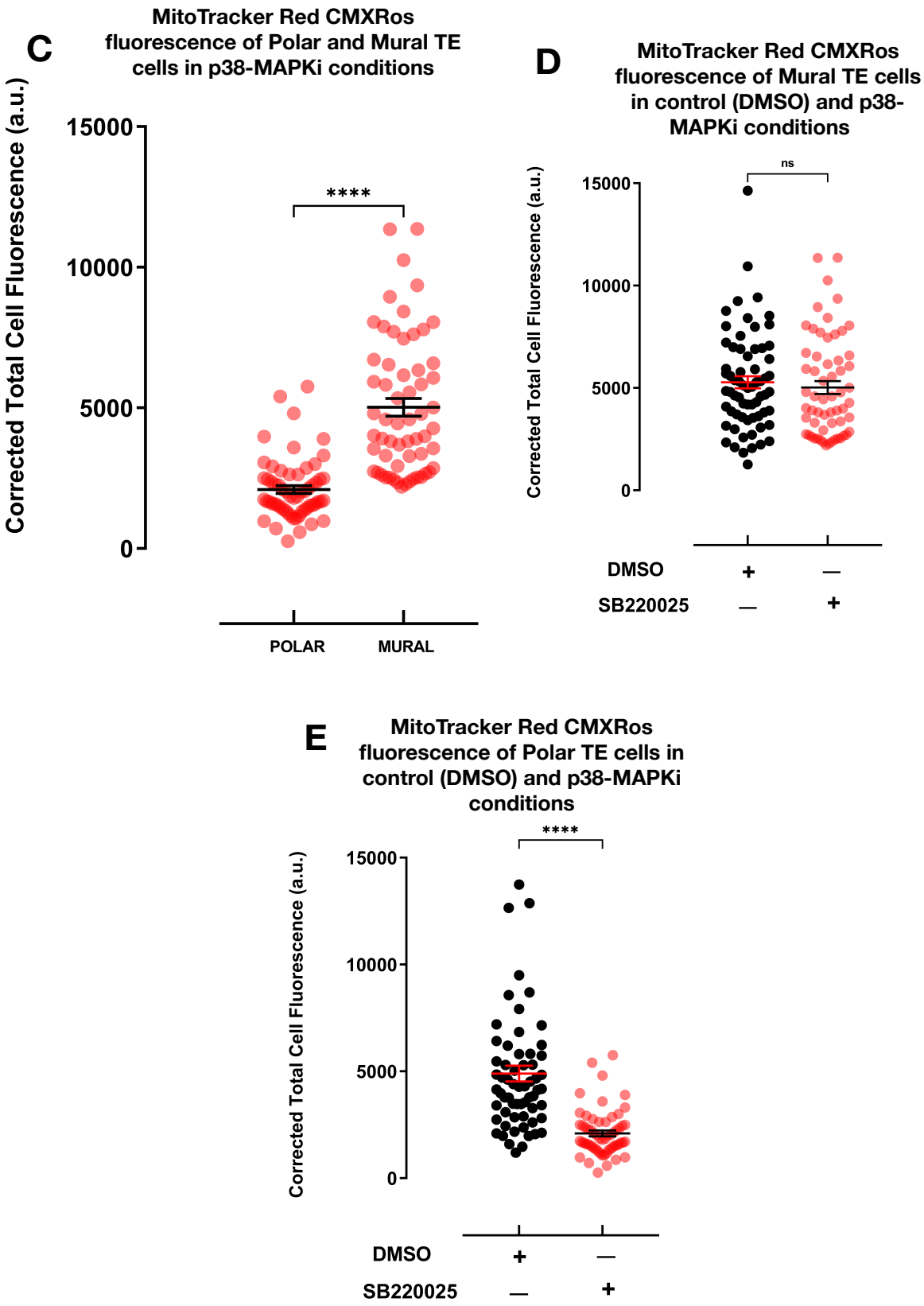

Figure 17. Scatter plots quantifying per cell (CTCF) levels of MTR (representing mitochondria membrane potential) in control (DMSO) and p38-MAPKi (SB220025) of E4.5 stage outer (TE) cells (A), further subdivided into polar and mural TE sub-lineages. Panels B and C detail statistical comparison of the polar and mural sub-lineages of TE in control (DMSO; B) and p38-MAPKi (C) conditions. Panels represent comparison of the mural (D) and polar (E) sub-lineages between inhibitor conditions.

The obtained data from TE-related experiments is an important discussion point regarding p38-MAPK influence on trophectoderm as the relationship between TE cell mitochondrial polarization via p38-MAPK regulation has not been presented and reported and these results may open opportunities for the study of novel regulatory mechanisms in mouse preimplantation embryo development, in the TE specifically.

Total ICM MMP intensity values were analysed next: conversely (in regard to the TE), the values of p38-MAPKi inhibited embryos (1914 ± 80.6 a.u.) were significantly higher compared to the control group (1538 ±88.5 a.u.; $p < 0.0001$; Figure 18).

To analyse in depth the ICM MMP values, summarily treated groups were immune-fluorescently stained for marker proteins for each lineage (NANOG, GATA4, GATA6; Figure 19). The EPI lineage comparison resulted in a slight, but statistically significant difference of intensity values between studied conditions, with inhibited embryos showing higher MMP activity (1626 ± 137.8 a.u. , in control groups vs 1705 76.1 ± a.u.; $p = 0.0477$). The PrE comparison demonstrated the biggest divergence in MMP intensity between the studied groups (1160 ±103.7 a.u. in control group vs 2798± 307.4 a.u. in inhibited; $p < 0.0001$), although, in p38-MAPKi condition there were far less GATA4+ PrE cells per embryo (Supplementary figure 3). While there was no significant differences observed between the uncommitted lineage in both conditions (1587 ±123.1 a.u. in control vs 1806± 123.1 a.u. in SB220025 treated; $p = 0.174$). Exemplar obtained and analysed confocal z-section projection micrographs, of these data sets, are shown in Figure 19.

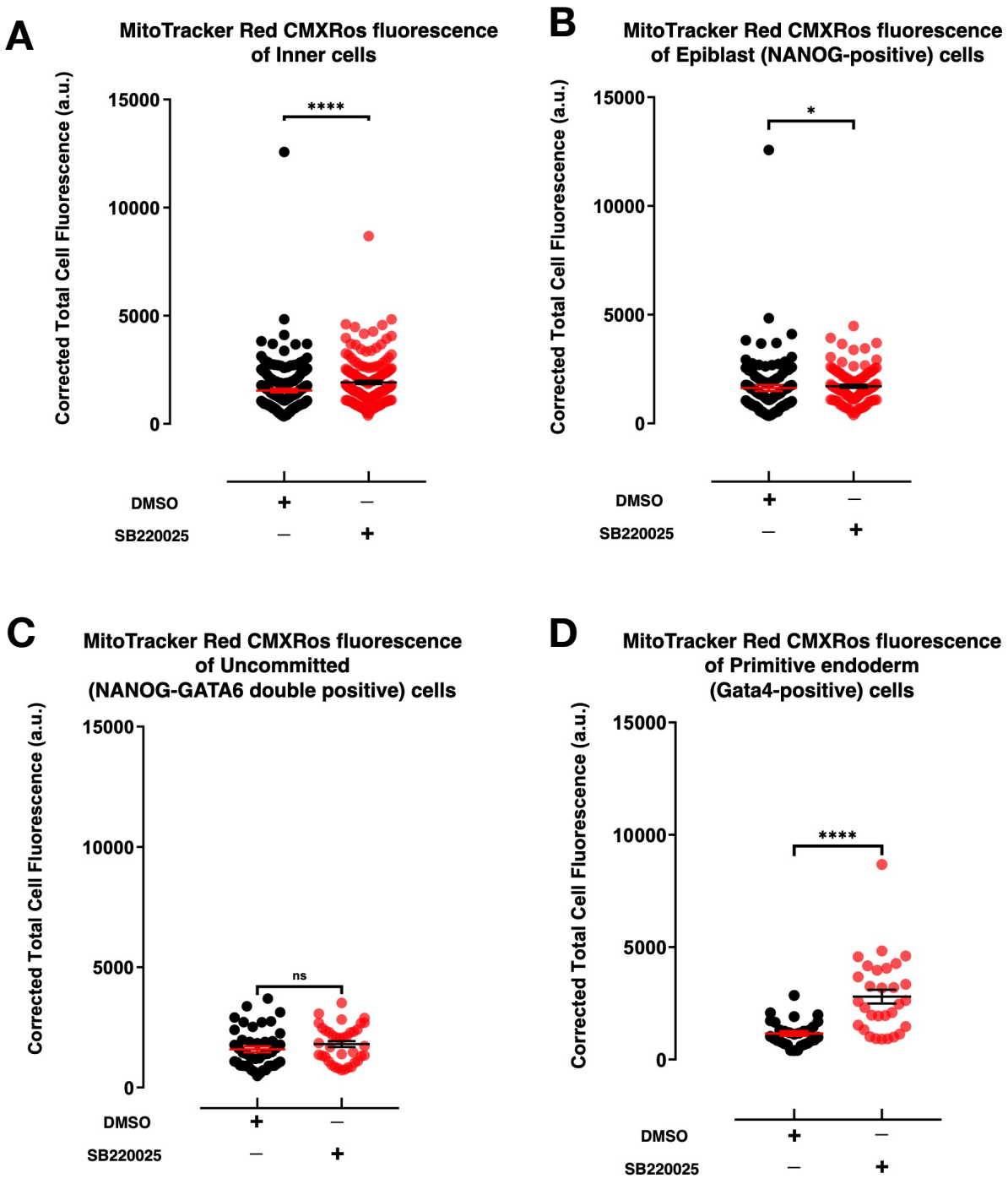

Figure 18. Scatter plots quantifying per cell (CTCF) levels of MTR (representing mitochondria membrane potential) in control (DMSO) and p38-MAPKi (SB220025) of inner (ICM) cells (A), further subdivided into epiblast (EPI, NANOG-positive; B) uncommitted lineage cells (C NANOG, GATA6 co-positive;) and primitive endoderm (PrE, GATA4-positive; D).

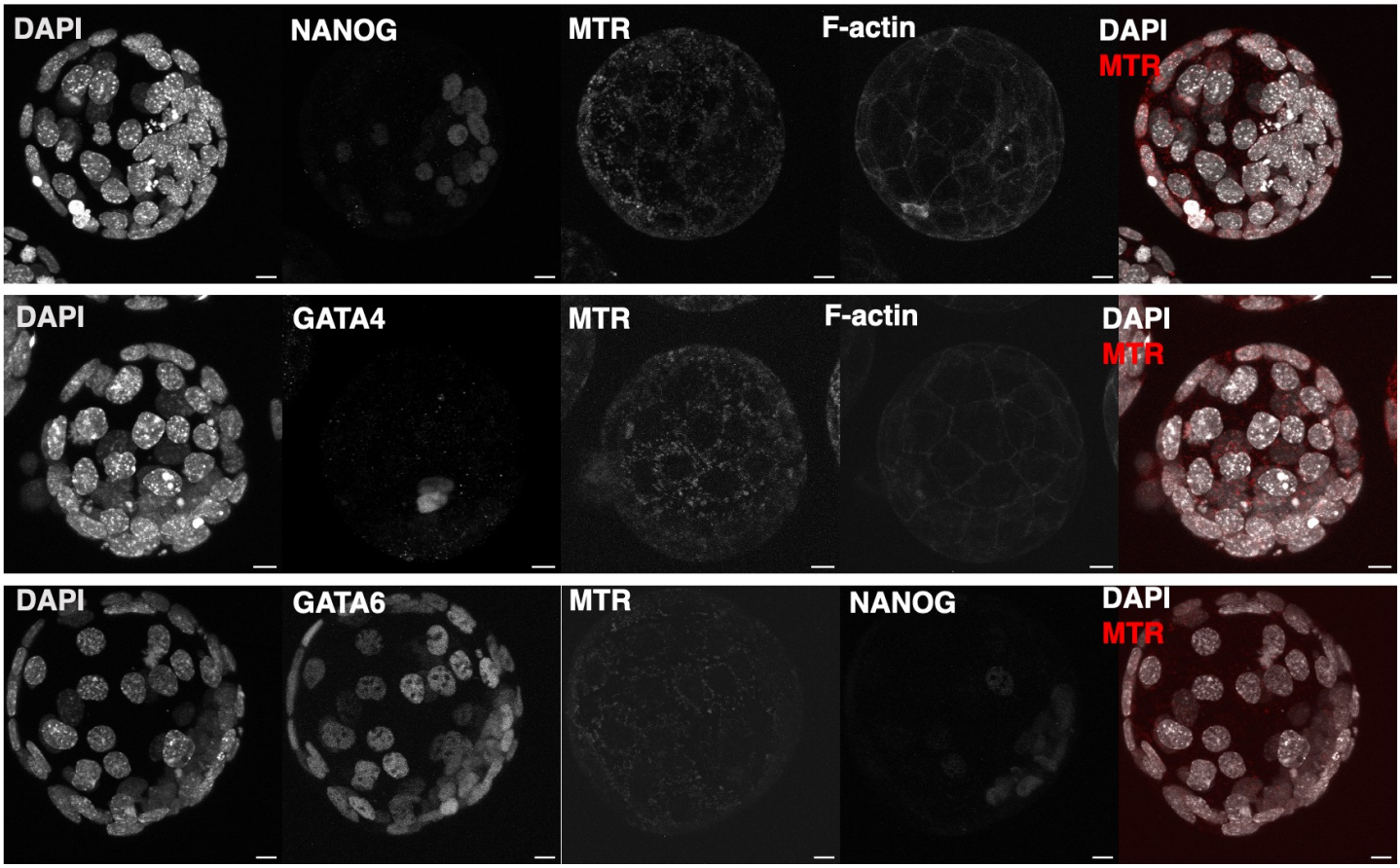

Figure 19. Confocal micrograph z-projections of an exemplar late (E4.5) stage blastocysts treated with MitoTracker Red and SB220025 p38-MAPK inhibitor (E3.5 - E4.5). Individual DAPI (gray pan-nuclear stain; total number of cells), NANOG (grayscale; EPI cells) and GATA4 (grayscale; PrE cells) and GATA6 and NANOG (grayscale; uncommitted cells) and F-actin (cellular membrane boundaries; grayscale) channel micrographs, plus a merged DAPI (grayscale), MitoTracker Red (red) image are shown (scale bar = 10μm).

4.3. p38-MAPK inhibition influences mitochondrial morphology

It is known that mitochondrial morphology is determined by a variance in states between fusion and fission, both processes remaining necessary for continuous development, as blocking either fusion or fission regulatory protein expression results in embryonic death by E11.5 stage (Chen *et al.,* 2003; Wakabayashi *et al.*, 2009). In order to investigate mitochondrial morphology in E4.5 stage p38-MAPK inhibited embryos, as well as controls, the software pipeline "Mitochondria Analyzer", developed by Chaudhry *et al.* was utilized: the analysis pipeline has proven to provide the best accuracy required for quantitative assessment of mitochondrial network dynamics, compared to similar solutions (Chaudhry *et al.*, 2020). This FIJI image analysis plugin option includes image parameter optimization, thresholding, and automated morphofunctional analysis of mitochondrial images (or confocal image stacks). To perform such fluorescence confocal analysis of mitochondria in preimplantation mouse embryonic cells, a series of crucial steps were followed to ensure high-quality results could be obtained. Initially, the mitochondria were labeled with AIF

antibody by IF staining. The image acquisition process was optimized to capture high-resolution images of sufficient quality for accurate analysis, while at the same time avoiding damage due to fluorescent bleaching effects. Imaging parameters and conditions used are detailed in Materials and Methods section.

The aim was set to examine mitochondrial morphology in normal and pathophysiological conditions involving p38-MAPK inhibition. Mouse embryos were cultured and treated according to the established p38-MAPK inhibition protocol as was used for the proceeding analysis, listed in the Materials and Methods section. Mitochondria were labeled with the mitochondrial membrane protein AIF IF staining (Figure 20). AIF IF signal provided the signal for pan mitochondrial detection and morphological characterization.

The initial confocal scans revealed an empirical difference in mitochondria structure between the control and treated conditions conditions: p38-MAPKi mitochondria exhibit an enhanced elongated and interconnected tubular morphology, forming a network-like structure, in contrast to control embryo group mitochondria that had a more fragmented morphology (Figure 20, 21, 22). Thus, further analysis, involving deeper quantitative approaches was deemed necessary. Quantitative analysis of the confocal images showed clear differences in mitochondrial morphology between p38-MAPKi and control conditions (Figure 23). The obtained data showed that p38-MAPKi mitochondria exhibited increased average mitochondrial size, a more tubular morphology, and a decreased sphericity value, suggesting decreased mitochondrial fission (or enhanced/maintained fusion). Skeletonization analysis also revealed that p38-MAPKi caused an overall increase in mitochondrial network connectivity, as evidenced by increased branch parameters (Figures 21, 22, 23). These collective data support previous findings linking DRP1/p38-MAPK-dependent fission/fusion regulatory pathways and demonstrates that the confocal imaging 3D digital analysis pipeline established by Chaudhry *et al.* is sensitive enough to allow for quantitative detection of subtle physiological changes in mitochondrial morphology and networking.

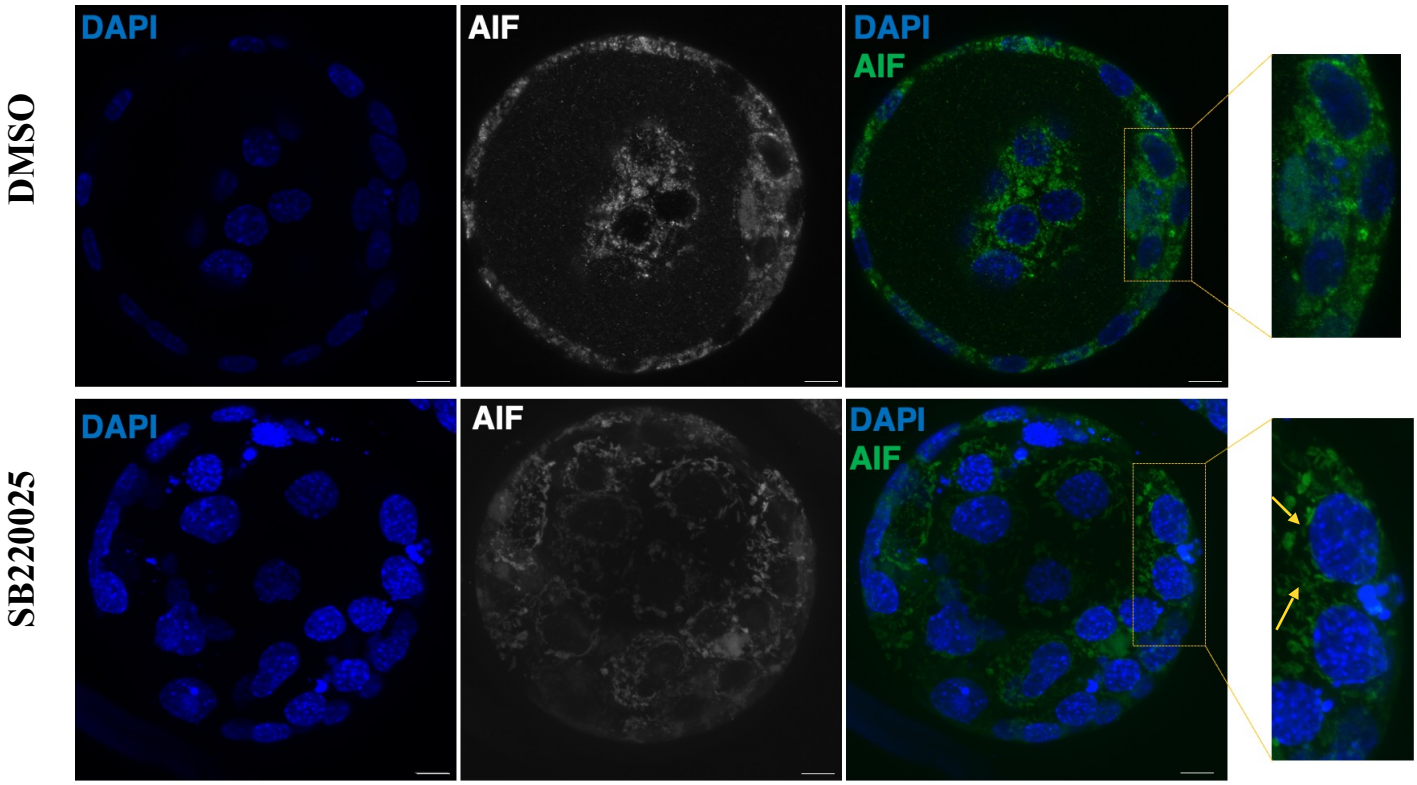

Figure 20. Confocal micrograph partial z-projections (comprising 3-slice z stack for better individual mitochondria visualization) of an exemplar late (E4.5) stage blastocysts treated with SB220025 p38-MAPK inhibitor, as well as control DMSO embryos. Individual DAPI (blue pan-nuclear stain; total number of cells) and AIF (mitochondrial network; gray), plus a merged DAPI (blue), AIF (green) image are shown. Note the tubular mitochondria morphology in p38-MAPKi embryonic cells (scale bar = 10μm).

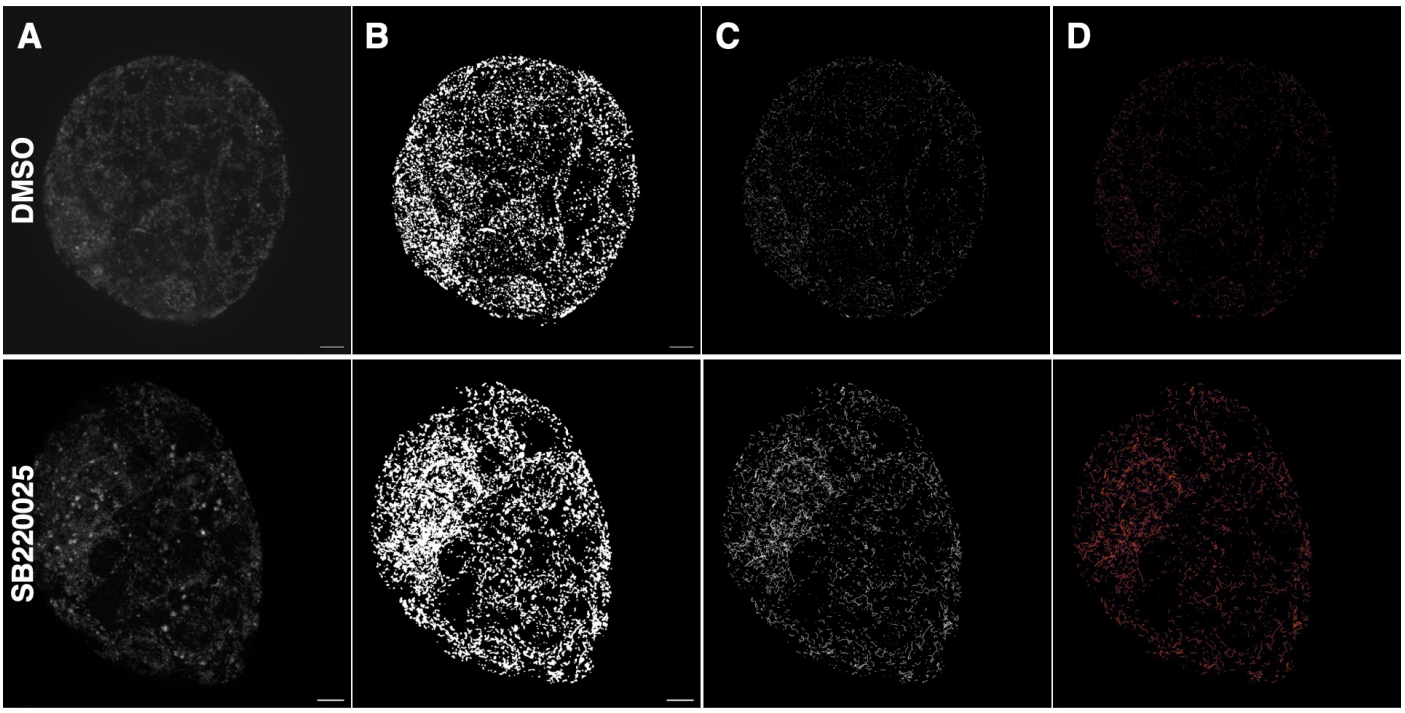

Figure 21. A quantitative comparison of mitochondrial morphology and network connectivity in three-dimensional (3D) confocal scans of E4.5-stage mouse embryos expressing mitochondria-targeted apoptosis-inducing factor protein (AIF). Exemplary z-projections of the AIF-labeled mitochondria in representative blastocysts from each condition are shown in panel A, and the objects identified by applying adaptive thresholding to the images are shown in panel B. A skeletonized and post-processed branch visualization of skeleton image outputs of the mitochondrial objects are shown in panels C and D respectively (scale bar = 10μm).

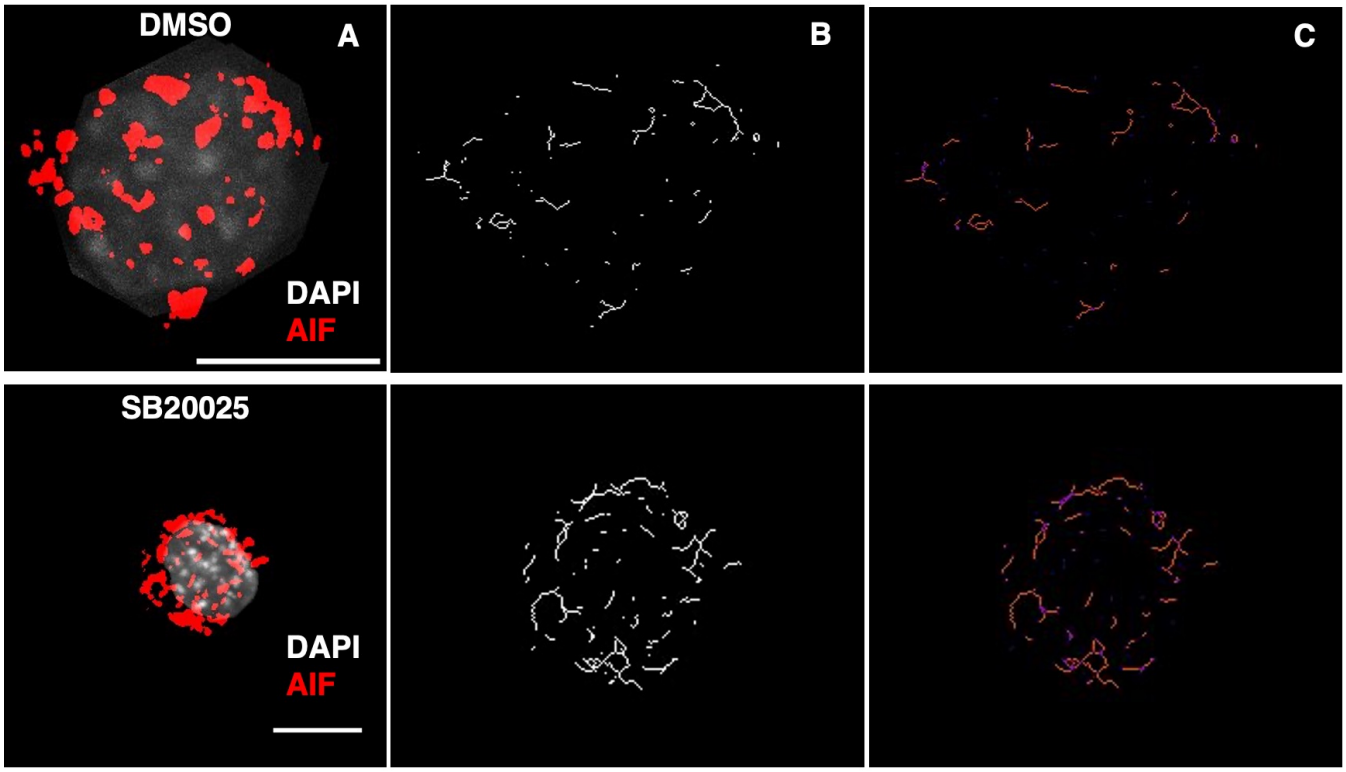

Figure 22. A representative image of mitochondrial morphology and network connectivity in three-dimensional (3D) confocal scans of and control (DMSO; top row) and p38-MAPKi (bottom row) E4.5-stage mouse single ICM cells expressing mitochondria-targeted AIF protein. Examples of the AIF-labeled mitochondria objects already processed with adaptive thresholding algorithm and merged with cell nucleous (visualized by DAPI staining) in representative cells from each group are shown in panel A. A skeletonization and analyzed skeleton image outputs of the mitochondrial objects are listed in panel B and C respectively (scale bar = 10μm).

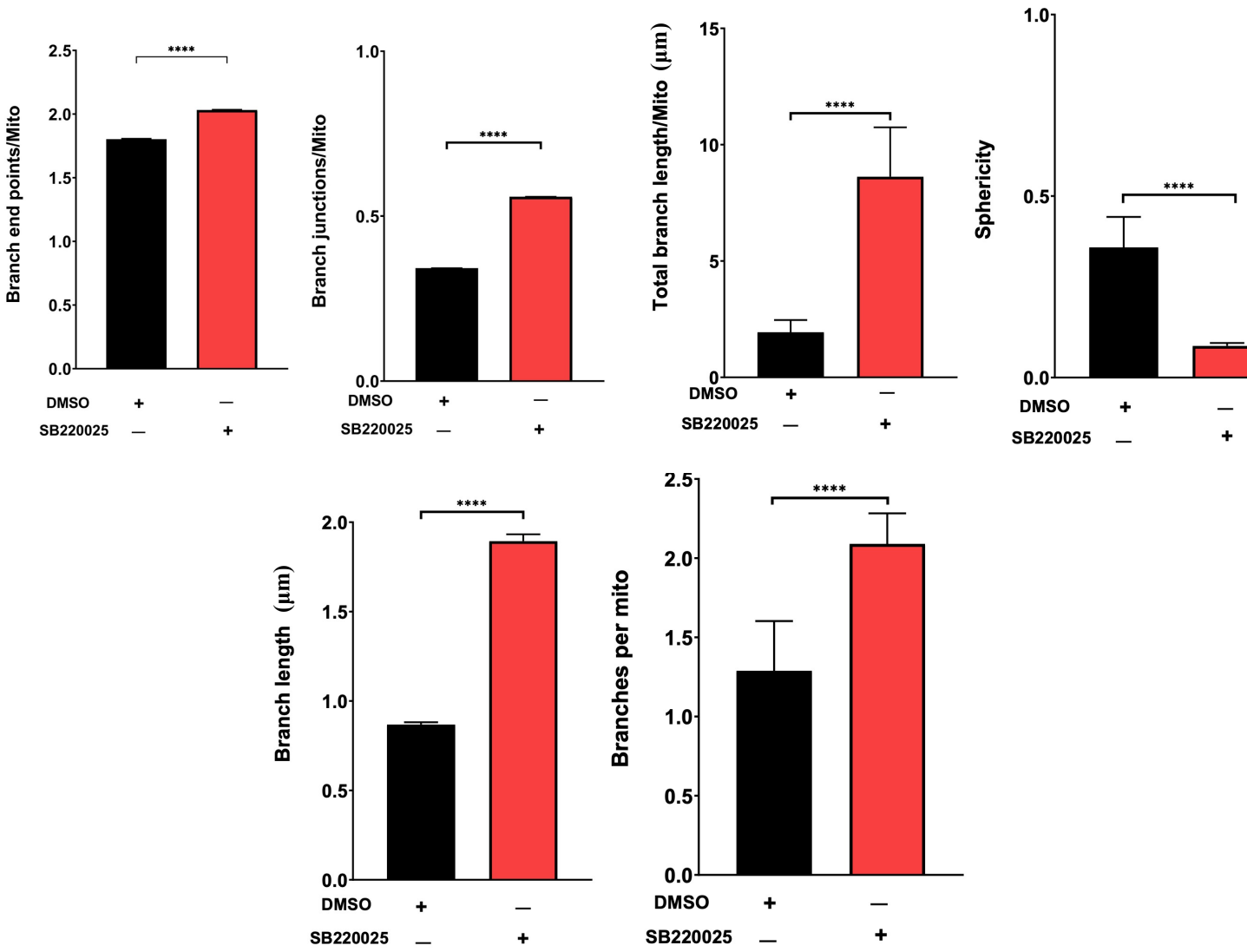

Figure 23. Bar graphs describing statistical comparisons of mitochondrial morphology and network connectivity in three-dimensional (3D) confocal scans of E4.5-stage mouse p38-MAPK inhibited and control blastocysts assayed by mitochondria-targeted apoptosis-inducing factor protein (AIF) expression.

4.4. p38-MAPK inhibition alters the ratio of membrane polarization in preimplantation mouse embryos

It was decided to investigate the proportion (%) of polarized mitochondria within the general mitochondrial pool; using AIF-stained embryos/cells as a reference indicator of mitochondrial network and MTR dye to detect polarized embryonic mitochondria. Although advances in microscopy and labelling techniques have made it possible to image such sensitive processes as MMP accumulation in preimplantation mouse embryos, the

interpretation of colocalization data required rigorous statistics and software solutions. However, there are limitations in the use of current software for visualizing the localization of reporters in biological samples and measuring colocalization, including the need for customization, unsuitability for experiments with low signal intensity or high levels of non-specific signal, and the presence of mixed localization patterns (all three are notoriously recognized and reoccurring problems in mitochondria analyses). While these challenges can be addressed by combining and customizing existing software programs, this requires programming proficiency, quantitative microscopy experience, and statistical knowledge, delving into a topic much beyond the scope of this thesis. Therefore, a single application that provides all the tools from start to finish of the analysis of colocalization and that could be easily customized was sought. The EzColocalization analysis toolset developed by Stauffer *et al.* was chosen for this purpose (Stauffer *et al.*, 2018).

EzColocalization utilization involve analyzing single-cell confocal images of E4.5 stage mouse embryos to determine the colocalization patterns between AIF- and MTR-stained scans. The process starts with creating three stacks of reporter images: the first one includes F-actin labeled with phalloidin-488 or phalloidin-647; the second and third ones are anti-AIF antibodies and MTR dye. F-actin labelling is important for identifying single cells and cellular boundaries in the TE and ICM regions of the mouse embryo, while AIF is important for visualizing the total mitochondrial network. To identify individual cells, a threshold is applied to the F-actin images and a cell filter is used to remove any background noise. Subsequently, cell selection for analyses consisted of 4 groups: control and p38-MAPKi cells localized in ICM and TE.

Following the selection of cells, cellular heat maps and scatterplots were used to examine the intensity of the reporter signals. To quantify colocalization ratio, linear threshold overlap scores (TOS) were used as universal metrics for pixel colocalization values, as these represent the quantifiable degree of overlap of pixels that are above the intensity thresholds for two signals, while rescaling obtained values, allowing direct comparison, representing colocalized/anti-colocalized pixels between collected data at different thresholds (Sheng *et al.,* 2016). The resulting mean TOS colocalization values calculated were 0.654 ± 0.0179 and 0.605 ± 0.0238 for control and p38-MAPKi TE cells, respectively and 0.187 ± 0.0191 and 0.388 ± 0.0318 for control and p38-MAPK inhibited ICM cells, respectively (Figure 24). Multiple comparison tests showed significant statistical differences between the degree

of colocalization in each analyzed condition except TE cells of control (DMSO) versus p38-MAPKi ($p < 0.0001$ for every statistical comparison of each condition; $p = 0.519$ for control TE versus p38-MAPKi TE). TOS values were further visually assessed by generating a matrix with median TOS values, indicating colocalization (positive pixel correlation, TOS > 0.1), anti-colocalization (negative pixel correlation, TOS < 0.1) and non-colocalization (no pixel correlation, TOS ~ 0) at various thresholds for the signal intensities of AIF and MTR. This outcome is consistent with the matrix heat maps and pixel colocalization scatterplots (Figure 24). Obtained results revealed that the reporters in TE cells of both p38-MAPKi and control (DMSO) conditions did colocalize at high signal level, and there was a direct relationship between their signal intensities, as shown in Figure 25. An opposite trend was observed in ICM cells in both conditions, while control cells exhibited lowest linear TOS score, indicating the least polarized mitochondria pool out of all conditions.

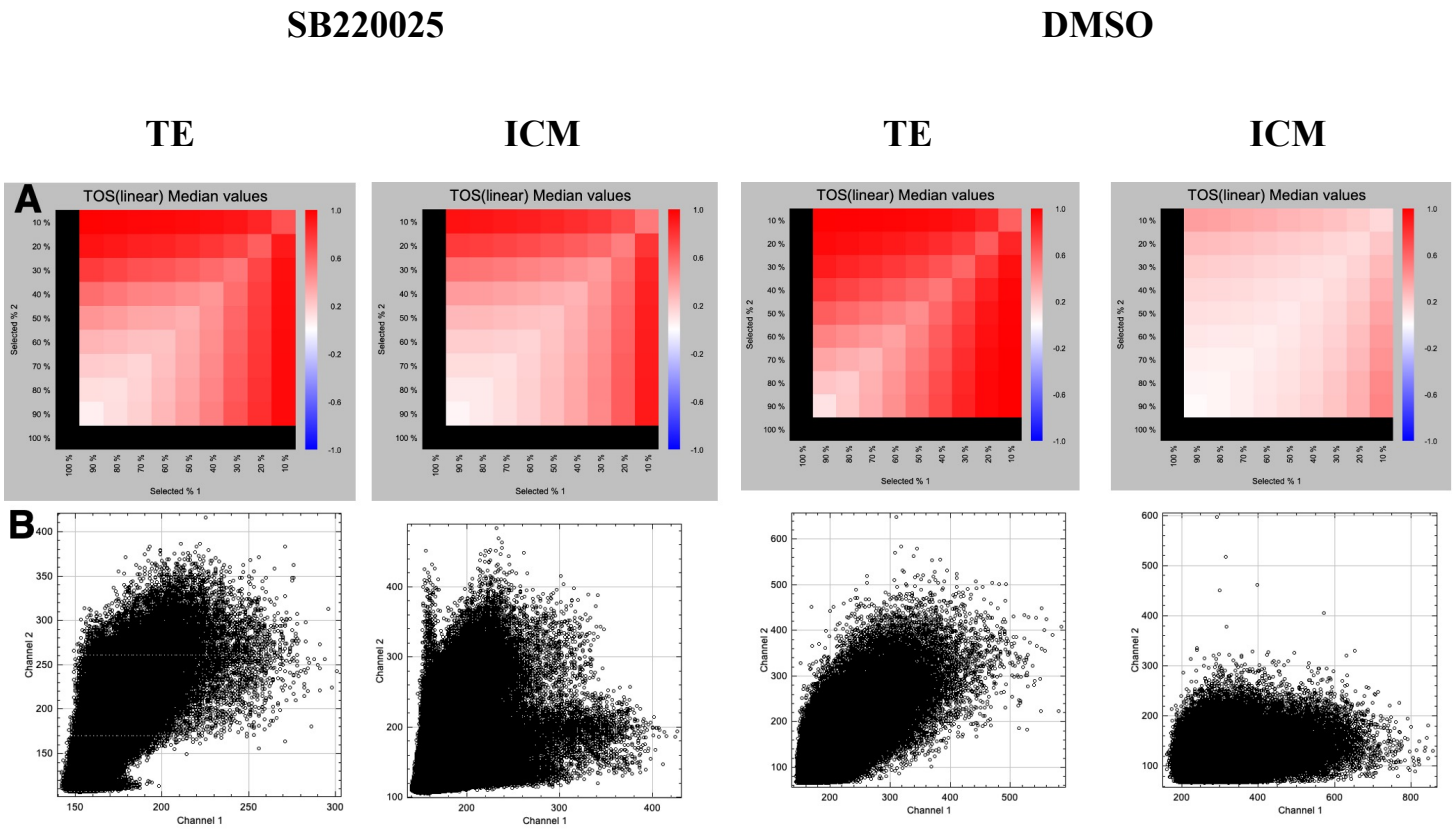

Figure 24. Metric matrix heatmaps for TOS (linear scaling) between AIF (Y axis) and MTR (X axis) pixel overlaps for a representative E4.5 stage single cell from p38-MAPKi and control (DMSO) conditions (A), coupled with the corresponding scatterplot of AIF (Y axis) and MTR (X axis) (B). Heatmaps are detail the top percentage of pixels overlap (indicating colocalization) between the AIF (Y axis) and MTR (X axis) fluorescence values.

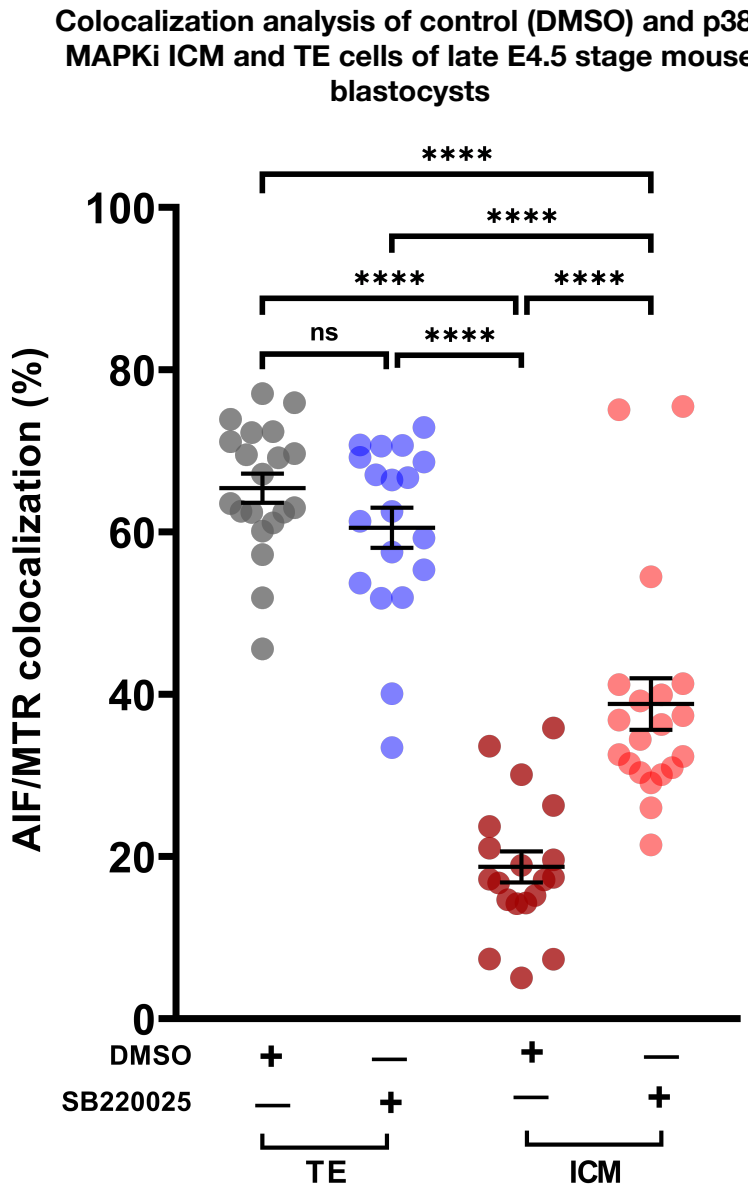

Figure 25. Scatterplot showcasing TOS colocalization values (in percentage) in control and p38-MAPK inhibited ICM and TE E4.5 stage cells.

The obtained results reveal that the colocalization patterns between the ICM and TE cells of normal and p38-MAPKi E4.5 stage mouse blastocysts exhibit a more pronounced level of pixel colocalization between AIF (representing general cellular mitochondria pool) and MTR (representing polarized mitochondria, as demonstrated by MMP fluorescence) specifically in the TE cells. The degree of colocalization reflect the percentage of actively respiring mitochondria (via OXPHOS) within the embryonic cellular pool and are consistent with a low percentage of actively respiring mitochondria observed in ICM cells. These findings

once again suggest variations in mitochondria metabolic rate between ICM and TE at the E4.5 stage of control, as well as p38-MAPKi mouse blastocysts.

4.5. p38-MAPK inhibition affects transcription activity of electron transport chain (ETC) subunit genes

In order to investigate the gene expression profile of ETC mRNA transcripts under p38-MAPKi conditions, six specific genes belonging to ETC complexes were selected, namely *Ndufa5*, *Uqcr10*, *Uqcrq*, *Cox17*, *Atp5e* and *Atp5k*; be analysed in late blastocyst stage embryos (E4.5). Figure 26 highlights the protocol procedure for obtaining E4.5 embryos ready for mRNA isolation and RT-qPCR.

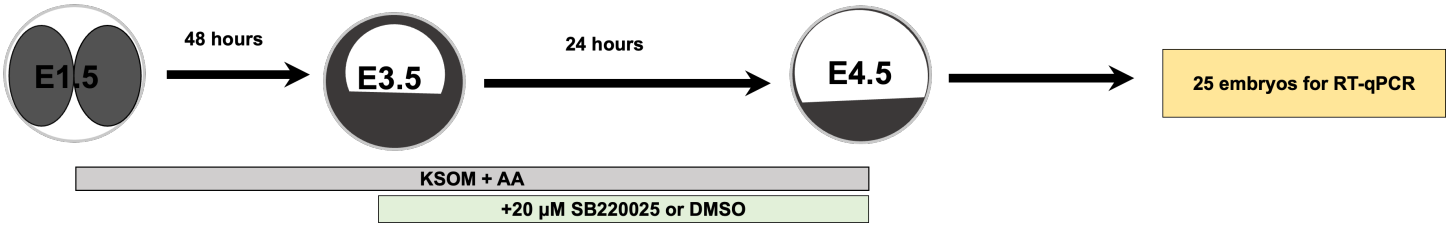

Figure 26. Experimental design for analysing the role of p38-MAPK on mRNA expression of ETC-related genes in maturing blastocysts (E4.5).

Upon conducting this mRNA expression analysis, a universal downregulation of all of the transcripts responsible for protein production in complexes I (*Ndufa5*), III (*Uqcr10*), IV (*Cox17*), V (*Atp5e*, *Atp5k*) (*Uqcrq*, transcript for complex II was excluded due to technical problems during experiments) that were studied was revealed (Figure 27). The obtained findings suggests that there may be a broad regulation of the ETC, potentially influenced by p38-MAPK signalling, occurring during the blastocyst stage of development (E3.5 - E4.5), and is also in agreement with already published RNA-Seq and (phospho)proteomics data from our lab (Bora *et al.*, 2021), Although in this publication an established upregulation of mitochondria respiration-related RNA transcription at E3.5+7h stage, with respect to the control cohort, with subsequent return to control levels at E3.5+10h, was observed rather than a downregulation of the same units at the much later E4.5 stage.

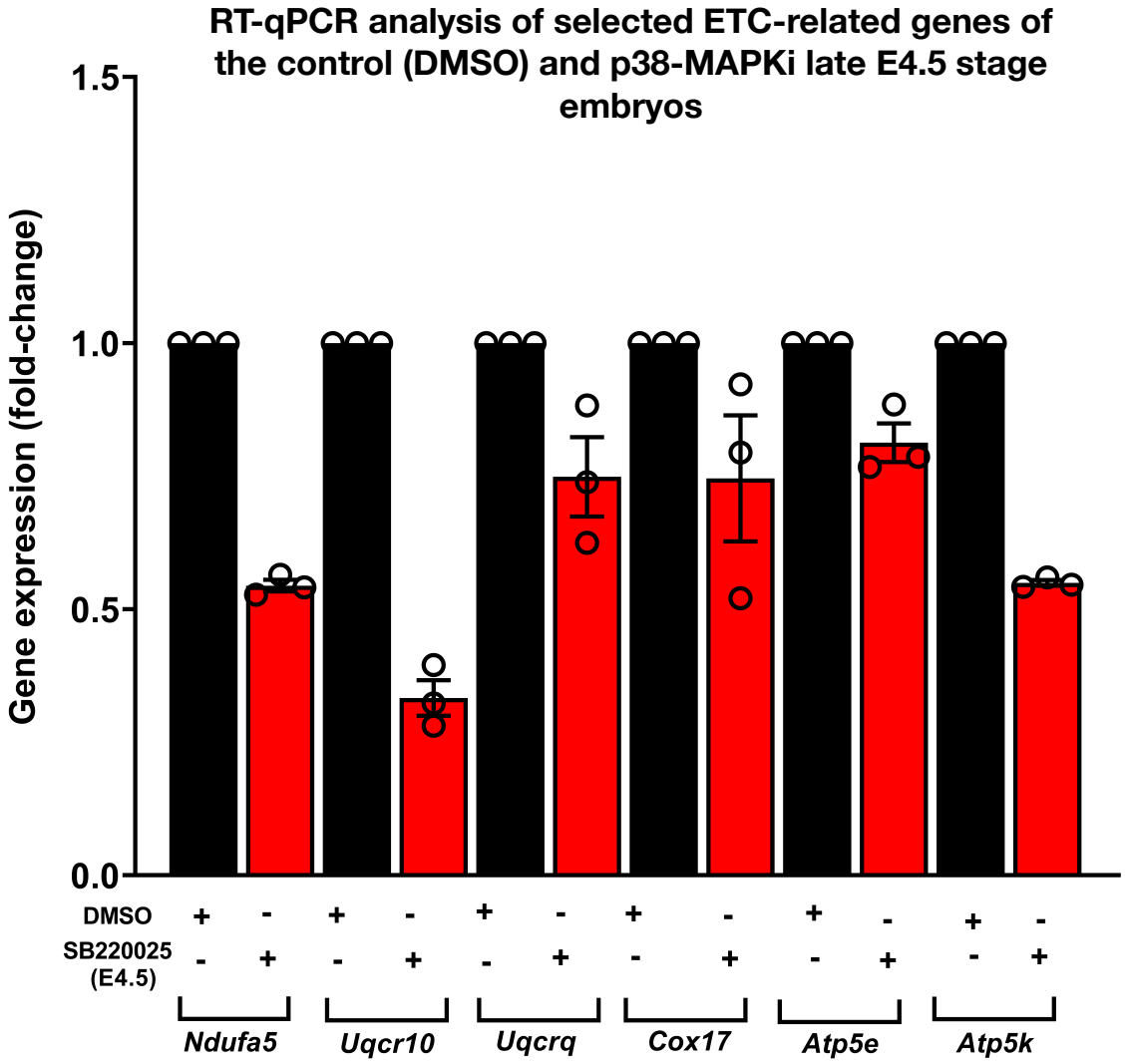

Figure 27. Quantification of the relative transcript expression levels of *Ndufa5*, *Uqcr10*, *Uqcrq*, *Cox17*, *Atp5e*, *Atp5k* internally normalized to *H2afz* levels, across the control (DMSO) and p38-MAPKi conditions in mouse blastocysts of E4.5 stage.

To summarize, the chemical inhibition of p38-MAPK, which is already known to play a role in many translational processes involved in mitochondria maturation during early blastocyst development (Bora *et al.*, 2021), affects the transcriptional activity of ETC complex genes at the E4.5 stage as well. Once again, these findings implicate p38-MAPK not only as a signalling cascade involved in mitochondrial fission regulation but also potentially in OXPHOS and ATP production activity, the extent of which is difficult to separate at this stage as cause or effect.

5. Discussion

Mitochondrial physiology and signalling are crucial for most aspects of cellular function and survival, underpinned by the importance of mitochondrial morphology and dynamics. Mitochondrial adaptation to stress and selective turnover of damaged parts of the network by mitophagy are crucial for the integrity of the organelle and the metabolic health of the cell and in the context of the present study. These processes rely on the balance between mitochondrial fusion and fission dynamics, that require sensitive cell imaging approaches to study. Our current understanding of mitochondrial dynamics in mouse preimplantation embryonic cells is mainly based on utilization of molecular and electron microscopy approaches, but accurately quantifying embryonic cell mitochondrial morphology and dynamics in preimplantation stage embryo cells, by such methods are not descriptive enough to completely fill the research gap. Therefore, the main goal of this thesis was to investigate the structural organization of preimplantation mitochondria networks in the mouse model, utilizing novel computational approaches, coupled with traditional techniques employed in mitochondrial membrane potential (MMP) research and in the emerging blastocyst stage cell lineages; plus the transcriptional activity of electron transport chain subunits genes following p38-MAPKi.

Prior research on mitochondrial MMP and its association with the regulation of mitochondrial morphogenesis presents apparently conflicting results in the context of cell viability and physiology. For instance, Gilkerson *et al.* report dysregulation of mitochondrial MMP, caused by either increased, decreased or total depolarization, triggers reversible mitochondrial network fragmentation in different cell types (Gilkerson *et al.*, 2000), while the findings of Parone *et al.* state that mitochondrial fragmentation itself leads to reduced MMP and as a consequence, decreasing ATP synthesis and increasing susceptibility to apoptosis (Parone *et al.*, 2008). The existence of overly-polarized mitochondria is also hypothesised to serve as a marker of a cellular pathophysiological state, often being a cause of developmental arrest or abnormal mitochondrial fragmentation (reviewed in Zorova *et al.*, 2018).

Addressing the described results, pertaining to MMP activity in all mouse blastocyst cell lineages (in both control and p38-MAPKi conditions), significant statistical differences were observed. While control embryos exhibited the same levels of MMP in ICM, which were uniformly smaller compared to the outer TE lineage, p38-MAPK inhibited cells manifested

an increase in MMP activity across all three types of ICM cells (EPI/PrE/uncommitted); accompanied by a significantly decreased population of PrE cells that nevertheless displayed the most robust MMP increase (to levels comparable to the TE lineage). Moreover, a comparison of outer cell MMP between control and p38-MAPKi conditions revealed a noticeable and specific depolarization of the polar TE sub-lineage across the p38-MAPKi embryos. It is noteworthy that polar TE cells play a role in the establishment of the embryonic-abembryonic axis, shortly after implantation, as well as being responsible for the development of the extra-embryonic ectoderm and its derivatives, such as the ectoplacental cone and chorionic ectoderm (reviewed in Christodoulou *et al.*, 2019). These structures contain trophoblast stem and progenitor cells that generate various trophoblast tissues later in development, essential for successful pregnancy establishment (Kumar *et al.*, 2018). Earlier investigations have hypothesized that p38-MAPK inhibition in mouse embryos may result in a decreased or delayed hatching rate compared to control embryos, proposing a potential role for p38-MAPK in regulating the cellular mechanisms underlying successful embryo hatching (Bora *et al.*, 2021). Therefore, the abnormal downregulation of mitochondrial membrane potential in polar TE cells, as well as increased MMP in ICM (specifically the compromised PrE lineage) might contribute to post-implantation developmental impairments associated with p38-MAPK inhibition. Thus, the obtained results may indicate that stable maintenence of MMP levels (in part contributed to be germane p38-MAPK activity/signalling) are crucial in ensuring successful preimplantation development and subsequent implantation. However, additional research is needed to confirm whether p38-MAPKi mediated alterations in MMP in the ICM and TE are the cause or effect, regarding the observed changes in mitochondria morphological development and how they correlate with the shifting metabolic demands of the developing embryo and its emerging cell lineages (summarized in introduction, Figure 9).

A number of hypotheses can be proposed addressing the increased MMP levels of PrE cells, compared to the rest ICM lineages after p38-MAPKi. The first possibility suggests that PrE cell specification requires increased ATP production to overcome the activation threshold needed for PrE specification and differentiation. This could be related to the rising ATP demand from increased protein translation, which is known to be a factor in the p38-MAPKi PrE phenotype (Bora *et al.*, 2021). However, it is important to note that there is no evidence to suggest that this is the case in control ICM cells, where PrE, EPI and uncommitted cell

MMP maintains similar levels, which are equally low when compared to TE lineage. The second possibility implies, that the few cells that differentiate in p38-MAPKi ICMs are already stressed from the process of PrE specification and differentiation. Indeed, Bessonnard *et al.* demonstrated that maintaining high levels of GATA6 expression in PrE, unlike NANOG levels in EPI, requires active transcription during the second maturation period (from E3.5 to E3.75) (Bessonnard *et al.*, 2019), that suggest PrE specification is a two-step process — one early around the 16-32-cell transition and one later during early blastocyst maturation (E3.5 - E3.75, coinciding with the p38-MAPKi sensitive window). Thus, the observed PrE MMP phenotype in p38-MAPKi conditions represents only a cohort of PrE cells that specified earlier (16-32-cell stage) and managed to sustain increased translational output, required for the PrE lineage specification. This is further backed up by the fact that maintaining high levels of GATA6 expression in the PrE, unlike NANOG levels in EPI, requires active transcription during the second maturation period (from E3.5 to E3.75). Unfortunately, confirming this hypothesis through applying p38-MAPK inhibitor prior to the first round of PrE specification in order to observe MMP phenotype in lately-specified PrE cells is impossible due to the compromised blastocyst formation and further preimplantation development (Paliga *et al.*, 2005). Indeed, further investigations beyond this thesis are required to explore the potential connection between altered MMP activity in the TE/ICM and the impaired developmental competence of cells in p38-MAPKi embryos in general (Bora *et al.*, 2019; Bora *et al.*, 2021; Bora *et al.*, 2021(a); Thamodaran *et* Bruce, 2016).

To provide deeper insight to the observed p38-MAPKi MMP phenotypes, it was decided to perform multi-parameter statistical comparisons by analyzing mouse blastocyst cells stained with MitoTracker Red CMXRos (MTR) and IF against AIF, to simultaneously record changes in MMP (plus co-localisation analyses, indicating the percentage pool of mitochondria exhibiting MMP and likely under-going OXPHOS/respiration). Although, the obtained data demonstrated the same patterns of MMP as assayed using only MTR (highly-polarized TE in both control and p38-MAPKi conditions and a significantly reduced degree of polarization in control ICM), there was a noticeably elevated percentage of colocalization in p38-MAPKi ICM (with the caveat that this analysis was performed on a much more sensitive scale, utilizing different confocal microscopy methods and higher magnification objective lenses, in contrast to the previous experiments). Comparing our results to the

findings of Wilding *et al.*, studying human oocytes and embryos derived from IVF, the increased ratio of high-to-low polarized mitochondria pools could indicate abnormal mitochondrial distributions in the oocyte and metabolic deficiencies in the embryo, that may lead to fatal chromosomal segregation errors (Wilding *et al.,* 2003). In a study by Acton *et al.*, it was noted that differences in the competency of mouse oocytes and embryos are inversely correlated with the ratio of high-to-low polarized mitochondria populations, which in turn depended on whether fertilization occurred *in vitro* or *in vivo*. The same study also revealed that an increased ratio of highly-polarized mitochondria was linked to greater levels of mitochondrial fragmentation during the cleavage of human embryos after IVF (Acton *et al.*, 2004). Thus, an observed elevated percentage of highly-polarised mitochondria, specifically in the ICM of p38-MAPK inhibited embryos, might serve as another marker of impaired developmental competence and inability to implant. Future research on this topic can be performed using the colocalization pipeline developed by Stauffer *et al.*, permitting any number of mitochondrial parameters to be quantified using shape- and intensity-based descriptors (*e.g*. quantification of mitochondria fragmentation). Further experiments involving combining a stable mitochondrial label with other fluorescent biosensors for mitochondrial redox state, ROS analysis *etc*. could provide valuable insights into mitochondrial structure-function relationships in preimplantation embryo development. For example, we know from research in our lab that p38-MAPKi during blastocyst maturation causes elevated detectable ROS generation, exacerbated by removal of exogenous amino acid supplementation to the culture media (Bora *et al.*, 2019).

The presented results in this thesis are also focused on a comprehensive examination of the mitochondrial network organization within mouse blastocysts. The described results, detailing quantitative characteristics of mitochondrial network arrangement/morphology in relation to active p38-MAPK signalling, were obtained and analyzed. Preliminary experiments were dedicated to searching the most suitable and precise pipeline for software analysis of generated mitochondrial network from acquired confocal microscopy images. A solid number of relevant software solutions and protocols using 3D IF stained mitochondrial protein images were trialed (primarily driven by the relatively smaller size of mitochondria in preimplantation embryos, compared to pancreatic β-cells or neuronal cells – a frequently utilized and exemplary model culture system for such mitochondrial analyses). Utilized softwares included, the Mamito algorithm by Ouellet *et al.* (Ouellet *et al.*, 2017),

MetaMorph package (trialed protocol taken from Song *et al.*, 2008), Image-Pro Plus software (trialed protocol taken from Nikolaisen *et al.*, 2014) and others. Mitochondria Analyzer by Chaudhry *et al.* was eventually chosen for the more in-depth analyses presented here, due to its user-friendly, automated and comprehensive nature, coupled with a high accuracy and customization flexibility. Unfortunately, this thesis does not include quantitative comparison of TE versus ICM mitochondria networks due to many difficulties associated with appropriate image capture and isolation of solely ICM or outer trophectodermal areas of E4.5 embryos, obtainable from confocal microscopy scans; although a potential development, arising from this work, could be to employ the lessons learnt in the presented analyses and protocols to obviate these hurdles in the future. Another potential development could be the utilization of TE-deprived (immuno-surgically treated) and isolated ICMs derived from 32-cell blastocysts (as demonstrated in Wigger *et al.*, 2017), for a quantitative comparison of the mitochondrial network between the TE and ICM. This approach could overcome the previously described challenges and provide a deeper understanding of the lineage organization of mitochondrial networks in early embryonic development (this technique has recently been successfully been adopted by our laboratory, and used to show PrE specification/differentiation deficits caused by p38-MAPKi are essentially ICM autonomous and minimally contributed to be TE/blastocyst cavity expansion-related biology; Bohuslavova *et al.*, *manuscript in preparation*). Existing studies (e.g. Kumar *et al.*, 2018) have also addressed the topic of mitochondrial network formation and morphological dynamics (utilizing an electron microscopy approach); confirming the hypothesised robust mitochondrial network of mouse embryo/blastocyst TE cells (most probably associated with increased metabolic activity of fluid-pumping proton pumps), when compared to the relatively underdeveloped ICM state. The work presented in this thesis was solely aimed to explore the role of p38-MAPK in regulating general mitochondrial morphology and it was discovered that inhibiting p38-MAPK indeed alters the mitochondrial network in comparison to the control condition. Specifically, that inhibiting p38-MAPK activity during mouse blastocyst maturation is a postulate cause of impaired mitochondrial fission, resulting in an increased and consolidated mitochondrial network (as demonstrated by quantitative characteristic analyses); including an increase in branch length, number of branches and branch junctions, and a more tubular shape, leading to a robust mitochondrial network alignment. However, despite the involvement of other members of the MAPK

superfamily, such as ERK and JNK, in the regulation of DRP1-mediated mitochondrial fission (Cook *et al.*, 2017; reviewed in Ren *et al.*, 2020), little is generally known about how MAP kinases specifically regulate mitochondrial dynamics in preimplantation mouse embryos. However, some clues, in the context of the data presented here, can be found in human disease research, as p38-MAPK over expression in a post-subarachnoid haemorrhage (a type of stroke, caused by a pathological accumulation of blood into the subarachnoid space of the brain) model lead to depolarization of mitochondria and subsequent ROS leakage to cytoplasm (Huang *et al.*, 2013; reviewed in Ki *et al.*, 2013). The relationship between this data and that presented regarding potential p38-MAPK activity would seem to be consistent, however in regard to ROS generation they would appear to contrast the report of Bora *et al.* describing how p38-MAPKi also caused significantly increased ROS levels in E4.5 mouse blastocysts, especially after amino acid depletion from the culture media (Bora *et al.*, 2019); indicating these cellular processes are almost certain to be highly context dependent. An essential niche of p38 MAPK-mediated regulation of mitochondria activity has been also described in the central nervous system, as chemical inhibition of p38-MAPK reduced DRP1 phosphorylation and mitochondrial fission, thus maintaining synaptic plasticity (Gui *et al.*, 2020). Moreover, p38-MAPK inhibition in neuroblastoma, Parkinson's disease, and other types of neuronal cell culture models, results in a balanced mitochondrial fission and fusion rate, whilst also increasing cell viability and reducing cell apoptosis, both *in vitro* and *in vivo* (Bohush *et al.*, 2018; reviewed in Canovas *et* Nebreda, 2021). Indeed, p38-MAPK has a number of known fission protein-related substrates, such as DRP1, FIS1, MFF (Ren *et al.*, 2020). Evaluating obtained data from the embryonic 3D mitochondrial network reconstruction, presented here, the apparent morphological alterations of p38-MAPKi treated embryo mitochondria could reflect a blocked mitochondrial fission sensor mechanism; that can also be governed by ROS accumulation, a vital component in inducing mitophagy, promotion of mitochondrial fission and impairments in signal transduction pathways (Brownlee, 2001). Accordingly, it may be derived that the underdeveloped morphology and metabolic rate of mitochondria in early mouse embryos, specifically the pluripotent ICM (Houghton, 2006; Kumar *et al.*, 2018), may play a role in limiting their OXPHOS capacity and organelle size, thereby reducing the production of ROS at levels that could harm mitochondrial function or trigger apoptosis; especially during early development, during which total embryo cell numbers are low. Previous research has suggested the

existence of a cell sorting mechanism during waves of asymmetric division, as inappropriately (in relation to lineage-specific cell position within ICM) positioned PrE and EPI cells, that failed to correct their position, are subjected to apoptosis (Morris *et al.*, 2010). Although the authors noted, that not all cell death is caused by cells being mispositioned, however, our results might suggest that mitochondrial morphology may also play a role in cell elimination. It is plausible that the observed apoptosis in ICM cells may not solely be related to their positioning, but also increased ROS accumulation within such cells. In publications by Dumollard *et al.* and Van Blerkom, the authors derived a similar theory through their research on mouse oocytes, as both oocytes with excessively high mitochondrial numbers struggled to regulate nutrient supply and cell metabolic demand, leading to toxic levels of ROS following fertilization (Dumollard *et al.*, 2004; Van Blerkom, 2004). Although the direct impact of p38-MAPK in relations to DRP1-mediated fission was not assayed and presented in this thesis, a major increase of the mitochondrial network parameters coupled with general MMP increase in ICM, imply increased OXPHOS activity and, as a side effect, the potential for increased ROS accumulation.

The final goal of this thesis was to investigate transcriptional activity of ETC complex genes under p38-MAPKi conditions. It was found that p38-MAPKi during the blastocyst maturation stages of development (E3.5 - E.4.5) leads to a universal downregulation of several mRNA transcripts responsible for protein production in ETC complexes I, III, IV, and V. The selected analysed genes included *Ndufa5*, *Uqcr10*, *Uqcrq*, *Cox17*, *Atp5e*, and *Atp5k*. The observed downregulation of ETC mRNA transcripts suggests that p38-MAPK signalling may have a broader mitochondrial regulatory role in OXPHOS and ATP production activity during mouse blastocyst development. These findings are consistent with previous studies that have shown the involvement of p38-MAPK in mitochondrial function and maturation during mouse embryonic development. For instance, Bora *et al.* reported that p38-MAPK signalling regulates translational output in early embryos, and demonstrated that p38-MAPK inhibition (from E3.5) leads to a decrease in the abundance of several mitochondrial proteins, including ETC-related genes analyzed in this thesis (Bora *et al.*, 2021). Moreover, the obtained results in this thesis complement the RNASeq experiments from the same publication by Bora *et al.*, since they add the E4.5 stage as an additional assay time-point, as the the initial analysis detailed elevation in expression of these mitochondria-related mRNAs at E3.5 +4h/7h, that then drop to control levels by E3.5+10h (Bora *et al.*,

2021); we now know these transcripts are eventually downregulated by the E4.5 stage (under p38-MAPKi, E3.5 - E4.5, conditions). Collectively, these findings demonstrate a significant susceptibility of the chosen ETC-related gene transcripts to active p38-MAPK signalling during blastocyst maturation. Intriguingly, the observed dynamic mRNA expression not only applies to mitochondrial respiration-related mRNAs, but also to translation-governing units (Bora *et al.*, 2021); thus, implying most active time-window for mitochondria maturation is likely to be between E3.5+4h and E3.5+7h. Moreover, these findings suggest a decelerated morphological maturation of mitochondria network after E3.5+10h, which can be potentially interesting to investigate in the context of given topic.

Overall, the results in this thesis provide further evidence for the role of p38-MAPK in regulating mitochondrial function during early mouse blastocyst development. In addition to its hypothesised involvement in mitochondrial network dynamics (Supplementary figure 6), p38-MAPK signalling appears to have a broader regulatory role in OXPHOS and potential ATP production activity. These findings have important implications for the understanding of early embryonic development and may have potential applications in assisted reproductive technologies.

6. References

1. Absalón-Medina, V. A., Butler, W. R., & Gilbert, R. O. (2014). Preimplantation embryo metabolism and culture systems: experience from domestic animals and clinical implications. *Journal of assisted reproduction and genetics*, 31(4), 393–409.
2. Acton, B. M., Jurisicova, A., Jurisica, I., & Casper, R. F. (2004). Alterations in mitochondrial membrane potential during preimplantation stages of mouse and human embryo development. *Molecular human reproduction*, 10(1), 23–32.
3. Ajduk, A., Biswas Shivhare, S., & Zernicka-Goetz, M. (2014). The basal position of nuclei is one pre-requisite for asymmetric cell divisions in the early mouse embryo. *Developmental biology*, 392(2), 133–140.
4. Alberio R. (2020). Regulation of Cell-fate Decisions in Early Mammalian Embryos. *Annual review of animal biosciences*, 8, 377–393.
5. Anani, S., Bhat, S., Honma-Yamanaka, N., Krawchuk, D., & Yamanaka, Y. (2014). Initiation of Hippo signaling is linked to polarity rather than to cell position in the pre-implantation mouse embryo. *Development* (Cambridge, England), 141(14), 2813–2824.
6. Artus, J., & Cohen-Tannoudji, M. (2008). Cell cycle regulation during early mouse embryogenesis. *Molecular and cellular endocrinology*, 282(1-2), 78–86.
7. Bell, C. E., & Watson, A. J. (2013). p38 MAPK regulates cavitation and tight junction function in the mouse blastocyst. *PloS one*, 8(4), e59528.
8. Bessonnard S., De Mot L., Gonze D., Barriol M., Dennis C., Goldbeter A., Dupont G., Chazaud C. (2014) Gata6, Nanog and Erk signaling control cell-fate in the inner cell mass through a tristable regulatory network. *Development*, 141(19): 3637-3648.
9. Bessonnard, S., Vandormael-Pournin, S., Coqueran, S., Cohen-Tannoudji, M., & Artus, J. (2019). PDGF Signaling in Primitive Endoderm Cell Survival Is Mediated by PI3K-mTOR Through p53-Independent Mechanism. *Stem cells* (Dayton, Ohio), 37(7), 888–898.
10. Bhakta, H. H., Refai, F. H., & Avella, M. A. (2019). The molecular mechanisms mediating mammalian fertilization. *Development (Cambridge, England)*, *146*(15), dev176966.
11. Bohush, A., Niewiadomska, G., & Filipek, A. (2018). Role of mitogen activated protein kinase signaling in Parkinson's disease. *International journal of molecular sciences*, 19(10), 2973.
12. Bora, P., Gahurova, L., Hauserova, A., Stiborova, M., Collier, R., Potěšil, D., Zdráhal, Z., Bruce, A. W. (2021 (a)). DDX21 is a p38-MAPK-sensitive nucleolar protein necessary for mouse preimplantation embryo development and cell-fate specification. *Open Biology*, 11(7), 210092.
13. Bora, P., Gahurova, L., Mašek, T., Hauserova, A., Potěšil, D., Jansova, D., Susor, A., Zdráhal, Z., Ajduk, A., Pospíšek, M., & Bruce, A. W. (2021). p38-MAPK-mediated translation regulation during early blastocyst development is required for primitive endoderm differentiation in mice. Communications biology, 4(1), 788.Bora, P., Thamodaran, V., Šušor, A., Bruce, A. W. (2019). p38-Mitogen Activated Kinases Mediate a Developmental Regulatory Response to Amino Acid Depletion and Associated Oxidative Stress in Mouse Blastocyst Embryos. *Frontiers in cell and developmental biology*, 7, 276.
14. Brand, M. D., & Nicholls, D. G. (2011). Assessing mitochondrial dysfunction in cells. *The Biochemical journal*, 435(2), 297–312.

15. Brownlee M. Biochemistry and molecular cell biology of diabetic complications. *Nature*. 2001;414(6865):813–820.
16. Bruce, A. W., & Zernicka-Goetz, M. (2010). Developmental control of the early mammalian embryo: competition among heterogeneous cells that biases cell-fate. *Current opinion in genetics & development*, 20(5), 485–491.
17. Buckman, J. F., Hernández, H., Kress, G. J., Votyakova, T. V., Pal, S., Reynolds, I. J. (2001). MitoTracker labeling in primary neuronal and astrocytic cultures: influence of mitochondrial membrane potential and oxidants. *Journal of neuroscience methods*, 104(2), 165-176.
18. Canovas, B., Nebreda, A.R. (2021). Diversity and versatility of p38 kinase signalling in health and disease. *Nat Rev Mol Cell Biol* 22, 346–366.
19. Chaudhry, A., Shi, R., & Luciani, D. S. (2020). A pipeline for multidimensional confocal analysis of mitochondrial morphology, function, and dynamics in pancreatic β-cells. *American journal of physiology*. *Endocrinology and metabolism*, 318(2), E87–E101.
20. Chazaud, C., & Yamanaka, Y. (2016). Lineage specification in the mouse preimplantation embryo. *Development* (Cambridge, England), 143(7), 1063–1074.
21. Cheeseman, L. P., Boulanger, J., Bond, L. M., & Schuh, M. (2016). Two pathways regulate cortical granule translocation to prevent polyspermy in mouse oocytes. *Nature communications*, *7*, 13726.
22. Chen, H., Detmer, S. A., Ewald, A. J., Griffin, E. E., Fraser, S. E., & Chan, D. C. (2003). Mitofusins Mfn1 and Mfn2 coordinately regulate mitochondrial fusion and are essential for embryonic development. *The Journal of cell biology*, *160*(2), 189–200.
23. Christodoulou, N., Weberling, A., Strathdee, D., Anderson, K. I., Timpson, P., & Zernicka-Goetz, M. (2019). Morphogenesis of extra-embryonic tissues directs the remodelling of the mouse embryo at implantation. *Nature communications*, 10(1), 3557.
24. Cook, S. J., Stuart, K., Gilley, R., and Sale, M. J. (2017). Control of cell death and mitochondrial fission by ERK1/2 MAP kinase signalling. *FEBS J*. 284, 4177–4195
25. Cuenda, A., & Rousseau, S. (2007). p38 MAP-kinases pathway regulation, function and role in human diseases. *Biochimica et biophysica acta*, 1773(8), 1358–1375.
26. Cummins J. (1998). Mitochondrial DNA in mammalian reproduction. *Reviews of reproduction*, 3(3), 172–182.
27. Deluao, J. C., Winstanley, Y., Robker, R. L., Pacella-Ince, L., Gonzalez, M. B., & McPherson, N. O. (2022). OXIDATIVE STRESS AND REPRODUCTIVE FUNCTION: Reactive oxygen species in the mammalian pre-implantation embryo. *Reproduction (Cambridge, England)*, *164*(6), F95–F108.
28. De Vries, W. N., Evsikov, A. V., Haac, B. E., Fancher, K. S., Holbrook, A. E., Kemler, R., Solter, D., & Knowles, B. B. (2004). Maternal beta-catenin and E-cadherin in mouse development. *Development* (Cambridge, England), 131(18), 4435–4445.
29. Diaz, G., Setzu, M. D., Zucca, A., Isola, R., Diana, A., Murru, R., Sogos, V., & Gremo, F. (1999). Subcellular heterogeneity of mitochondrial membrane potential: relationship with organelle distribution and intercellular contacts in normal, hypoxic and apoptotic cells. *Journal of cell science*, 112 (Pt 7), 1077–1084.
30. Diez-Juan, A., Rubio, C., Marin, C., Martinez, S., Al-Asmar, N., Riboldi, M., Díaz-Gimeno, P., Valbuena, D., & Simón, C. (2015). Mitochondrial DNA content as a viability score in human euploid embryos: less is better. *Fertility and sterility*, 104(3), 534–41.e1.

31. DiMauro, S., & Schon, E. A. (2003). Mitochondrial respiratory-chain diseases. *New England Journal of Medicine*, 348(26), 2656-2668.
32. Dumollard, R., Duchen, M., & Carroll, J. (2007). The role of mitochondrial function in the oocyte and embryo. *Current topics in developmental biology*, 77, 21-49.
33. Dumollard, R., Marangos, P., Fitzharris, G., Swann, K., Duchen, M., & Carroll, J. (2004). Sperm-triggered [Ca2+] oscillations and Ca2+ homeostasis in the mouse egg have an absolute requirement for mitochondrial ATP production. *Development* (Cambridge, England), 131(13), 3057–3067.
34. Dumortier, J. G., Le Verge-Serandour, M., Tortorelli, A. F., Mielke, A., de Plater, L., Turlier, H., & Maître, J. L. (2019). Hydraulic fracturing and active coarsening position the lumen of the mouse blastocyst. *Science* (New York, N.Y.), 365(6452), 465–468.
35. Fleming T. P. (1987). A quantitative analysis of cell allocation to trophectoderm and inner cell mass in the mouse blastocyst. *Developmental biology*, 119(2), 520–531.
36. Gardner, D. K., & Harvey, A. J. (2015). Blastocyst metabolism. *Reproduction, fertility, and development*, 27(4), 638–654.
37. Gilkerson, R. W., Margineantu, D. H., Capaldi, R. A. and Selker, J. M. (2000). Mitochondrial DNA depletion causes morphological changes in the mitochondrial reticulum of cultured human cells. *FEBS Lett*. 474, 1-4.
38. Gui, C., Ren, Y., Chen, J., Wu, X., Mao, K., Li, H., Yu, H., Zou, F., & Li, W. (2020). p38 MAPK-DRP1 signaling is involved in mitochondrial dysfunction and cell death in mutant A53T α-synuclein model of Parkinson's disease. *Toxicology and applied pharmacology*, 388, 114874.
39. Harvey, A. J. (2019). Mitochondria in early development: linking the microenvironment, metabolism and the epigenome. *Reproduction*, 157(5), R159-R179.
40. Hayashi, Y., Saito, S., Bai, H., Takahashi, M., & Kawahara, M. (2021). Mitochondrial maturation in the trophectoderm and inner cell mass regions of bovine blastocysts. *Theriogenology*, *175*, 69–76.
41. Houghton F. D. (2006) Energy metabolism of the inner cell mass and trophectoderm of the mouse blastocyst. *Differentiation* 74, 11e8
42. Huang, L., Wan, J., Chen, Y., Wang, Z., Hui, L., Li, Y., Xu, D., & Zhou, W. (2013). Inhibitory effects of p38 inhibitor against mitochondrial dysfunction in the early brain injury after subarachnoid hemorrhage in mice. *Brain research*, 1517, 133–140.
43. Hunt, P.A., Koehler, K.E., Susiarjo, M., Hodges, C.A., Ilagan, A., Voigt, R.C., Thomas, S., Thomas, B.F., and Hassold, T.J. (2003). Bisphenol a exposure causes meiotic aneuploidy in the female mouse. *Current Biology*. 13, 546–553
44. Johnson M. H. (2009). From mouse egg to mouse embryo: polarities, axes, and tissues. *Annual review of cell and developmental biology*, 25, 483–512.
45. Kang, M., Garg, V., & Hadjantonakis, A. K. (2017). Lineage Establishment and Progression within the Inner Cell Mass of the Mouse Blastocyst Requires FGFR1 and FGFR2. *Developmental cell*, 41(5), 496–510.e5.
46. Konstantinidis, M., Alfarawati, S., Hurd, D., Paolucci, M., Shovelton, J., Fragouli, E., & Wells, D. (2014). Simultaneous assessment of aneuploidy, polymorphisms, and mitochondrial DNA content in human polar bodies and embryos with the use of a novel microarray platform. *Fertility and sterility*, 102(5), 1385-1392.
47. Korotkevich, E., Niwayama, R., Courtois, A., Friese, S., Berger, N., Buchholz, F., & Hiiragi, T. (2017). The Apical Domain Is Required and Sufficient for the First Lineage Segregation in the Mouse Embryo. *Developmental cell*, 40(3), 235–247.e7.

48. Ki, Y. W., Park, J. H., Lee, J. E., Shin, I. C., & Koh, H. C. (2013). JNK and p38 MAPK regulate oxidative stress and the inflammatory response in chlorpyrifos-induced apoptosis. *Toxicology letters*, 218(3), 235-245.
49. Krupa, M., Mazur, E., Szczepańska, K., Filimonow, K., Maleszewski, M., & Suwińska, A. (2014). Allocation of inner cells to epiblast vs primitive endoderm in the mouse embryo is biased but not determined by the round of asymmetric divisions (8→16- and 16→32-cells). *Developmental biology*, 385(1), 136–148.
50. Kumar, R. P., Ray, S., Home, P., Saha, B., Bhattacharya, B., Wilkins, H. M., Chavan, H., Ganguly, A., Milano-Foster, J., Paul, A., Krishnamurthy, P., Swerdlow, R. H., & Paul, S. (2018). Regulation of energy metabolism during early mammalian development: TEAD4 controls mitochondrial transcription. *Development* (Cambridge, England), 145(19), dev162644.
51. Lima, A., Lubatti, G., Burgstaller, J., Hu, D., Green, A. P., Di Gregorio, A., Zawadzki, T., Pernaute, B., Mahammadov, E., Perez-Montero, S., Dore, M., Sanchez, J. M., Bowling, S., Sancho, M., Kolbe, T., Karimi, M. M., Carling, D., Jones, N., Srinivas, S., Scialdone, A., … Rodriguez, T. A. (2021). Cell competition acts as a purifying selection to eliminate cells with mitochondrial defects during early mouse development. *Nature metabolism*, 3(8), 1091–1108.
52. Livak, K. J., & Schmittgen, T. D. (2001). Analysis of relative gene expression data using real-time quantitative PCR and the 2(-Delta Delta C(T)) Method. *Methods* (San Diego, Calif.), 25(4), 402–408.
53. Maekawa, M., Yamamoto, T., Tanoue, T., Yuasa, Y., Chisaka, O., & Nishida, E. (2005). Requirement of the MAP kinase signaling pathways for mouse preimplantation development. Development (Cambridge, England), 132(8), 1773–1783.
54. Marcondes, N.A., Terra, S.R., Lasta, C.S., Hlavac, N.R.C., Dalmolin, M.L., Lacerda, L.d.A., Faulhaber, G.A.M. and González, F.H.D. (2019), Comparison of JC-1 and MitoTracker probes for mitochondrial viability assessment in stored canine platelet concentrates: A flow cytometry study. *Cytometry*, 95: 214-218.
55. May-Panloup, P., Boguenet, M., Hachem, H. E., Bouet, P. E., & Reynier, P. (2021). Embryo and Its Mitochondria. *Antioxidants* (Basel, Switzerland), 10(2), 139.
56. McCubrey, J. A., Steelman, L. S., Chappell, W. H., Abrams, S. L., Wong, E. W., Chang, F., Lehmann, B., Terrian, D. M., Milella, M., Tafuri, A., Stivala, F., Libra, M., Basecke, J., Evangelisti, C., Martelli, A. M., & Franklin, R. A. (2007). Roles of the Raf/MEK/ERK pathway in cell growth, malignant transformation and drug resistance. *Biochimica et biophysica acta*, 1773(8), 1263–1284.
57. Menchero, S., Rayon, T., Andreu, M.J. and Manzanares, M. (2017), Signaling pathways in mammalian preimplantation development: Linking cellular phenotypes to lineage decisions. *Dev. Dyn.*, 246: 245-261.
58. Menchero S., Rollan I., Lopez-Izquierdo A., Maria Jose Andreu Julio Sainz de Aja Minjung Kang Javier Adan Rui Benedito Teresa Rayon Anna-Katerina Hadjantonakis Miguel Manzanares (2019) Transitions in cell potency during early mouse development are driven by Notch *eLife* 8:e42930.
59. Mihajlović, A. I., & Bruce, A. W. (2017). The first cell-fate decision of mouse preimplantation embryo development: integrating cell position and polarity. *Open biology*, 7(11), 170210.

60. Mihajlović, A. I., Thamodaran, V., & Bruce, A. W. (2015). The first two cell-fate decisions of preimplantation mouse embryo development are not functionally independent. *Scientific reports*, 5(1), 1-16.
61. Mitchell, M., Cashman, K. S., Gardner, D. K., Thompson, J. G., & Lane, M. (2009). Disruption of mitochondrial malate-aspartate shuttle activity in mouse blastocysts impairs viability and fetal growth. *Biology of reproduction*, 80(2), 295–301.
62. Mohr L.R., Trounson A.O. Comparative ultrastructure of hatched human, mouse and bovine blastocysts. *J Reprod Fertil* 1982
63. Morris, S. A., Teo, R. T., Li, H., Robson, P., Glover, D. M., & Zernicka-Goetz, M. (2010). Origin and formation of the first two distinct cell types of the inner cell mass in the mouse embryo. *Proceedings of the National Academy of Sciences of the United States of America, 107(14)*, 6364–6369.
64. Morris, S. A., & Zernicka-Goetz, M. (2012). Formation of distinct cell types in the mouse blastocyst. *Results and problems in cell differentiation*, 55, 203–217.
65. Mudgett, J. S., Ding, J., Guh-Siesel, L., Chartrain, N. A., Yang, L., Gopal, S., & Shen, M. M. (2000). Essential role for p38alpha mitogen-activated protein kinase in placental angiogenesis. *Proceedings of the National Academy of Sciences of the United States of America*, 97(19), 10454–10459.
66. Nagaraj, R., Sharpley, M. S., Chi, F., Braas, D., Zhou, Y., Kim, R., Clark, A. T., & Banerjee, U. (2017). Nuclear Localization of Mitochondrial TCA Cycle Enzymes as a Critical Step in Mammalian Zygotic Genome Activation. *Cell*, 168(1-2), 210–223.e11.
67. Nikolaisen, J., Nilsson, L. I., Pettersen, I. K., Willems, P. H., Lorens, J. B., Koopman, W. J., & Tronstad, K. J. (2014). Automated quantification and integrative analysis of 2D and 3D mitochondrial shape and network properties. *PloS one*, 9(7), e101365.
68. Nolfi-Donegan, D., Braganza, A., & Shiva, S. (2020). Mitochondrial electron transport chain: Oxidative phosphorylation, oxidant production, and methods of measurement. *Redox biology*, 37, 101674.
69. Ouellet, M., Guillebaud, G., Gervais, V., Lupien St Pierre, D.& Germain ,M. (2017). A novel algorithm identifies stress-induced alterations in mitochondrial connectivity and inner membrane structure from confocal images. *PLoS Comput. Biol*. 13, e1005612.
70. Paliga, A. J., Natale, D. R., & Watson, A. J. (2005). p38 mitogen-activated protein kinase (MAPK) first regulates filamentous actin at the 8–16-cell stage during preimplantation development. *Biology of the Cell*, 97(8), 629-640.
71. Papanayotou, C., & Collignon, J. (2014). Activin/Nodal signalling before implantation: setting the stage for embryo patterning. *Philosophical transactions of the Royal Society of London. Series B, Biological sciences*, 369(1657), 20130539.
72. Parone, P. A., Da Cruz, S., Tondera, D., Mattenberger, Y., James, D. I., Maechler, P., Barja, F., & Martinou, J. C. (2008). Preventing mitochondrial fission impairs mitochondrial function and leads to loss of mitochondrial DNA. *PloS one*, 3(9), e3257.
73. Perkins, A.T., Das, T.M., Panzera, L.C., and Bickel, S.E. (2016). Oxidative stress in oocytes during midprophase induces premature loss of cohesion and chromosome segregation errors. *Proc. Natl. Acad. Sci. USA* 113, E6823–E6830.
74. Pikó, L., & Taylor, K. D. (1987). Amounts of mitochondrial DNA and abundance of some mitochondrial gene transcripts in early mouse embryos. *Developmental biology*, 123(2), 364-374.

75. Plusa, B., Piliszek, A., Frankenberg, S., Artus, J., & Hadjantonakis, A. K. (2008). Distinct sequential cell behaviours direct primitive endoderm formation in the mouse blastocyst. *Development* (Cambridge, England), 135(18), 3081–3091.
76. Posfai, E., Petropoulos, S., de Barros, F. R. O., Schell, J. P., Jurisica, I., Sandberg, R., Lanner, F., & Rossant, J. (2017). Position- and Hippo signaling-dependent plasticity during lineage segregation in the early mouse embryo. *eLife*, 6, e22906.
77. Prieto, J., León, M., Ponsoda, X., Sendra, R., Bort, R., Ferrer-Lorente, R., Raya, A., López-García, C., & Torres, J. (2016). Early ERK1/2 activation promotes DRP1-dependent mitochondrial fission necessary for cell reprogramming. *Nature communications*, 7, 11124.
78. Prowse ABJ, Chong F, Elliott DA, Elefanty AG, Stanley EG, Gray PP, et al. (2012) Analysis of Mitochondrial Function and Localisation during Human Embryonic Stem Cell Differentiation In Vitro. *PLoS ONE* 7(12): e52214.
79. Remy, G., Risco, A. M., Iñesta-Vaquera, F. A., González-Terán, B., Sabio, G., Davis, R. J., & Cuenda, A. (2010). Differential activation of p38-MAPK isoforms by MKK6 and MKK3. *Cellular signalling*, *22*(4), 660–667.
80. Ren, L., Chen, X., Chen, X., Li, J., Cheng, B., & Xia, J. (2020). Mitochondrial Dynamics: Fission and Fusion in Fate Determination of Mesenchymal Stem Cells. *Frontiers in cell and developmental biology*, 8, 580070.
81. Rojansky, R., Cha, M. Y., & Chan, D. C. (2016). Elimination of paternal mitochondria in mouse embryos occurs through autophagic degradation dependent on PARKIN and MUL1. *eLife*, 5, e17896.
82. Rovini, A., Heslop, K., Hunt, E. G., Morris, M. E., Fang, D., Gooz, M., Gerencser, A. A., & Maldonado, E. N. (2021). Quantitative analysis of mitochondrial membrane potential heterogeneity in unsynchronized and synchronized cancer cells. *FASEB journal : official publication of the Federation of American Societies for Experimental Biology,* 35(1), e21148.
83. Rubio, C., & Simón, C. (2021). Embryo Genetics. *Genes*, 12(1), 118.
84. Ryan, A. Q., Chan, C. J., Graner, F. & Hiiragi, T. Lumen Expansion Facilitates Epiblast-Primitive Endoderm Fate Specification during Mouse Blastocyst Formation. *Dev. Cell* 575282 (2019).
85. Saba-El-Leil, M. K., Vella, F. D., Vernay, B., Voisin, L., Chen, L., Labrecque, N., Ang, S. L., & Meloche, S. (2003). An essential function of the mitogen-activated protein kinase Erk2 in mouse trophoblast development. *EMBO reports*, 4(10), 964–968.
86. Saha, B., Ganguly, A., Home, P., Bhattacharya, B., Ray, S., Ghosh, A., Rumi, M. A. K., Marsh, C., French, V. A., Gunewardena, S., & Paul, S. (2020). TEAD4 ensures postimplantation development by promoting trophoblast self-renewal: An implication in early human pregnancy loss. *Proceedings of the National Academy of Sciences of the United States of America*, 117(30), 17864–17875.
87. Sathananthan, A. H., & Trounson, A. O. (2000). Mitochondrial morphology during preimplantational human embryogenesis. *Human reproduction* (Oxford, England), 15 Suppl 2, 148–159.
88. Schaefer, A. M., McFarland, R., Blakely, E. L., He, L., Whittaker, R. G., Taylor, R. W., Chinnery, P. F., & Turnbull, D. M. (2008). Prevalence of mitochondrial DNA disease in adults. *Annals of neurology*, 63(1), 35–39.
89. Schindelin J, Arganda-Carreras I, Frise E, Kaynig V, Longair M, Pietzsch T, Preibisch S, Rueden C, Saalfeld S, Schmid B, Tinevez JY, White DJ, Hartenstein V, Eliceiri K,

Tomancak P, Cardona A. Fiji: an open-source platform for biological-image analysis. *Nat Methods* 9: 676 – 682, 2012
90. Schulz, K. N., & Harrison, M. M. (2019). Mechanisms regulating zygotic genome activation. *Nature reviews. Genetics*, 20(4), 221–234.
91. Sheng, H., Stauffer, W., & Lim, H. N. (2016). Systematic and general method for quantifying localization in microscopy images. *Biology open*, 5(12), 1882–1893.
92. Simsek-Duran, F., Li, F., Ford, W., Swanson, R. J., Jones Jr, H. W., & Castora, F. J. (2013). Age-associated metabolic and morphologic changes in mitochondria of individual mouse and hamster oocytes. *PloS one*, 8(5), e64955.
93. Song, W., Bossy, B., Martin, O. J., Hicks, A., Lubitz, S., Knott, A. B., & Bossy-Wetzel, E. (2008). Assessing mitochondrial morphology and dynamics using fluorescence wide-field microscopy and 3D image processing. *Methods* (San Diego, Calif.), 46(4), 295–303.
94. Song, C. X., Chen, J. Y., Li, N., & Guo, Y. (2021). CTRP9 Enhances Efferocytosis in Macrophages via MAPK/Drp1-Mediated Mitochondrial Fission and AdipoR1-Induced Immunometabolism. *Journal of inflammation research*, 14, 1007–1017.
95. Soszyńska A, Klimczewska K and Suwińska A (2019) FGF/ERK signaling pathway: How it operates in mammalian preimplantation embryos and embryo-derived stem cells. *International Journal of Developmental Biology* 63 171–186.
96. Sozen, B., Ozturk, S., Yaba, A., & Demir, N. (2015). The p38 MAPK signalling pathway is required for glucose metabolism, lineage specification and embryo survival during mouse preimplantation development. *Mechanisms of development*, 138 Pt 3, 375–398.
97. Stauffer, W., Sheng, H., & Lim, H. N. (2018). EzColocalization: An ImageJ plugin for visualizing and measuring colocalization in cells and organisms. *Scientific reports*, 8(1), 1-13.
98. Stival, C., Puga Molina, L.delC., Paudel, B., Buffone, M. G., Visconti, P. E., & Krapf, D. (2016). Sperm Capacitation and Acrosome Reaction in Mammalian Sperm. *Advances in anatomy, embryology, and cell biology*, 220, 93–106.
99. Svoboda P. (2018). Mammalian zygotic genome activation. *Seminars in cell & developmental biology*, *84*, 118–126.
100. Thamodaran, V., & Bruce, A. W. (2016). p38 (Mapk14/11) occupies a regulatory node governing entry into primitive endoderm differentiation during preimplantation mouse embryo development. *Open biology*, 6(9), 160190.
101. Tokuhiro, K., & Dean, J. (2018). Glycan-Independent Gamete Recognition Triggers Egg Zinc Sparks and ZP2 Cleavage to Prevent Polyspermy. *Developmental cell*, *46*(5), 627–640.e5.
102. Tuppen, H. A., Blakely, E. L., Turnbull, D. M., & Taylor, R. W. (2010). Mitochondrial DNA mutations and human disease. *Biochimica et Biophysica Acta (BBA)-Bioenergetics*, 1797(2), 113-128.
103. Varelas, X., Samavarchi-Tehrani, P., Narimatsu, M., Weiss, A., Cockburn, K., Larsen, B. G., Rossant, J., & Wrana, J. L. (2010). The Crumbs complex couples cell density sensing to Hippo-dependent control of the TGF-β-SMAD pathway. *Developmental cell*, 19(6), 831–844.
104. Van Blerkom J. (2004). Mitochondria in human oogenesis and preimplantation embryogenesis: engines of metabolism, ionic regulation and developmental competence. *Reproduction* (Cambridge, England), 128(3), 269–280.

105. Van Blerkom, J. (2008). Mitochondria as regulatory forces in oocytes, preimplantation embryos and stem cells. *Reproductive biomedicine online*, 16(4), 553-569.
106. Van Blerkom, J. (2011). Mitochondrial function in the human oocyte and embryo and their role in developmental competence. *Mitochondrion*, 11(5), 797-813.
107. Van Blerkom J., Davis P., Mathwig V., Alexander S., Domains of high-polarized and low-polarized mitochondria may occur in mouse and human oocytes and early embryos, *Human Reproduction*, Volume 17, Issue 2, February 2002, Pages 393–406,
108. Van Blerkom, J., & Runner, M. N. (1984). Mitochondrial reorganization during resumption of arrested meiosis in the mouse oocyte. *American journal of Anatomy*, 171(3), 335-355.
109. Wagner, K., Rehling, P., Szklarz, L. K. S., Taylor, R. D., Pfanner, N., & van der Laan, M. (2009). Mitochondrial F1Fo-ATP synthase: the small subunits e and g associate with monomeric complexes to trigger dimerization. *Journal of molecular biology*, 392(4), 855-861.
110. Wai, T., Ao, A., Zhang, X., Cyr, D., Dufort, D., & Shoubridge, E. A. (2010). The role of mitochondrial DNA copy number in mammalian fertility. *Biology of reproduction*, 83(1), 52–62.
111. Wakabayashi, J., Zhang, Z., Wakabayashi, N., Tamura, Y., Fukaya, M., Kensler, T. W., Iijima, M., & Sesaki, H. (2009). The dynamin-related GTPase Drp1 is required for embryonic and brain development in mice. *The Journal of cell biology*, *186*(6), 805–816.
112. Wigger, M., Kisielewska, K., Filimonow, K., Plusa, B., Maleszewski, M., & Suwińska, A. (2017). Plasticity of the inner cell mass in mouse blastocyst is restricted by the activity of FGF/MAPK pathway. *Scientific reports*, 7(1), 15136.
113. Wilding, M., De Placido, G., De Matteo, L., Marino, M., Alviggi, C., & Dale, B. (2003). Chaotic mosaicism in human preimplantation embryos is correlated with a low mitochondrial membrane potential. *Fertility and sterility*, 79(2), 340–346.
114. Wilding, M., Dale, B., Marino, M., di Matteo, L., Alviggi, C., Pisaturo, M. L., Lombardi, L., & De Placido, G. (2001). Mitochondrial aggregation patterns and activity in human oocytes and preimplantation embryos. *Human reproduction* (Oxford, England), 16(5), 909–917.
115. Wu, M., Neilson, A., Swift, A. L., Moran, R., Tamagnine, J., Parslow, D., Armistead, S., Lemire, K., Orrell, J., Teich, J., Chomicz, S., & Ferrick, D. A. (2007). Multiparameter metabolic analysis reveals a close link between attenuated mitochondrial bioenergetic function and enhanced glycolysis dependency in human tumor cells. American journal of physiology. *Cell physiology*, 292(1), C125–C136.
116. Yamanaka, Y., Lanner, F., & Rossant, J. (2010). FGF signal-dependent segregation of primitive endoderm and epiblast in the mouse blastocyst. *Development* (Cambridge, England), 137(5), 715–724.
117. Yang, Y., & Wilson, M. J. (2015). Lhx9 gene expression during early limb development in mice requires the FGF signalling pathway. *Gene expression patterns : GEP*, 19(1-2), 45–51.
118. Yusoff, A. A. M. , Ahmad, F., Idris, Z., Hasnan Jaafar, H., & Abdullah, J. M. (2015). Understanding Mitochondrial DNA in Brain Tumorigenesis. In (Ed.), Molecular Considerations and Evolving Surgical Management Issues in the Treatment of Patients with a Brain Tumor. *Intech Open*.

119. Zernicka-Goetz, M., Morris, S. A., & Bruce, A. W. (2009). Making a firm decision: multifaceted regulation of cell-fate in the early mouse embryo. *Nature reviews. Genetics*, 10(7), 467–477.
120. Zhang, H., Menzies, K. J., & Auwerx, J. (2018). The role of mitochondria in stem cell-fate and aging. *Development*, 145(8), dev143420.
121. Zhang, T., Ikejima, T., Li, L., Wu, R., Yuan, X., Zhao, J., Wang, Y., & Peng, S. (2017). Impairment of Mitochondrial Biogenesis and Dynamics Involved in Isoniazid-Induced Apoptosis of HepG2 Cells Was Alleviated by p38 MAPK Pathway. *Frontiers in pharmacology*, 8, 753.
122. Zhou, W., Choi, M., Margineantu, D., Margaretha, L., Hesson, J., Cavanaugh, C., Blau, C. A., Horwitz, M. S., Hockenbery, D., Ware, C., & Ruohola-Baker, H. (2012). HIF1α induced switch from bivalent to exclusively glycolytic metabolism during ESC-to-EpiSC/hESC transition. *The EMBO journal*, 31(9), 2103–2116.
123. Ziomek, C. A., Johnson, M. H. (1980). Cell surface interaction induces polarization of mouse 8-cell blastomeres at compaction. *Cell*, 21(3), 935–942.
124. Zorova, L. D., Popkov, V. A., Plotnikov, E. Y., Silachev, D. N., Pevzner, I. B., Jankauskas, S. S., Babenko, V. A., Zorov, S. D., Balakireva, A. V., Juhaszova, M., Sollott, S. J., & Zorov, D. B. (2018). Mitochondrial membrane potential. *Analytical biochemistry*, 552, 50–59.

7. Appendix (supplementary data)

Total number of embryos assayed	64
Total embryos in control condition	29
Total embryos in experimental (inhibited) condition	35
Number of biological replicates	3
Total embryos in experimental condition at E4.5 stage (and possessing NANOG-positive cells)	29
Total embryos in control condition at E4.5 stage (and possessing NANOG-positive cells)	35
Total amount of NANOG cells in experimental condition	107
Total amount of NANOG cells in control condition	104
Mean CTCF values of MTR in NANOG-positive cells in experimental condition (A.U.)	1555
Mean CTCF values of MTR in NANOG-positive cells in control condition (A.U.)	1356
The statistical p-value (Mann-Whitney) describing the difference between the CTCF of MTR in each condition across all embryos.	P = 0.0476

Supplementary figure 1. Complementary data of MitoTracker Red fluorescence measuring experiment in EPI (NANOG+) cells showing all information about used embryos.

Total number of embryos assayed	46
Total embryos in control condition	20
Total embryos in experimental (inhibited) condition	26
Number of biological replicates	2
Total amount of outer cells in experimental condition	154
Total amount of outer cells in control condition	160
Mean CTCF values of MTR in outer cells in experimental condition (A.U.)	3550
Mean CTCF values of MTR in outer cells in control condition (A.U.)	4663
The statistical p-value (Mann-Whitney) describing the difference between the CTCF of MTR in each condition across all embryos.	P = 0.003

Supplementary figure 2. Complementary data of MitoTracker Red fluorescence measuring experiment in TE cells showing all information about used embryos.

Total number of embryos assayed	68
Total embryos in control condition	27
Total embryos in experimental (inhibited) condition	41
Number of biological replicates	3
Total embryos in experimental condition at E4.5 stage (and possessing GATA4-positive cells)	17
Total embryos in control condition at E4.5 stage (and possessing GATA4-positive cells)	27
Total amount of GATA4 cells in experimental condition	30
Total amount of GATA4 cells in control condition	30
Mean CTCF values of MTR in GATA4-positive cells in experimental condition (A.U.)	2521
Mean CTCF values of MTR in GATA4-positive cells in control condition (A.U.)	1076
The statistical p-value (Mann-Whitney) describing the difference between the CTCF of MTR in each condition across all embryos.	$P < 0.0001$

Supplementary figure 3. Complementary data of MitoTracker Red fluorescence measuring experiment in PrE (GATA4+) cells showing all information about used embryos.

Total number of embryos assayed	46
Total embryos in control condition	28
Total embryos in experimental (inhibited) condition	18
Number of biological replicates	2
Total embryos in experimental condition at E4.5 stage (and possessing NANOG-GATA6 double-positive cells)	18
Total embryos in control condition at E4.5 stage (and possessing NANOG-GATA6 double-positive cells)	28
Total amount of uncommitted cells in experimental condition	44
Total amount of uncommitted cells in control condition	38
Mean CTCF values of MTR in NANOG-GATA6 double-positive cells in experimental condition (A.U.)	1394
Mean CTCF values of MTR in NANOG-GATA6 double-positive cells in control condition (A.U.)	1784
The statistical p-value (Mann-Whitney) describing the difference between the CTCF of MTR in each condition across all embryos.	$P < 0.174$

Supplementary figure 4. Complementary data of MitoTracker Red fluorescence measuring experiment in uncommitted lineage (NANOG GATA6 double-positive) cells showing all information about used embryos.

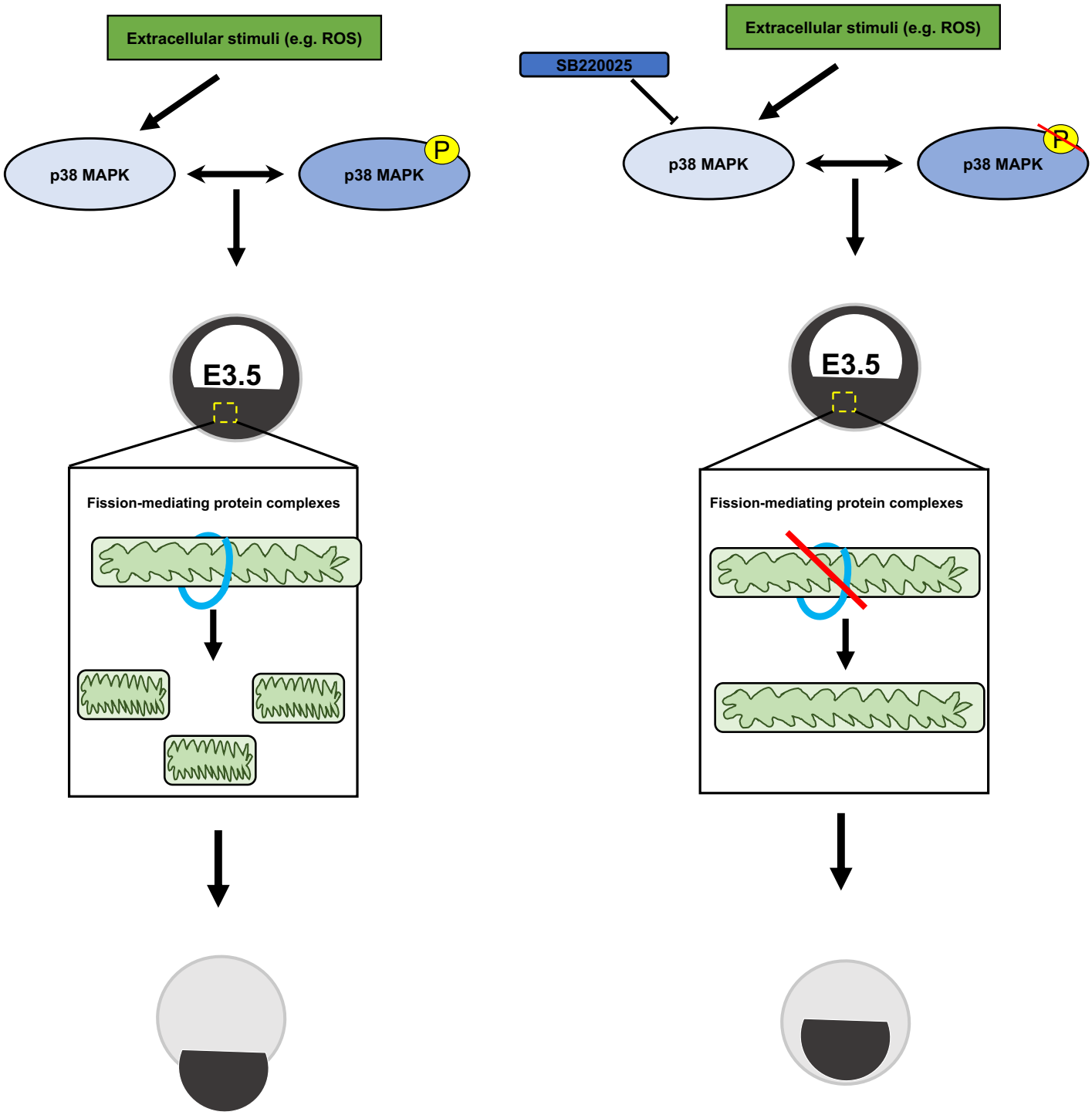

Supplementary figure 5. Working model of the role of p38-MAPK regulating mitochondria fission rate during preimplantation stage embryo development.

		RT-qPCR oligonucleotide primers list	
#	**Gene name**	**Forward primer (5'-3')**	**Reverse primer (3'-5')**
1	*Ndufa5_*	GGCTTGCTGAAAAAGACAAC	ACCTCTTCCACTTCACCAC
2	*Uqcr10_*	AACTTCCACCTTTGCCCTC	TGTTTCCACAGTTTCCCCTC
3	*Uqcrq_*	TCAGCAAAGGCATCCCCAAC	GGCTGGATTCTTCCTTTTCGAC
4	*Cox17_*	AGAAGAAGCCACTGAAGCC	TCTCCTTTCTCAATGATGCAC
5	*Atp5e_*	CTCAGCTACATCCGGTTTTC	CAATTTTTATGCTGCTGCCC
6	*Atp5k_*	GGTCTCTCCACTCATCAAGTTC	TTCCTCCGCTGCTATTCTC
7	*H2afz*	GCGCAGCCATCCTGGAGTA	CCGATCAGCGATTTGTGGA

Supplementary figure 6. Information on oligonucleotide primers used in RT-qPCR analysis

#	Antigen	Cat. Number	Supplier	Type	Species raised in	Dilution used
Immunofluorescence imaging						
1	Nanog	14-5761	Affymetrix/ eBioscience	Primary; monoclonal	rat	1:200 in PBST (3% BSA)
2	Gata6	AF1700	R&D systems	Primary; polyclonal	goat	1:200 in PBST (3% BSA)
3	Gata4 (C20)	sc-1237	Santa Cruz	Primary; polyclonal	goat	1:200 in PBST (3% BSA)
4	Gata4 (H112)	sc-9053	Santa Cruz	Primary; polyclonal	rabbit	1:200 in PBST (3% BSA)
5	Cdx2	MU392A-UC	BioGenex	Primary; monoclonal	mouse	1:200 in PBST (3% BSA)
6	AIF/ apoptosis inducing factor	5318T	CST	Primary; monoclonal	rabbit	1:200 in PBST (3% BSA)
7	donkey anti-rabbit IgG Alexa-488	ab150073	Abcam	Secondary; polyclonal	donkey	1:500 in PBST (3% BSA)
8	donkey anti-rabbit IgG Alexa-647	ab150075	Abcam	Secondary; polyclonal	donkey	1:500 in PBST (3% BSA)
9	donkey anti-mouse IgG Alexa647	ab150107	Abcam	Secondary; polyclonal	donkey	1:500 in PBST (3% BSA)
10	donkey anti-goat IgG Alexa647	ab150131	Abcam	Secondary; polyclonal	donkey	1:500 in PBST (3% BSA)
11	Donkey anti-mouse Alexa 488	A21202	Invitrogen	Secondary; polyclonal	donkey	1:500 in PBST (3% BSA)
12	Donkey anti-rat Alexa 488	A21208	Invitrogen	Secondary; polyclonal	donkey	1:500 in PBST (3% BSA)
13	Donkey anti-goat Alexa 488	A11055	Invitrogen	Secondary; polyclonal	donkey	1:500 in PBST (3% BSA)

Supplementary figure 7. List of antibodies used.